The Phanerozoic Stratabound/Stratiform Ore Deposits of Egypt: Their Mode of Occurrence and Formation in Accordance with the Phanerozoic Geological Evolution

Mortada Mourad Taha El Aref

Abstract

The present work provides an integral and comprehensive view on the mode of occurrence and the mode formation of the ores hosted in outcropped Egyptian Phanerozoic rock sequences. The main goal of this work is to discuss the time/space problem of the formation of these deposits and to clarify the regional and local geological factors controlled their formation, in order to be fundamental guides for future exploration and investment plans. Also focusing has been bayed to clarify the sedimentary environments, parageneses, geochemical characteristics, possible source, and economic potentiality of each ore type as well as detailed explanation of the depositional, digenetic, and post-diagenetic (supergenetic) processes involved during the ore formation. The work shed some light on the mining advantages and investment opportunities of some of these ore deposits, as well as the challenges facing the development of their economic return. The ore deposits under consideration are of stratabound/stratiform types, being confined within certain stratigraphic horizons of different ages and paleo-geographic settings which concurrent well with the Phanerozoic geologic history of North Africa and the associated paleo-geographic evolution patterns of the paleo-shorelines and the simultaneous paleo-topographic configurations. The stratiform deposits show conspicuous depositional and diagenetic features of shallow near-shore environments and are hosted within certain marginal stratigraphic units of regional or local magnitudes. The stratabound deposits are genetically related to paleo-erosion surfaces (sequence boundaries) and the related supergenesis as they constitute the main product of deep weathering processes. The concluded basic factors which controlled the formation of these ores at the time(s) and in the place(s) of their formation, can be summed up as follows: (a) the paleo-geography of the paleo-shorelines, (b) the paleo-topographic configurations and distribution of paleo-highs and paleo-lows, (c) the prevailed paleo-climates, (d) the simultaneous availability of the ore components, either from the local medium or from the adjacent hinterlands (d) the availability of a suitable paleo-environments with the related facies hierarchy and possible lateral facies changes, and (e) the prevailed sedimentary dynamics and sedimentation and post-sedimentation processes.

Keywords

Stratabound deposits • Digenetic processes • Paleo-Tethys • Neo-Tethys • Sedimentary dynamics • Egypt

1 Introduction

Egypt is located in the northeastern part of the African continent and consists of Precambrian igneous and metamorphic rock association followed by Phanerozoic sedimentary successions. The Precambrian rocks have been affected by various deformational episodes, ended by the Proterozoic Pan-African tectonothermal deformation. According to Schandelmeir et al. (1987), the erosion and deposition of the Phanerozoic rock successions are generally controlled by reactivated faults and global sea level changes. The Phanerozoic history of Egypt is a part of the Phanerozoic evolution of the African continent which reflect the assembly of Pangea and the poly-phase breakup and the

The original version of this chapter has been revised. The chapter was published with incorrect words [paleo–karst] that have been corrected. The correction to this chapter can be found at https://doi.org/10.1007/978-3-030-95637-0_27.

Present Address:
M. M. T. El Aref (✉)
Department of Geology, Faculty of Science, Cairo University, Giza, Egypt
e-mail: elaref@sci.cu.edu.eg

Z. Hamimi et al. (eds.), *The Phanerozoic Geology and Natural Resources of Egypt*, Advances in Science, Technology & Innovation, https://doi.org/10.1007/978-3-030-95637-0_18

related tectonic phases of the Gondwana supercontinent. The details of the Phanerozoic geological history of North Africa have carefully studied and reviewed by distinguished scientists, among them are: Klitzsch and Wycisk (1987), Klitzsch (1984), Morgan (1990), Meshref (1990), Said (1990a, 1990b, 1990c), Stern (1994), Wilson and Guiraud (1998), Bosworth et al. (1999), Guiraud and Bosworth (1999), Guiraud et al. (2001, 2005), Issawi (2002) and Issawi et al. (1999, 2009). During the Phanerozoic time, North Africa including Egypt comprises an essential part of the southern boundary of the paleo- and new-Tethian seas. Accordingly, its Phanerozoic geological history was based mainly on the following dominating factors: (a) the effect of many structural events and successive periods of rifting phases accompanied by basaltic magmatic activities, (b) the domination of the paleo-Tethys and neo-Tethys shorelines along the northeast African margin, (c) sea level fluctuation, and southward transgression and northward regression of the seas, and (d) the geographic distribution and diversity of sedimentary environments and the related rock facies associations. With the context of the identification of the geology of the Egyptian Phanerozoic time span, it is necessary to clarify the geological setting and genesis of the ore deposits hosted in the Phanerozoic rock sequences.

This chapter aims to update the previously published contribution of El Aref (1996) on the origin of The Egyptian Phanerozoic stratabound and/or stratiform ore deposits. The inevitability, re-revision, updating, and republication of this version are due to the following objective reasons: (a) the original version is available only in the limited version and locally distributed proceeding of the second International Conference on the Geology of the Arab World (GAW II, Cairo, 1994, published in 1996), (b) there are many consequent scientific additions published after 1996 by the author and his colleagues, containing more explanations and detailed discussions on the nature and mode of formation of the ores involved, and (c) the dealt stratabound ore deposits constitute integral parts of the Egyptian Phanerozoic successions and coincided well with the geological history of this Epoch. The current comprehensive view, which is enhanced by new additional and redirected illustrations, throws more light on the main geological factors that controlled the development of the Phanerozoic stratabound/stratiform deposits of Pb. Zn, Cu, Fe, Mn, Sr, Ba, Al, P, and carbonate ore (the so-called Egyptian Alabaster) in their spaces and times of formation (Fig. 1; Table 1). The paleo-environments of these ores and the processes involved during their formation are clarified and discussed in detail. The other Phanerozoic geological resources such as the varieties of building stones, industrial non-metallic mineral resources, salts and evaporites, mineral fuels and fluvial and heavy mineral concentrates are not intended in this work. The chapter provides a compiled and an integrated genetic scheme, exhibiting the intimate genetic relation between the ore formation and multiple regional and local geological processes (i.e. tectonic events, sedimentary environments, paleo-drainage, and volcanic activities), and also the general directions of the paleo-shorelines (transgression and regression trends), which all or some of them gathered at certain time(s) in a certain geological and geographic site(s) during the Phanerozoic history of Egypt (Table 1). The stratiform deposits show conspicuous depositional and diagenetic features of shallow near-shore environments and are hosted within certain stratigraphic units of regional or local magnitudes. The stratabound deposits are genetically related to paleo-erosion surfaces (sequence boundaries) and the related supergenesis as they constitute the main product of the related deep weathering processes. Besides the concerned ore deposits, wide varieties of the stratigraphic rock sequences and environments in which the deposits were accumulated were carefully studied. For clarification, the formal lithostratigraphic nomenclature is used for the viewed rock units, while the term time rock unit (sequence) is applied to those sandwiched between major unconformities or stratigraphic gaps.

The achievement of this work is based mainly on a very systematic way of deep observations and interpretations (i.e. inductive reasoning, "bottom-up approach"), moving from regional and local field investigations and mapping of the mine areas with stratigraphic correlations and verification of breaks of sedimentation and sequence boundaries to more detailed megascopic and microscopic examinations of representative and oriented polished slabs and thin and polished sections as well as much-sophisticated "nono-scopic" inspections of representative textures and spots, major and trace chemical analyses and isotope measurements. The fine (high resolution) stratigraphy of the ore intervals and the ore architecture, ore geometry, and the degree of congruency (fabric characteristics, fabric relations, and evolution), in all scales, are essentially considered. Considerable attention is attributed to the main characteristic features of the different ore types, their regional or local paleo-geographic concordances with the host rocks as well as the processes involved during their formation. This is accompanied by the interpretation of the several geological aspects that controlled the structural, sedimentological, and paleo-topographical setting of the host rocks and the associated deposits and the accompanied distribution of paleo-highs and paleo-lows that fairly settled at certain times and in certain places during the Phanerozoic history of Egypt.

As a general main outcome, the concluded integral scheme clarifies the situation (space and time) of the ore formation which may hopefully assist further exploration programs for new economic ore sites. It is important to clarify that the present work did not neglect attention to the geological setting, characteristics, and mode of the formation of many small-scale mineral occurrences or shows, in order for

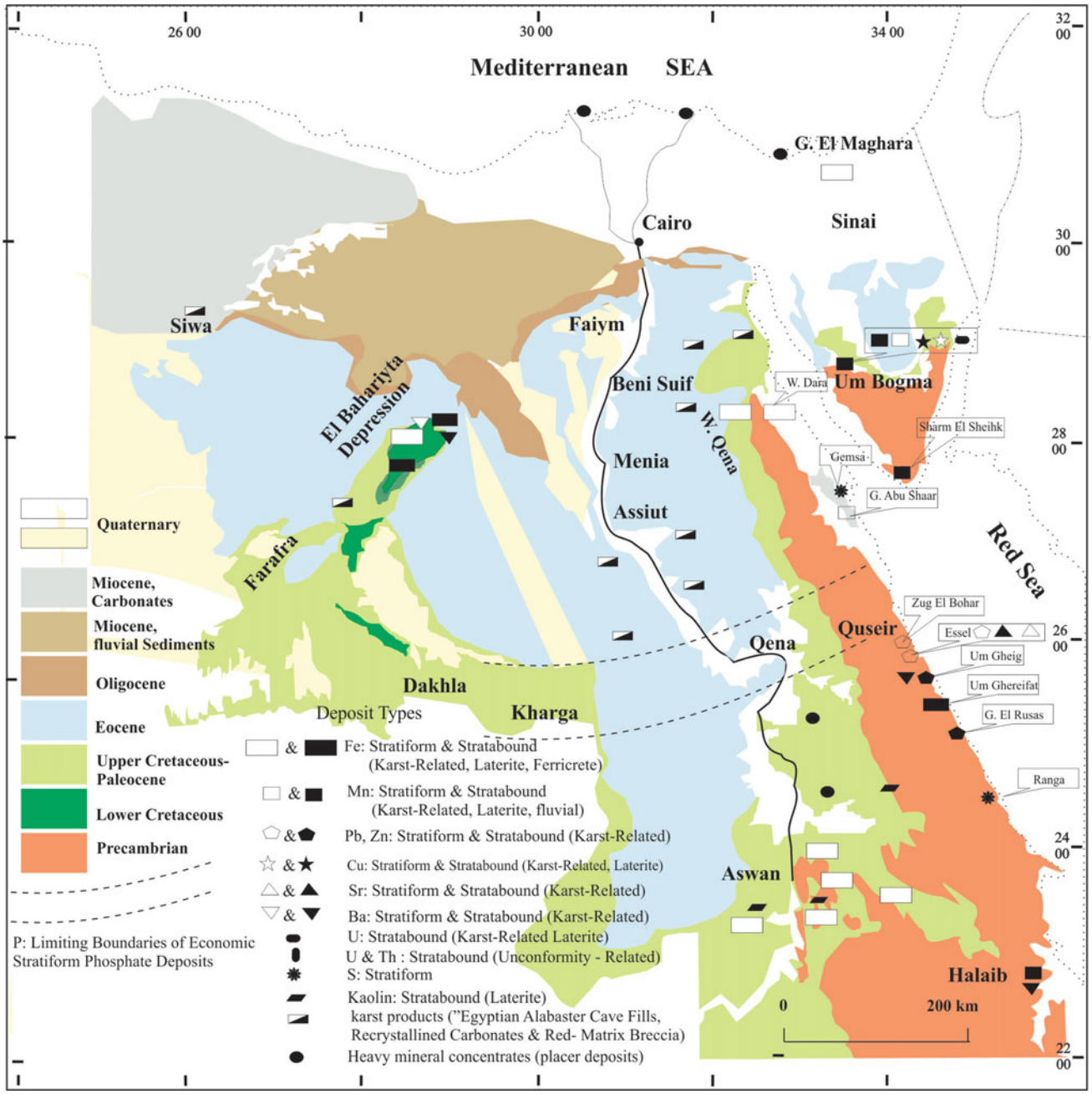

Fig. 1 Simplified geological map of Egypt and distribution of the Phanerozoic stratabound/stratiform ore deposits (modified after El Aref, 1996)

these occurrences to be fundamental necessities to future evaluation or exploration plans for similar new more economic places of the same geological setting or even to encourage their investment as small or very small enterprises.

The different genetic classifications of the Egyptian ore deposits including those confined within Phanerozoic rock units are reviewed and discussed by El Shazly (1957) and Hussein and El Sharkawi (1990). Hussein and El Sharkawi (op. cit.) presented a modified classification which follows the general scheme outlined by Hilmy and Hussein (1978). El Aref (2001) has outlined the geologic setting of the Phanerozoic sedimentary hosted deposits within the chronologic framework of the Egyptian geological column of the metallurgical map of Egypt. Most if not all of the Egyptian ore deposits under consideration, occurred within the Phanerozoic sediments, has previously been attributed by the pioneer Egyptian epigenetists to epigenetic replacement processes by hydrothermal solutions of the Oligocene volcanisms or of unknown sources. Meneisy (1990) in his study of the Phanerozoic volcanic activities of Egypt related

Table 1 Phanerozoic tectonic events, environmental evolution, and the related Phanerozoic stratabound and stratiform ore deposits (modified after El Aref, 1996)

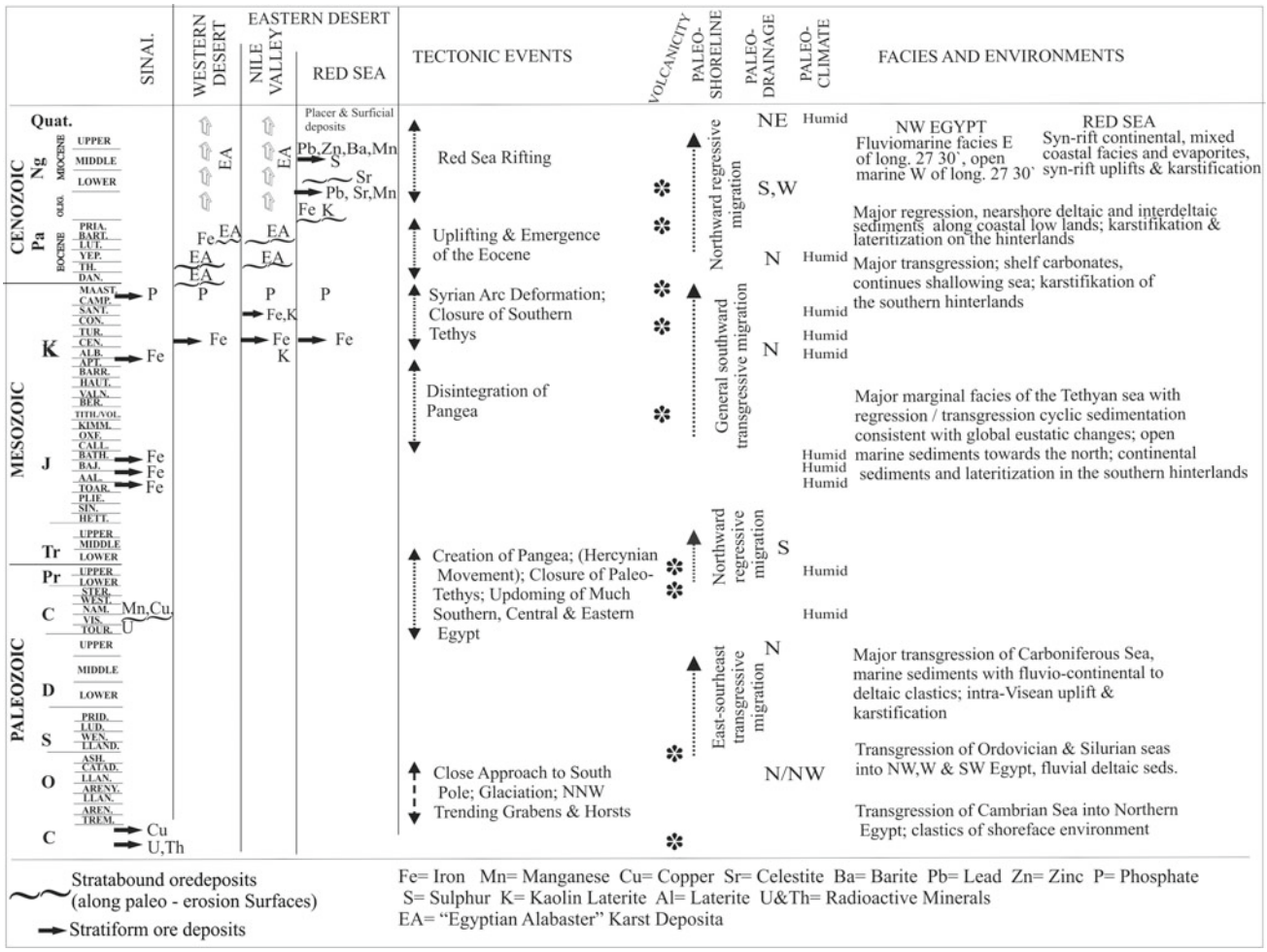

almost all the Phanerozoic Mn, Fe, and Cu to hydrothermal processes of the Tertiary volcanism. He assumed that the Red Sea metalliferous deposits are a product of seafloor spreading and the related hot brines. The stratiform oolitic Coniacian-Santonian oolitic ironstones of Aswan environ are also recently related to a successive hydrothermal-sedimentary origin by hypogene ascending poured acidic iron-rich solution associated with the activation of the Upper Cretaceous alkaline syenitic ring complex (Hassan et al., 2004, 2006, 2018). Hassan (1990, 2002, 2016, 2018) has grouped the different ore types of the Red Sea Coast, Gulf of Suez and Sinai as metallogenic province of hypogene hydrothermal origin. Hassan (2002, 2018) correlated the formation of these deposits with the Miocene-Recent rift-related Aden volcanic rocks, disregarding the geology and time of formation of each ore type as well as the sedimentation and geodynamic mechanisms of the Red Sea and Gulf of Aden rift system and ignoring that no record of any deep marine sediments or signs of hot brine pools have been yet proven within the Egyptian Syn-Rift Neogene sequences. Some authors still support the epigenetic hydrothermal replacement origin for the iron ores of El Bahariya Depression (e.g. Afify, 2017; Afify et al., 2015a, 2015b; Baioumya et al., 2014). Also, this conclusion is lacking concrete evidences for the source and composition of the proposed hydrothermal solution and its relationship with the geological setting and evolutional history of the iron ore and the host limestones.

Since 1996, the present author together with his eminent colleagues, co-authors, and students continued focusing their deep geological, mineralogical, and geochemical investigations on the Phanerozoic stratabound deposits of all over Egypt, accentuating and explaining their intimate relation with certain sedimentary horizons and/or fossilized paleo-erosion surfaces (Fig. 1; Table 1). Furthermore, special attention has been paid to the formational environment and sub-environment of these

deposits and the role of diagenesis and/or supergenesis in their formation. More recently, El Aref (2020a, 2020b) has provided a compiled synopsis on the Egyptian Fe and Mn deposits. However, the present chapter includes more information than those revised in El Aref (1996) and much genetic details and illustrations than what has been inspected in El Aref (2020a, 2020b). Table 2 shows the chronological arrangement of the Phanerozoic ore deposits.

2 Paleozoic Framework and Related Ore Deposits

During the Early Paleozoic, Egypt as a part of Gondwana was drifting toward the south reaching a paleo-latitude 70º S during the Ordovician and subsequently moved northwards rotating 180º (Smith, 1981). The Phanerozoic history of the northern margin of North Africa including Egypt started after the culmination of the Pre-Cambrian tectonic deformations. The surface of the northern Africa generally slope toward the paleo-Tethys and became very irregular, being dominated by paleo-highs and paleo-lows. Throughout the Paleozoic Era, the northern margin of North Africa, including Egypt, exposed to significant tectonic activities of regional or local magnitudes accompanied by alternating episodes of sea transgression and regression (Guiraud et al., 2001; Issawi et al., 2009). The early sea transgression over Egypt is expressed by the deposition of the Infra-Cambrian (earliest Cambrian) terrigenous sediments in Sinai (Taba Formation). During the Late Early Cambrian, mixed platform (varied facies) of the Araba Formation deposited on irregular Pre-Cambrian topography and well exposed in central Sinai and north Wadi Qena (Fig. 2a). Marine regression took place during Mid-Late Cambrian, most probably related to the latest Cambrian-Ordovician tectonic event. Fluvio-glacial clastics of the Ordovician Naqus Formation deposited on the Early Cambrian Araba Formation (Fig. 2b). The Silurian and Devonian seas have advanced only up to the northwestern corner of Egypt, against high positive lands in most of Egypt (Fig. 2b). During Early Carboniferous, marine transgression invaded east central Sinai, depositing the Visean carbonate rock successions (Um Bogma Formation) in the Um Bogma Region (Fig. 2c, d), directly over the Cambrian-Ordovician sediments, while the southeastern sector remained positive land under erosion. Tensional tectonic activity prevailed during the Late Permian (Guiraud et al., 2001) followed the opening of the neo-Tethys. As a consequence of plate collision and construction of the supercontinent Pangaea (Late Paleozoic-Early Mesozoic tectonic event Klitzsch, 1986), Upper Egypt was uplifted along rejuvenated ENE trending faults (Schandelmeir et al., 1987) and volcanic activities predominate (Meneisy, 1990).

The end results of the Cambrian-Carboniferous paleotopographic evolution patterns together with the configurations of the paleo-shorelines during the Cambrian and Carboniferous times are well expressed in the Um Bogma region (Fig. 2c). The lithostratigraphic rock sequences and their environments of this region are shown in Table 3. As it is evident, the Early Cambrian (Araba), and the Ordovician (Naqus) sequences rest on irregular relief of the Pre-Cambrian rocks and are followed unconformably by Mn bearing carbonate unite of the well-known Um Bogma Formation (Visean) which is punctuated by intra-Um Bogma paleo-karst surface, separating this unite into two easily identifiable sequences, a lower Mn bearing sequence and an upper carbonate sequence. The Cambrian-Carboniferous stratigraphic sequences of this region include varieties of stratabound deposits (Table 1; Figs. 3, 4, 5, 6, 7 and 8), among which are: (a) Thorium-Uranium bearing heavy mineral concentrates, building up the basal polymictic conglomerates of the Cambrian sequence, (b) Cambrian stratiform malachite, and (c) Early Carboniferous stratabound/stratiform manganese deposits with copper and uranium enrichment.

2.1 Cambrian Stratabound Th–U and Cu Occurrences

In Um Bogma region, the Cambrian strata comprise the shore face clastic sediments of the Araba sequence (Araba "Formation") with its trilobites and bilobites tracks as well as detectable Th, U, and Cu occurrences.

2.1.1 Cambrian Th–U Occurrence

Cambrian radioactive conglomerates (up to 410–600 ppm Th and 170–238 ppm U) build up the basal polymictic conglomerate unit of the proximal fluvial clastics of the Cambrian sequence (Aita, 1996; Hussein et al., 1998). The radioactivity of these conglomerates is related to the concentration of detrital radioactive mineral grains including uranothorite, thorite, and xenotime and metamict zircon, probably derived from the nearby paleo-highs of the Precambrian igneous and metamorphic rocks, and shortly transported together with other components into the upper reaches of braided streams. Decomposition of the radioactive heavy grains during transportation, deposition, and diagenesis is responsible for the redistribution of Th and U in the Fe oxyhydroxides' matrix and hematite cement of the host rocks. The host conglomerates of this type could be more uraniferous and of economic interest if they are traced far from the weathering and oxidation zones, meaning secondary uranium, could be found on the surface.

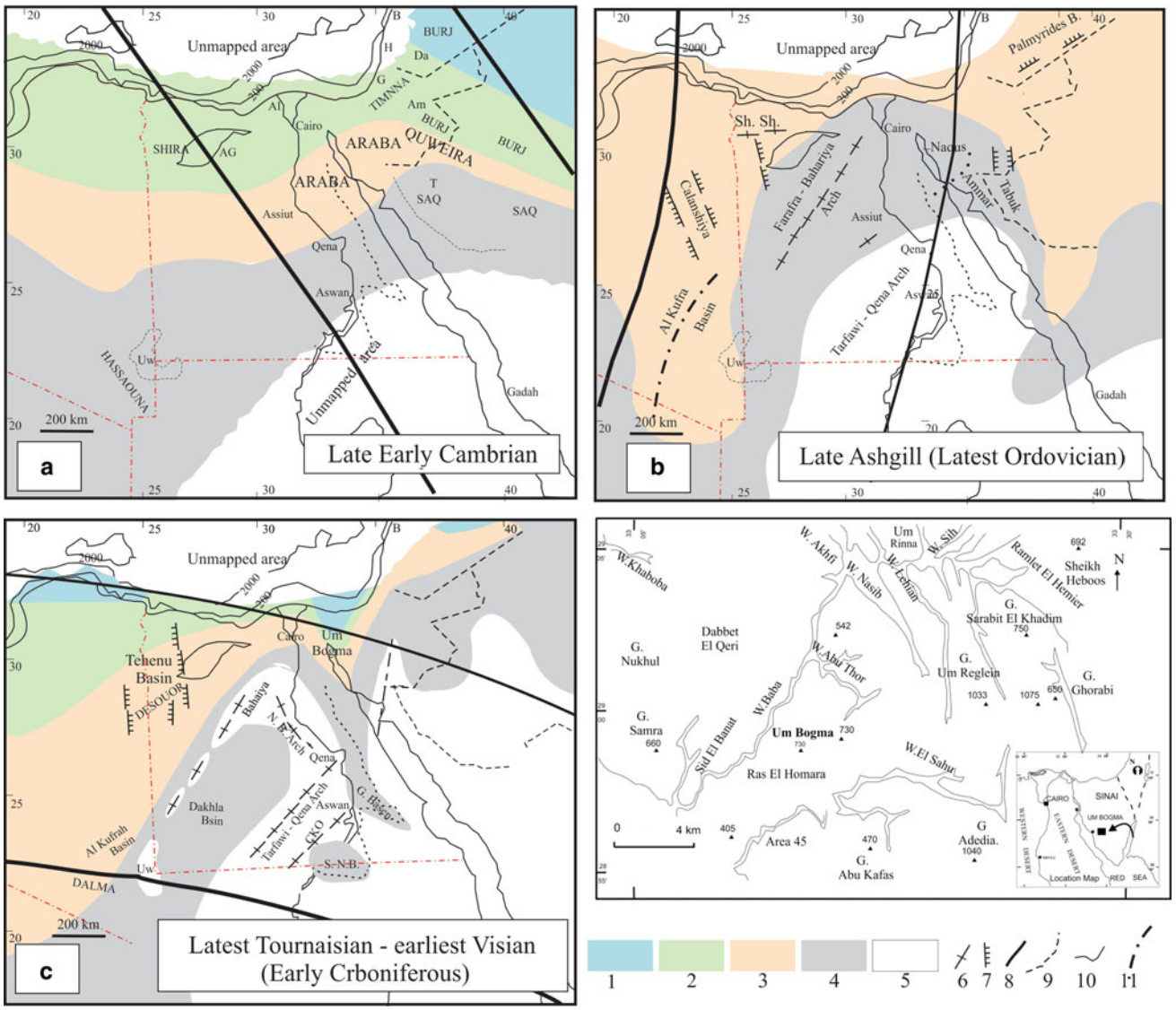

Fig. 2 (**a**–**c**): Late Early Cambrian, Latest Ordovician, and Latest Tournasian-earliest Visean (Early Carboniferous) paleo-geographic/paleo-tectonic map (simplified after Guiraud et al., 2001). 1 = carbonate platform, 2 = mixed platform (varied facies), 3 = terrigenous platform, 4 = fluvial—lacustrine environment, 5 = exposed land, 6 = uplifted arch, 7 = active normal fault, 8 = unspecified active fault, 9 = present-day Precambrian basement—sedimentary cover limit, 10 = present-day shoreline, 11 = depocenter. Figure (**d**): Location map of the Um Bogma Region and the study sites and measured stratigraphic sections

2.1.2 Cambrian Stratiform Malachite

Stratiform malachite is found within the upper part of the shore face clastics of the Cambrian Araba sequence which is correlated with the Cambrian cupriferous sediments of Timna, Israel and Wadi Dana, Jordan. The malachite is mostly confined to the middle green variegated part of the host rocks (Figs. 3 and 4). In the overlying and underlying parts, no malachite or other copper minerals are detected. The Malachite of this type occurs as interstitial material in the host sandstone, siltstone, and shale interbeds and is often associated with kaolinite, illite, chlorite, and calcite (El Sharkawi et al., 1990a).

The megascopic and microscopic geometric patterns of the malachite and the associated minerals are almost conformable with or even form the syn-sedimentary (syn-depositional, syn-deformational, and biogenic) structures of the host rocks, e.g. horizontal, adulatory, and cross-laminations; ripple marks, flasers, biogenic (burrowing), scour and fill structures and desiccation cracks (Fig. 3, sections A*– C** and Fig. 5). The close congruence of the geometric patterns of the malachite with the syn-sedimentary structures suggests that Cu has been leached from nearby copper bearing paleo-highs and transported with other land-derived clays into the basin of deposition as copper

Table 2 Chronological classification of the Phanerozoic stratabound ore deposits

Paleozoic		• Cambrian Th–U occurrence
		• Cambrian stratiform Malachite
		• Intra-Carboniferous stratabound/stratiform • Mn ores with Cu and U enrichment
Mesozoic		• Jurassic-lower Cretaceous ironstones
		• Upper Cretaceous ironstones, laterites, and phosphorite deposits
		• Cenomanian ironstones
		• Turonian laterites
		• Coniacian-Santonian oolitic ironstones
		• Campanian-Maastrichtian stratiform phosphorite deposit
Cenozoic	Paleogene	• Lutetian-Bartonian stratabound oolitic-oncolitic iron ores
		• Fe-rich lateritic blankets (surficial ferricrete duricrust)
		• Pre-rift fossilized alumino-ferruginous latosol
		• Karst economic carbonate stones (karst cave fills, "Egyptian Alabaeter") Paleogene-Quaternary (?)
	Neogene (rift-related ore deposits)	• Oligo-Miocene (?) flinty conglomeritic Mn ore
		• Middle Miocene stratiform to stratabound galena of beach environment
		• Middle Miocene stratiform oolitic-oncolitic Mn ore
		• Middle Miocene stratiform and post-Middle Miocene stratabound celestite
		• Middle to Late Miocene stratiform and stratabound barite
		• Middle to Late Miocene stratiform and stratabound biogenic sulfur deposit
		• Post-Late Miocene stratabound Pb, Zn sulfides, and calamine ore
		• Post-Miocene surficial Mn deposits
		• Post-Miocene-Quaternary (?) surficial conglomeritic Mn deposits

bicarbonate or microbial complex, where it was diagenetically crystallized into malachite during the drying-out of the host sediments (El Sharkawi et al., 1990a). The occurrence of this malachite type in Um Bogma environ may be attributed to the availability and proximity of copper bearing Pre-Cambrian or Cambrian hinterlands.

2.2 Intra-Carboniferous Stratabound/Stratiform Mn Ores with Cu and U Enrichment

- **Geologic and stratigraphic setting**

During the Carboniferous (Visean) time, the northeastern corner of Egypt, particularly the entire Um Bogma region, was transgressed by shallow Carboniferous sea, where carbonate sequences hosting Mn deposits (Um Bogma sequences) were laid down (Fig. 2).

The Carboniferous carbonates are of limited distribution and restricted only to the Um Bogma region. Meanwhile, the southern and eastern hinterlands remained positive land under erosion (Klitzsch & Wycisk, 1987). The Early Carboniferous Um Bogma carbonates rests unconformably above the Pre-Cambrian rocks and/or above different clastic horizons of the Cambrian Araba and Ordovician Naqus sequences (Figs. 6, 7 and 8). Toward east and south, the carbonate successions are highly attenuated and being divided into two distinguished sequences separated by intra-Um Bogma paleo-karst surface (Figs. 6, 7 and 8; Tables 3 and 4. The lower sequence is formed by laterally changed and intertongued stratabound/stratiform Mn facies associations (Fig. 7), sandwiched between two sequence boundaries, i.e. the Cambrian/Ordovician-Carboniferous sequence boundary and the intra-Um Bogma paleo-karst surface (Figs. 6 and 7). The lower Mn bearing sequence is covered by overstepped rhythmic alternations of dolostones and mudstones of the Upper Um Bogma sequence (Figs. 6 and 7). The lithofacies associations of the Mn deposits and the equivalent and overlying carbonates are summarized in Table 3.

The fluvial and near-surface sedimentations of the Late Visean–Early Namurian Abu Thora (Weissbrod, 1969) or Ataqa (Issawi et al., 2009) Formation (sequence) rests on different carbonate horizons of the upper carbonate sequence and/or directly on different horizons of the Mn facies of the lower Mn bearing sequence (Figs. 7 and 8). As clarified by Klizsch (1990), El Aref (1996), and El Aref and Adel

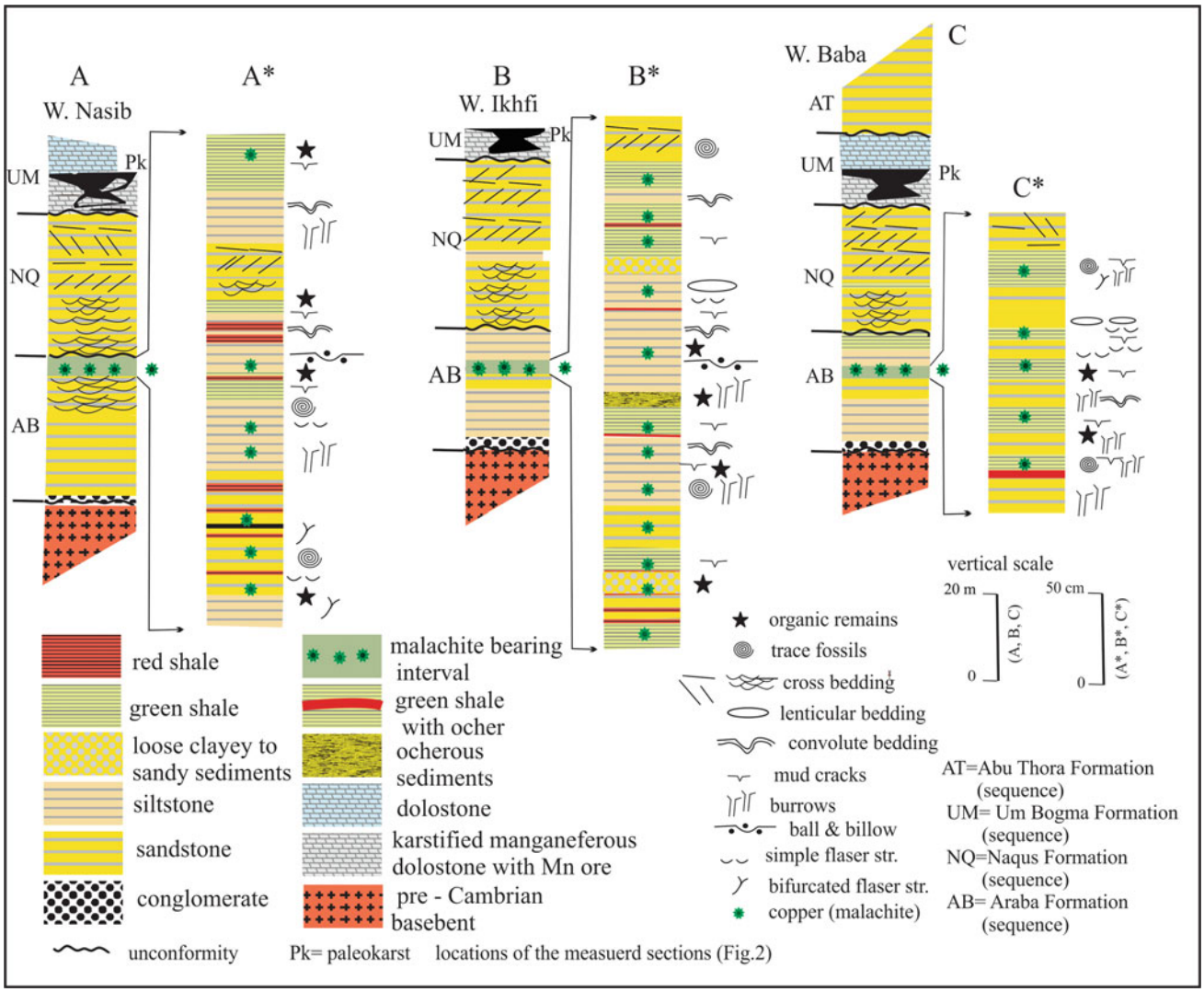

Fig. 3 General lithostratigraphic sections (**A**, **B**, and **C**) and fine (high resolution) stratigraphy (**A***, **B***, and **C***) showing the stratigraphic setting of the stratiform malachite interval of the Cambrian Araba Formation (sequence), Um Bogma region (El Sharkawi et al., 1990a)

Motelib (2001), the Um Bogma sequences are completely missing south of the Um Bogma environ. At northern Wadi Qena in the Eastern Desert, Abu Thora fluvial sequence unconformably deposited on the Cambrian clastics (Abdallah et al., 1992).

- **Mn ore facies (types) association**

The Lower Um Bogma sequence is composed of the following continental and marine Mn ore facies (Table 4; Figs. 6, 7 and 8 zones A–D):

1. Stratiform continental Mn ore type (facies),
2. Stratiform Lagoonal to swampy Mn ore type (facies), superimposed by Stratabound karst Mn ore type, and
3. Stratiform near-shore oncolitic Mn ore type (facies).

These Mn ore facies or types intertongue form east to west and change westward into up 0–45 m thick of continuous section of marine fossiliferous (oolitic) carbonates and shales (the type section of Um Bogma "Formation" at Gabal Khabuba), (Figs. 6, 7 and 8). The intra-Um Bogma paleo-karstification led to the destruction, dissolution, and decomposition of the manganiferous dolostones and mudstones of the lower sequence and re-concentration of the fourth enriched karst ore type.

The composition and main characteristics of the recognized ore facies (types) and the superimposed paleo-karst horizons are compiled and summarized by El Aref (2020b; Table 5).

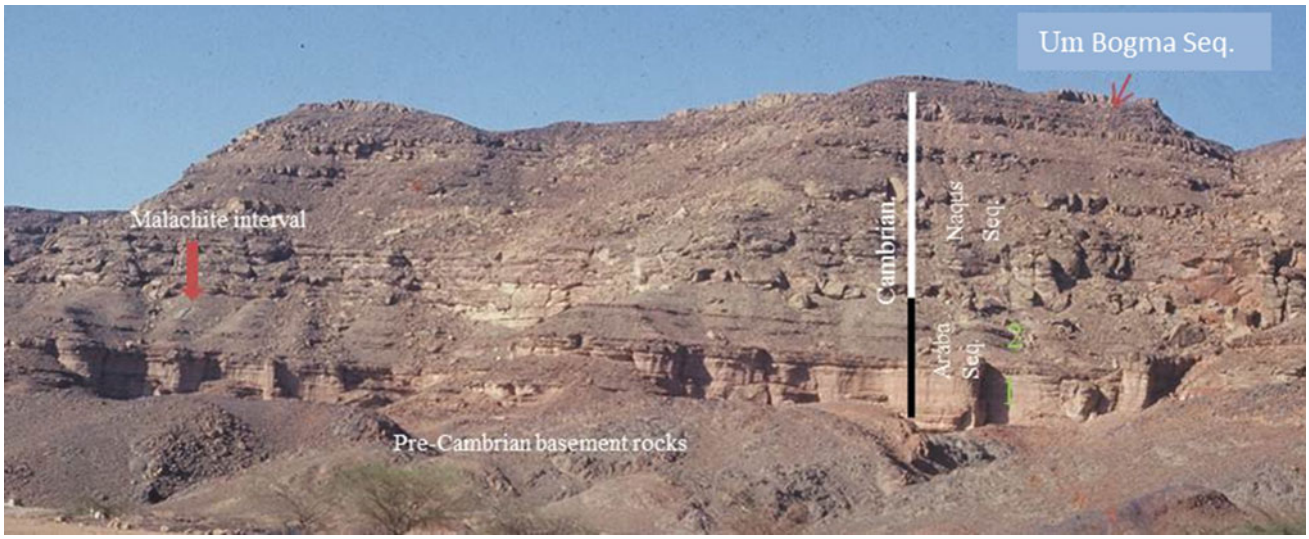

Fig. 4 Field photograph showing the Paleozoic sequences of Wadi Nasib, Um Bogma region, and the stratigraphic position of the stratiform malachite (red arrow) that is confined within the middle green shale of the upper part of the Araba sequence (2). 1 = the lower part of the Araba sequence

A. Stratiform continental Mn facies

This ore type is well-displayed in the extreme eastern zone of the Um Bogma region (Figs. 6, 7 and 8 zone D, Table 4). It consists of successive cyclic bodies (30–80 cm thick) being lenticular in shape and of fining-upward pattern, often interrupted by reactivation surfaces. The lower part is formed by Mn conglomerates followed upward by Mn sandstones and mudstones. The Mn-rich framework components (up to boulder, gravel, and sand sizes) are usually elongated parallel to the current direction and are flanked by cross-laminated sandstones or as lags along troughs of cross-sets. This ore type reflects deposition in braided streams by land-derived lateritic Mn-rich clastic and muddy materials, probably derived from nearby contiguous source (paleo-highs).

B. Stratiform manganiferous mudstones and dolostones (lagoonal to swampy facies)

This ore type is well-developed in the central zone of the Um Bogma region (Figs. 6, 7, and 8 zone C; Table 4). It forms stratified meter-scale sequences, each of which begins with manganiferous and ferruginous mudstones at the base, terminating upward by cyclic rhythmically alternating beds of karstified and rotten manganiferous dolostones and mudstones, earthy or sooty in part, and rich in evaporite nodules. It represents deposition in shallow shelf-restricted lagoonal environment enriched by land-derived Mn and Fe oxyhydroxides in association with marine influx. The depositional and marine diagenetic processes and textures of the Mn dolostones are simply illustrated in Fig 9.

Karst Ore

As a result of the uplifting and exposing of the lower Mn bearing sequence, the genuine lagoonal manganiferous dolostones were highly subjected to intensive post-digenetic processes (Fig. 10). These processes resulted in the formation of enriched karst ore (Figs. 6, 10, and 11; Tables 4, 5 and 6). The paleo-karst profile comprises three transitional horizons, including (a) a lower horizon of karstified manganiferous dolostones, (b) a middle subsoil (enrichment) breccia horizon, and (c) an upper variegated topsoil (lateritic) horizon (Figs. 10 and 11).

Along the paleo-karst surface, the karstified country rocks show varieties of vadose and vadose to phreatic solution features accompanied by telogenetic wall rock alteration processes and pyogenesis (Figs. 9 and 10). Among which are: dissolution, dedolomitization, pulverization, collapsing, and accumulation of lateritic earthy Mn and Fe products, vadose geopetal fillings, formation of coarse-grained Mn and Fe-rich dolomite, Ferron calcite, late orthosparite, and barite cementation (Fig. 9). The overlying gradational subsoil (enrichment, illuvial) horizon (2–8 m thick) is dominated by morphogenetic filled solution features of various shapes and diameters, ranging from small passages of network pattern, trough to V-shaped depressions as well as infilled solution cavities, that developed along cross-cutting cracks or/and bedding planes (Fig. 10). Predominant large scale infilled cavities connected through solution passages and small-scale sinkholes and collapse dolines, form detectable surface of cuspate form. The solution features are often bordered by crackled rocks and commonly filled with re-deposited crustified colloform layers of Mn oxides and hydroxides, mantling the cavities walls and ceils or surrounding collapse

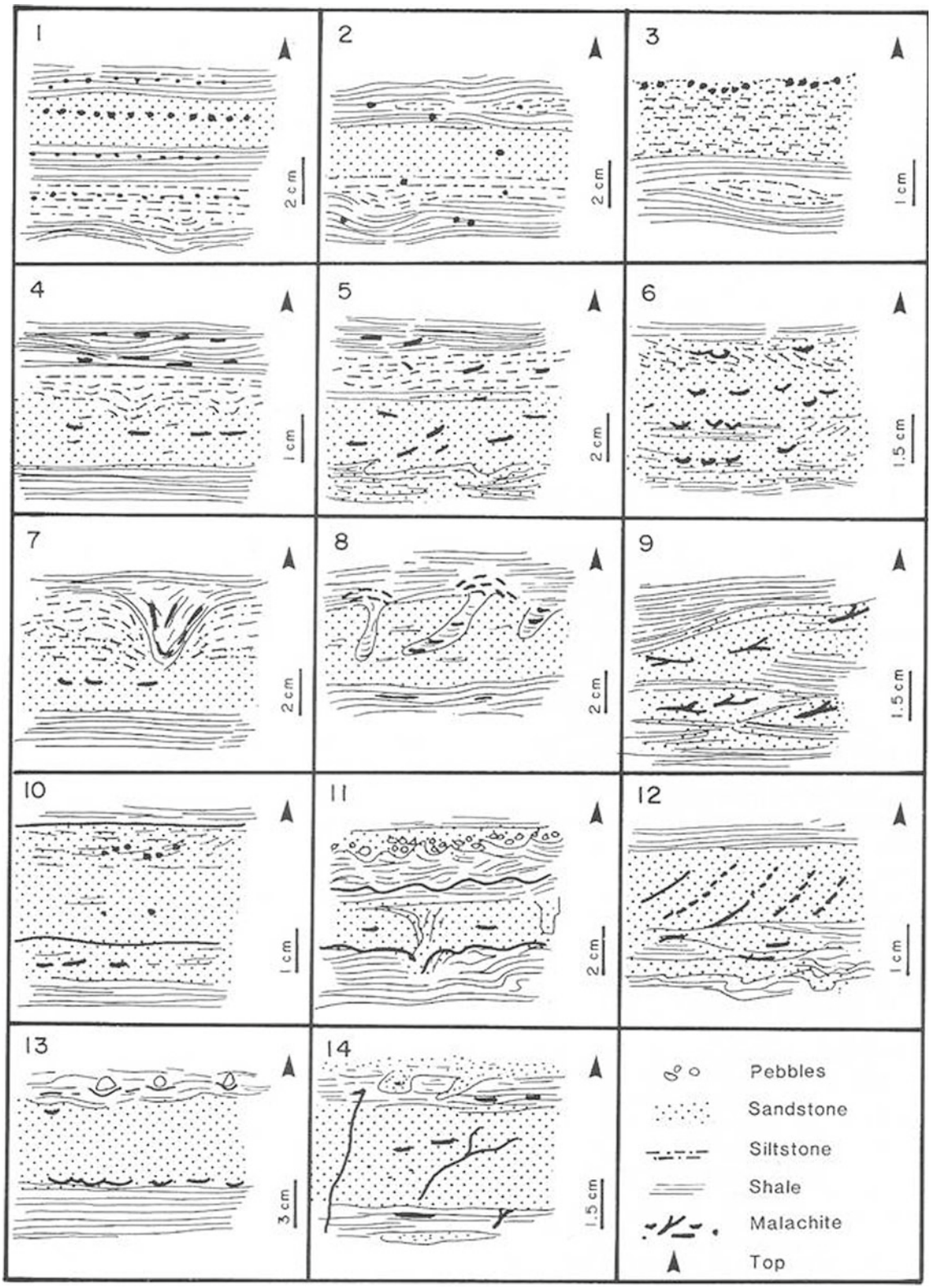

Fig. 5 Geometric distribution patterns of the Cambrian malachite (after El Sharkawi et al., 1990a). 1–3 = stratabound to stratiform malachite disseminations, 1 = dissected lamina, 2 = stratabound randomly distributed spots, 3 = spotty ripple marks. 4–6 = stratabound to stratiform streaks, 4 = stratified discontinuous streaks, 5 = planer non-parallel flasers, 6 = concave-convex oscillation ripples, 7 = filling scour and fill structure, 8 = filling shallow burrow pipes, 9 = bifurcated flasers, 10 = stratified lamination, 11 = undulated lamination, 12 = spotted cross-lamination, 13 = buried mud cracks, 14 = stratabound veinlet's

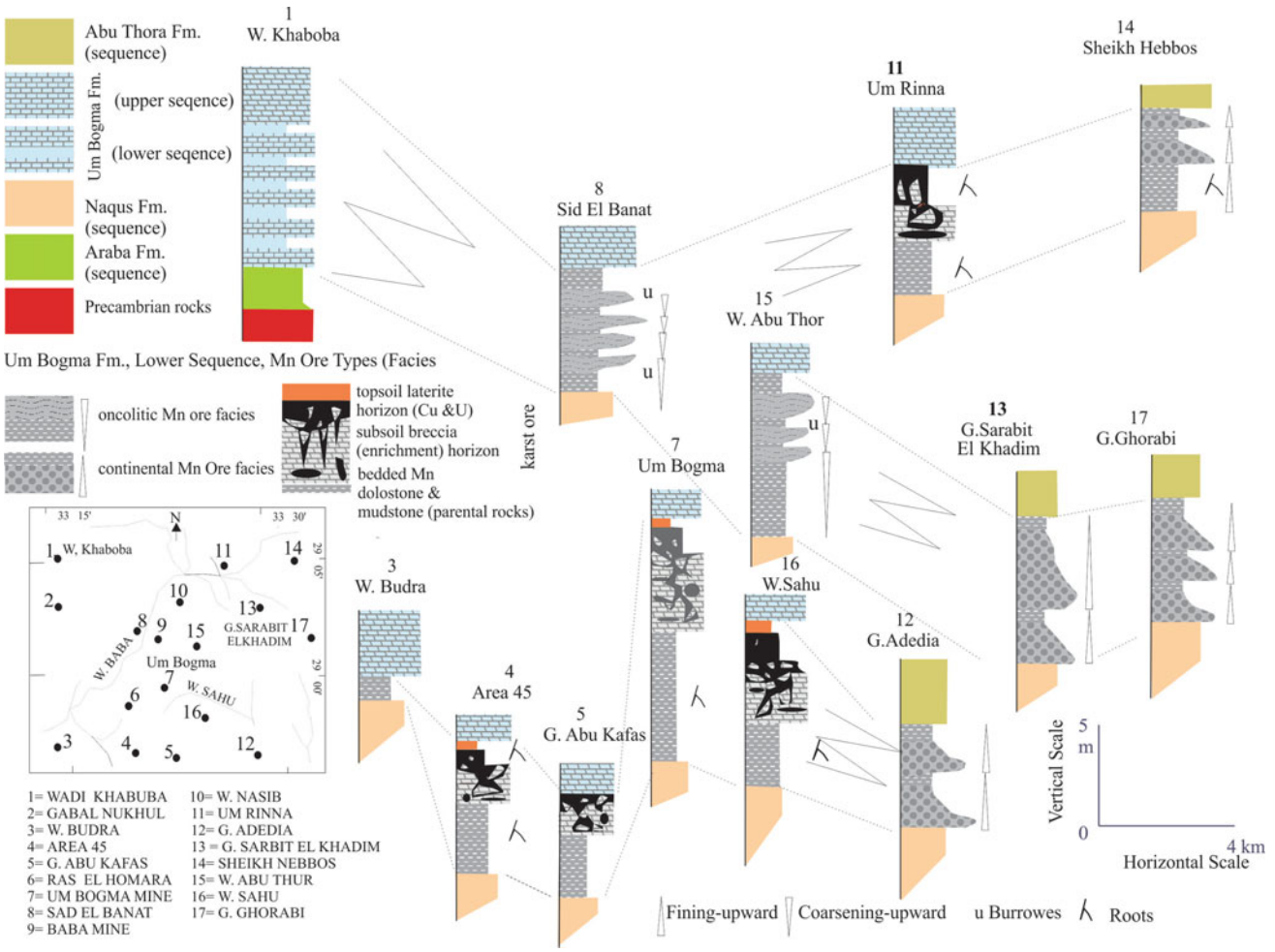

Fig. 6 Fine stratigraphy and lateral facies changes of the Carboniferous Um Bogma sequences (modified after El Aref & Abdel Motelib, 2001)

breccia fragments forming cockade textures, or may form isolated or grouped, nodules and concretions of variable diameters setting in earthy matrix. The topsoil horizon (20–60 cm, Figs. 10 and 11; Tables 5–7) is a leaching (eluvial) horizon being composed of multi-colored lenticular and patchy segregations of nodular kaolinite, gibbsite, and jarosite mixed with red and yellow ochers, black earthy manganiferous materials, alunite nodules, bituminous plant remains (woody particles and organic detritus) and land-derived palynomorphs. Barite and gypsum veinlets, nodules and rosette forms, circular pores, tubules, root molds and alveolar textures and desiccations are very common within these lateritic products. Mn, Cu, and U bearing carbonate, chloride, sulfate, silicate, phosphate, and vanadate minerals are frequently distributed within the topsoil horizon (Table 6) filling shrinkage cracks or may migrate downward through solution passages into the Mn-rich subsoil horizon. The Egyptian Nuclear Materials Authority (NMA) undertakes the study and evaluation of the radioactive elements concentrated in the intra-Um Bogma paleo-karst soil sediments. According to Abdel Motelib (1987), the subsequent erosion of the exposed Mn bearing carbonates in some sites led to gradual destruction and decomposition of the paleo-karst horizons and the Mn deposits and the associated Cu and U mineral associations.

C. Stratiform oncolitic Mn ore (Figs. 6 and 8 zone B; Table 4)

This ore type represents the northwest lateral facies change of the lagoonal Mn facies association. It is fairly bedded and consists of small-scale (30–80 cm) coarsening-upward sequences. Each sequence starts at the base by bioturbated manganiferous to ferruginous mudstones rich in organic matter, grading upward into manganiferous oncolitic

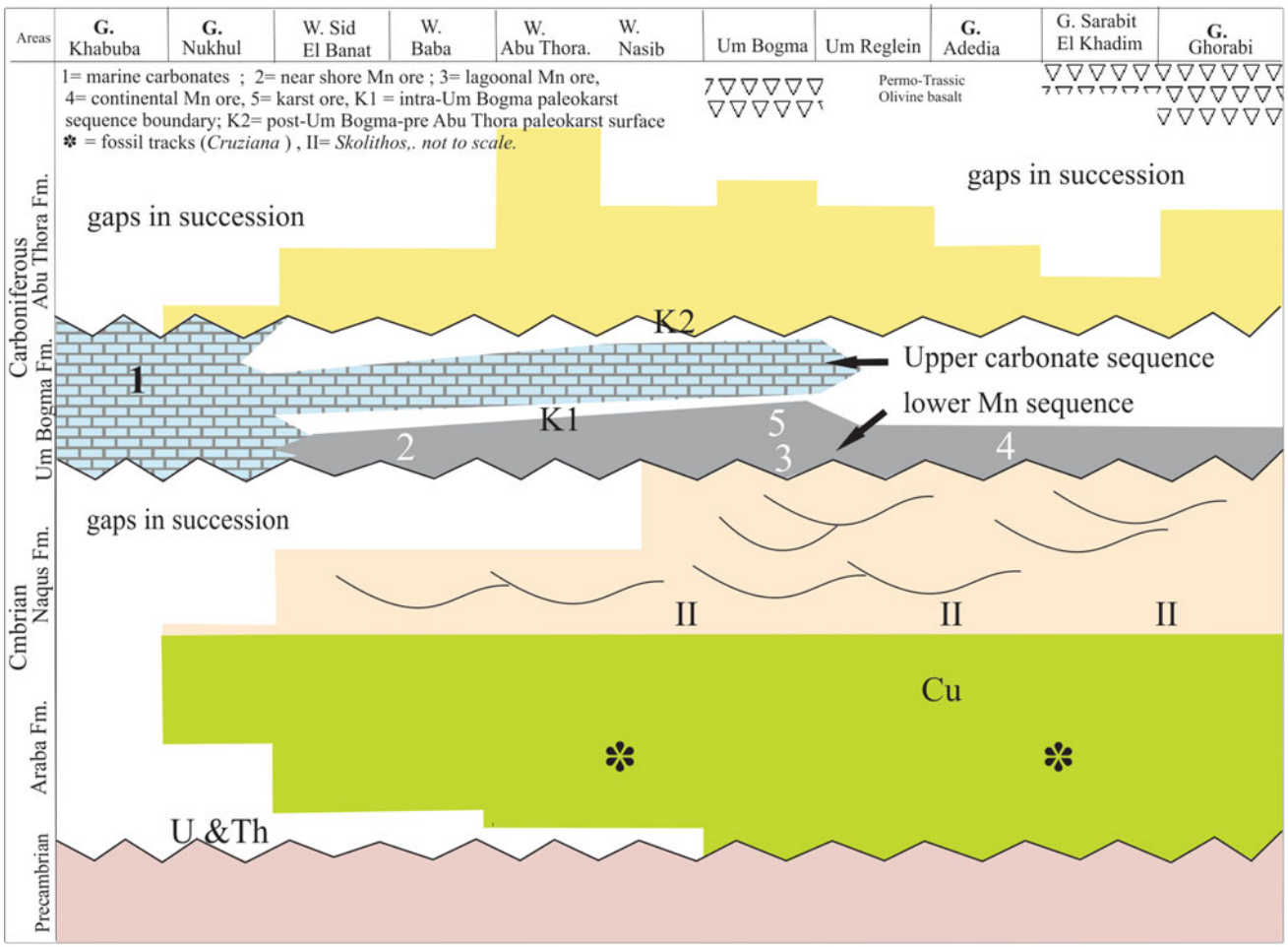

Fig. 7 Different gaps intervene of the Paleozoic sequences of Um Bogma Region and the stratigraphic setting of the associated stratabound ore types (El Aref & Adel Motelib, 2001). 1 = carbonate facies; 2 = oncolytic Mn facies; 3 = lagoonal Mn facies; 4 = continental Mn facies; 5 = karst ore

storm-generated beds or coarse lags consisting of manganiferous oncolites, goethitic in part, coarse skeletal fragments, and fossil molds. The framework components set in a Mn-rich clayey matrix. The sedimentological characters of this ore type reflect formation under marginal marine conditions with the deposition of land-derived manganefirous materials from suspension in a calm environment followed by storm-generated deposition responsible for the accumulation of the oncolite and skeletal components.

- **Genetic considerations**

1. The intra-Carboniferous Um Bogma Mn ore is confined within the lower Um Bogma sequence and consists of laterally changed stratiform continental and shallow marine Mn facies. The paleo-geography, stratigraphic setting, composition, and paleo-environments of the different recognized Mn ore facies indicate the following:
   (a) The Um Bogma Mn ore is of sedimentary origin developed along the Visean paleo-shoreline.
   (b) Land-derived lateritic Mn-rich lateritic clasts and/or suspensions were transported from the adjacent lateretized hinterlands and deposited as fluvial Mn facies in the eastern zone.
   (c) The land-derived lateritic products moved into the Visean shoreline, depositing lagoon to shallow marine Mn ore type in the central zone, contemporaneous with the deposition of the equivalent oolitic marine carbonates further west.
   (d) The different Mn facies exhibits varieties of syn-depositional textures and subjected to a series of diagenetic processes. The central Mn carbonates undergone subaerial dissolution and enrichment as a result of paleo-karstification processes of humid paleo-climatic condition.
2. The detailed field, megascopic, and microscopic investigations, chemical analyses and radioactive

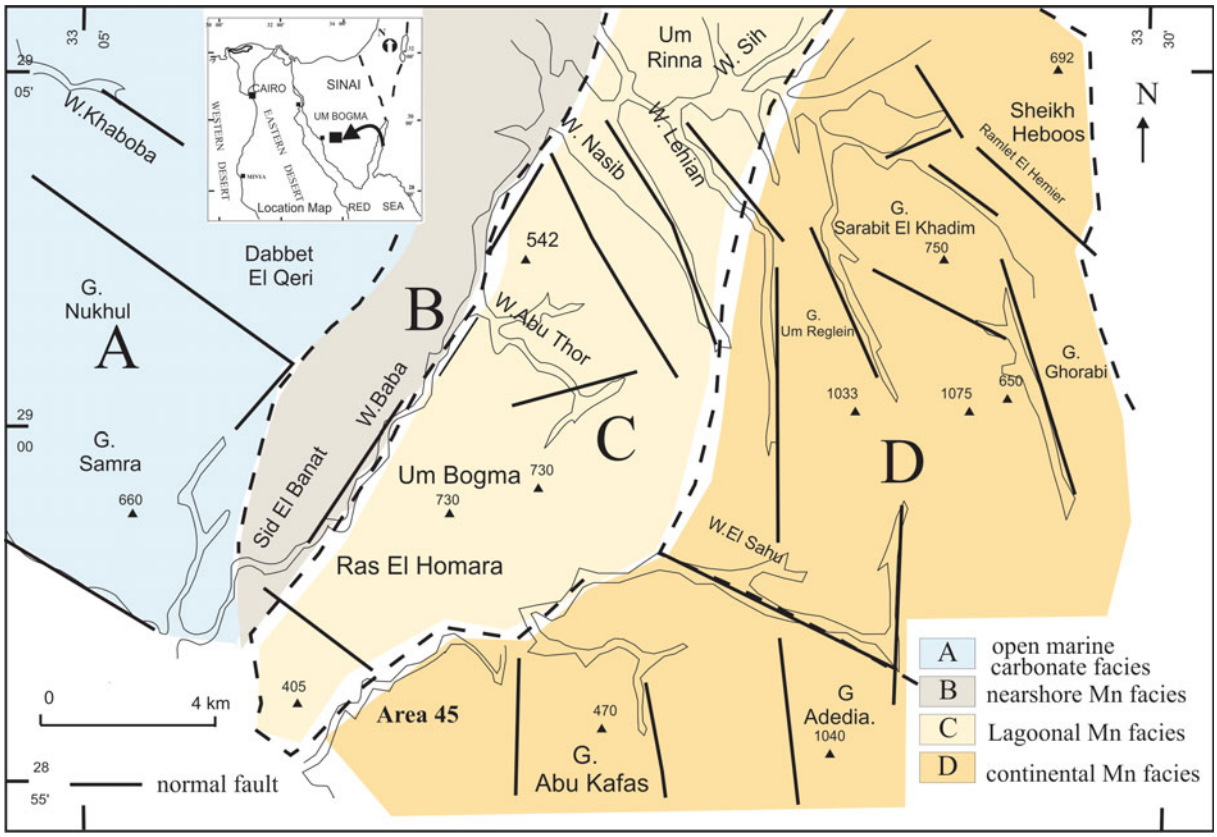

Fig. 8 Simplified structural map of Um Bogma region showing the geographic distribution of the recognized Mn facies and the equivalent carbonates of the lower Um Bogma sequence (El Aref & Abdel Motelib, 2001)

measurements of the karst Mn products, carried out by: Hilmy and Mohsen (1965), Hilmy et al. (1958), El Sharkawi et al. (1990a, 1990b), El Aref (1996), Abdel Motelib (1987, 1996), Aita (1996), El Aref et al., 1998; Hussein et al. (1998), El Aref and Abdel Motelib (2001), and El Aref (2000) enable the recognition of the detailed genetic processes prevailed during the intra-Carboniferous paleo-karstification and the formation of the different mineral assemblages throughout the karst profile, as has been briefly reviewed below: Three main progressive processes have been taken place during the periods of active weathering under humid condition, including

a. Carbonate dissolution with desilication, hydrolysis, enrichment of Fe and Al and formation of kaolinitic latosol along the surface of the weathered carbonates, forming the upper soil horizon, accompanied by Mn separation and concentration in the subsoil horizon.
b. Secondary bauxitization through continuous desilication and hydrolysis together with Mn–Si–Al–Fe dissociation and gibbsite formation, and
c. Subsequent alunitization and formation of alunite and evaporitic Cu and U minerals during the general desiccation of the lateritic products under arid to semiarid paleo-climate.
3. During the humid periods, the dissolution of the exposed manganiferous dolostones is favored during the increase in the pH and CO_2 content of the soil water, resulting from the plant and organic matter decomposition. During the carbonate dissolution, the mobile cations and anions (e.g. Ca^{2+}, Mg^{2+}, Na^{+}, K^{+}, Sr^{2+}, Ni^{2+}, CO^{2+}, Pb^{2+}, Zn^{2+}, Cu^{2+}, Ba^{+}, V^{3+}, U^{4+}, Th^{4+}. $CO_3{}^{2-}$, $SO_4{}^{2-}$, OH^{-}, $CO_3\,H^{-}$, Cl^{-}, $PO_4{}^{3-}$. NO^{3-}, and $H^{2+}VO^{-}{}_4$) moved in the soil water. The less mobile elements Fe^{3+}, Mn^{2+}, Si^{2+}, and Al^{3} left as residual products, i.e. formation of kaolinite and Fe oxides and hydroxides under fairly acidic condition.
4. The concentration of the Mn oxides and hydroxides in the subsoil solution openings as infilling crustified (colloform) layers indicate the differential leaching of the less mobile elements (i.e. Si, Al, Fe, Mn) from the uppermost acidic topsoil (leaching horizon) during the soilification processes with changing pH and Eh values. The leached Mn migrated downward toward the subsoil horizon (enrichment horizon) and deposited under more suitable pH-Eh conditions, leaving behind the more resistant Si, Al, and Fe bearing minerals.

Table 3 Lithostratigraphic sequences and their depositional environments of Um Bogma Region (modified after Abdel Motelib, 1996)

Age			Thick	Sequences ("formations")		Lithology			Environment		
Permo-Triassic			20 m	Volcanics		Olivine basalt					
Carboniferous Permo-Triassic unconformity											
Paleozoic	Carboniferousa		200 m	Abu Thora		Conglomerate, sandstone, mudstone, coal			Shallow marine to fluvial paralic sedimentation		
			Intra-Carboniferous paleo-karst surface (sequence boundary)								
			0–45 m	Um Bogma sequences	Upper dolostone sequence (0–25 m)	Dolostone and shale intercalations			Marine transgression, tidal flat to open marine		
					Intra-Um Bogma paleo-karst surface (sequence boundary)						
					Lower dolostone sequence (0–20 m)	Western part	Central part	Eastern part	Western part	Central part	Eastern part
						Dolostone and shale intercalation	Karst Mn ore karstified Mn dolostone and mudstone	Mn conglomerates, sandstones and mudstone	Shallow marine env.	Swampy to lagoonal env. + karst processes	Continental fluvial env.
	Unconformity										
	Late Ordovician-Early Silurian			Naqus sequence		Gravely cross-bedded sandstones and conglomerates					Continental env.
	Unconformity										
	Early Cambrian		130 m	Araba sequence		Upper part		Variegated coarsening-upward successions of sandstones and mudstones with *Cruziana* Sp.		Deltaic to shallow marine env.	
						Lower part		Fining-upward successions of conglomerate, gravely sandstone and sandstone and mudstone		Channel–near-shore env.	
Precambrian-Cambrian unconformity											
Precambrian granites, granodiorites, schists, gneisses and migmatites											

Table 4 Mn ore Facies and the equivalent carbonate Facies of the early Carboniferous Um Bogma sequences (Abdel Motelib, 1996; El Aref & Abdel Motelib, 2001; El Sharkawi et al., 1990b)

		Western facies	Central facies		Eastern facies
Carboniferous Um Bogma sequences	Locations in Fig. 2	W. Khaboba, G. Nukhul	Sid El Banat, W. Kharig	Um Bogma, W. Nasib	G. Sarabit El Khadim
	Upper Um Bogma sequence (rock unit facies)	Oolitic Grst			Sandy dolomitic Grst
		Fosiliferous shale			
		Argillaceous Echainoidal Wkst–Pkst			
		Brachipod Pkst			
	m Intraformatiomal paleo-karst + paleosol unconformity				
	Lower Um Bogma sequence (Mn ore and carbonate facies)	Fossiliferous shale–Grst–sandy oolitic Grst	Oncolitic Mn facies	Karst ore bedded Mn dolostone and mudstone	Mn conglomerate, sandstone and mudstone
Grst = grainstone; Pkst= packstone; Wkst= wackestone					
Grst = grainstone, Pkst = packstone, Wkst = wackestone, Mdst = mudstone					

5. Cu and U minerals were deposited from pore soil solution containing Cu^{2+}, Cl^{-}, SO_4^{2-}, CO_3^{2-}, PO_4^{3-}, SiO_3^{2-}, V^{3+}, and Al^{3+} ions and entrapped within the topsoil products. The geochemical behavior of U during the soilification and its concentration in the topsoil products is mostly controlled by the Eh and the amount of CO_2 in the system and the concentration of vanadium and phosphorous and other soluble cations and anions. The humic constituents of the soil products are very effective trapping material and the Fe, Al, and Mn hydroxides. Clays can also adsorb uranium. The formation of copper minerals was prevailed during low moister regimes or periods of evaporation and under neutral to alkaline conditions. Veinlet's of copper minerals cutting through certain karst ore or karst alteration products indicate the mobilization of the above-mentioned ions during the subsequent acidic leaching and their re-deposition during the drying out of the soil moister.
6. The late cements and dripstones of carbonate and sulfate minerals reflect crystallization during the arid periods, as a result of ultimate evapotranspiration of the soil moister and decrease in the biological activity and CO_2 content.
7. More details on the mechanism and geochemical behaviors of the constituent elements and minerals during their formation appear in the mentioned relevant publications.

3 Mesozoic Framework and Related Ore Deposits

The Late Paleozoic "Hercynian" tectonic event was followed by Triassic sea transgression depositing marine rock association in the structurally low area of Arif El Naqa, northeast Sinai. Southwards, along the Gulf of Suez, Permo-Triassic paracontinital sediments (Quseib Formation) were accumulated. In general, during Jurassic-Early Tertiary, coastal plains and shallow shelfs of low relief prevailed in the northern and central parts of Egypt, separating erosive paleo-highs and continental sediments toward the south from the marine Tethian Sea to the north, as shown in Table 1 and Fig. 12 and as has been discussed and explained in detail by Bosworth et al. (1996, 1999), Derocourt et al. (1993), Guiraud and Bosworth (1999), Guiraud et al. (2001, 2005), and Issawi et al. (1999, 2009). The marginal shorelines of North Africa continued transgression southward until reaching north Sudan at the Early Eocene time (Derocourt et al., 1993) depositing the Thebes Formation (Fig. 16).

Stratiform oolitic and non-oolitic ironstones are mostly congruent with the marginal paralic facies of the Jurassic to Santonian Tethyan paleo-shorelines (Figs. 12, 13 and 14). During the Campanian–Maastrichtian time duration, stratiform phosphorite deposits accumulated along the relatively stable epicontenental marginal facies of the Tethys. Mesozoic oolitic and non-oolitic ironstones of considerable Fe content are recorded in:

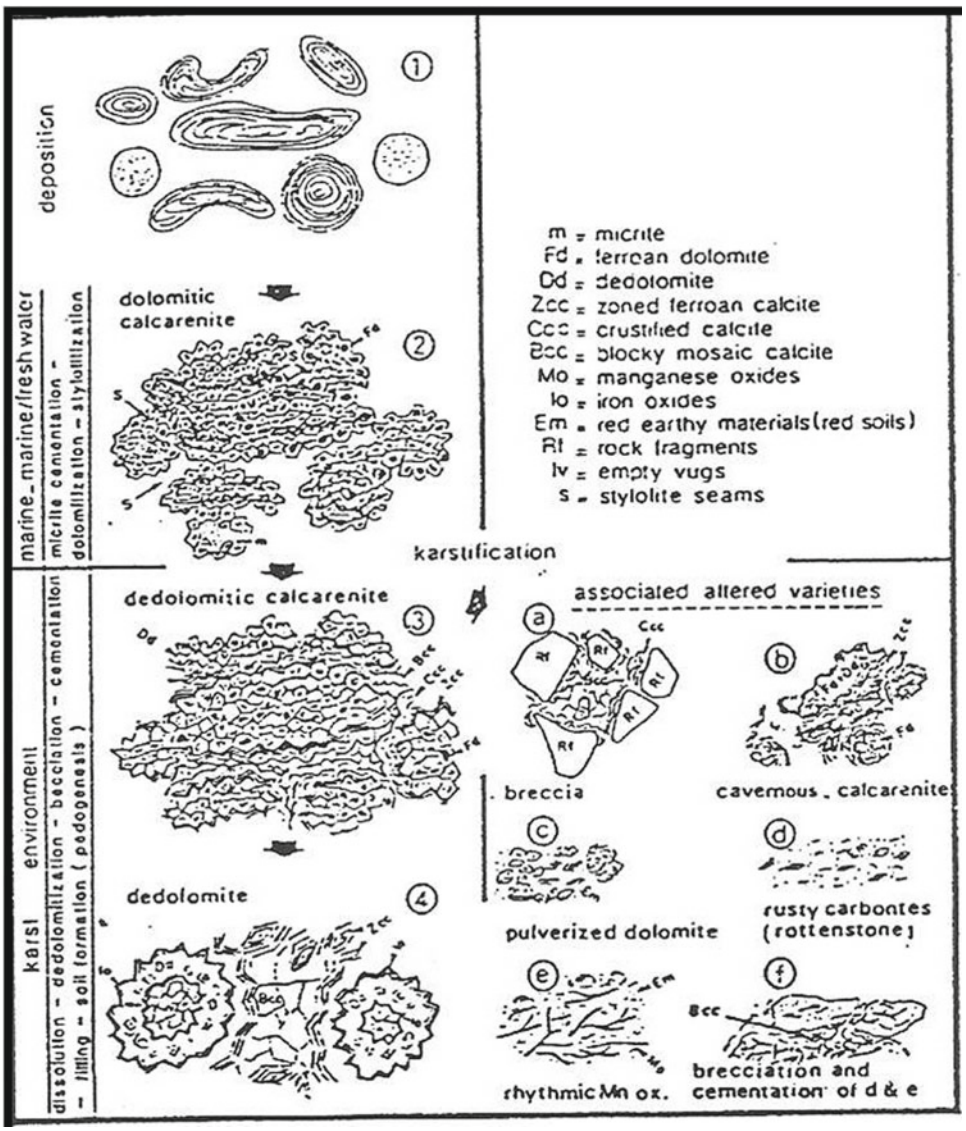

Fig. 9 Digenetic and wall rock alteration processes of the karstified manganiferous carbonates in the lower Um Bogma sequence (Abdel Motelib, 1987)

(a) North Sinai (El Maghara environ)
(b) North Eastern Desert (Wadi Qena)
(c) Gulf of Sues (W. Dara)
(d) Aswan region
(e) Central Western Desert.

The paleo-topographic and stratigraphic settings and paleo-facies of the ironstones of these sites clearly demonstrate their development along the paralic marginal facies of the southward migrating Tethyan paleo-shorelines (Figs. 12, 13 and 14), which support their formation simultaneously with lateritization (in situ or transported laterite) and continental sedimentation on the adjacent hinterlands. Although the well-known Mesozoic oolitic ironstone of Egypt is encountered within the Coniacian-Santonian sequence of east and eastwest Aswan, however the other equivalent and older occurrences were carefully studied in order to clarify the mode of formation of this ore type in accordance with the regional and local geological parameters which controlled their formation and also to shed light on the geology and geographic distributions of the host rocks, as a fundamental data required for further geological exploration and ore evaluation. Figures 13 and 14 show the geology of each site and the detailed stratigraphy of the encountered non-oolitic and oolitic ironstone intervals. The age, mode of occurrence, the average Fe content of these ironstones and their economic potentiality as well as their detailed sedimentological and mineralogical aspects are compiled and summarized in Table 8. The youngest rather most economic Phanerozoic (Tertiary) oolitic-oncolitic ironstone of Egypt is the Middle Eocene iron ore of El Bahariya Depression, Western Desert (Section 4).

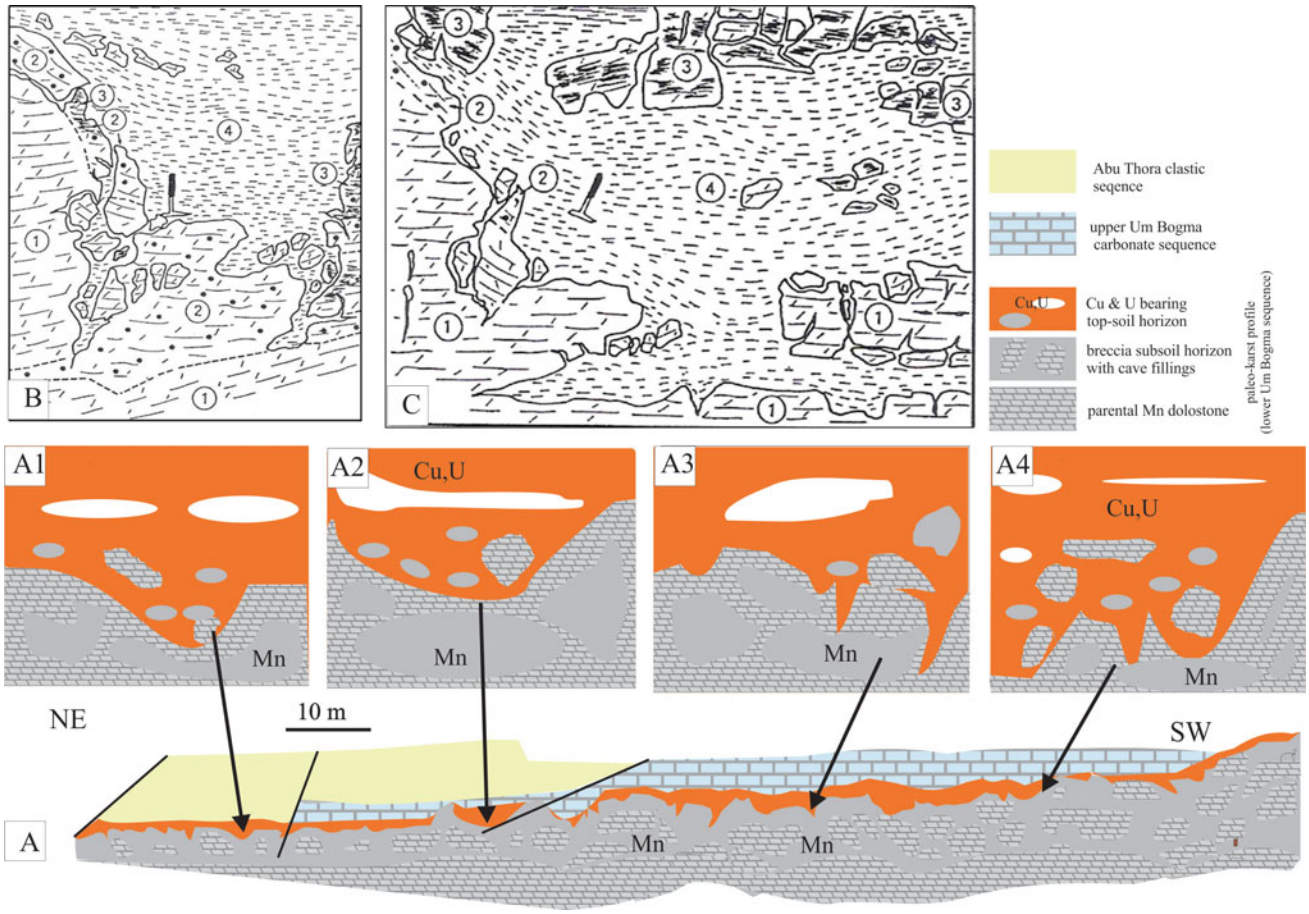

Fig. 10 **A** = representative drawing of the intra-Carboniferous fossilized paleo-karst profile and the related Mn ore and Cu and U concentration. A1–A4 = enlargement of solution features (A1 and A2 = trough-like depressions, A3 and A4 = V-shaped depressions) filled with collapse breccia and soil materials. **B** and **C** = representative drawings of solution hole (**B**) and subsurface solution cavity (**C**) showing the alteration varieties developed along the walls and roofs of the solution features, 1 = intact bed rock, 2 = pulverized dolomite, 3 = rusty carbonate, 4 = residual and infiltrated red soily materials (modified and simplified after Abdel Motelib, 1987)

3.1 Jurassic—Lower Cretaceous Ironstones

The Jurassic sea covered northern Egypt (Fig. 12). The thickest Jurassic succession crop out in northern Sinai at Gabal El Maghara (Fig. 13) and comprises an alternation of transregressive marine and regressive paralic sequences. The paralic facies association includes seams and ironstone bands (Fig. 14). Albian-Aptian carbonates including ironstone bands are also exposed in Gabal Manzur, east of Gabal El Maghara (Fig. 14). During the Jurassic-Early Cretaceous transgressive–regressive cycles on northern Sinai, the hinterlands were under erosion with the deposition of the continental clastics and the associated currently quarried kaolinite-rich laterites and paleosols of the Ragqaba, Temmariya, and Malha formations in Sinai and the continental clastics of Gilf Kebir, Six Hill, and Sabaya formations in the Western Desert. The Jurassic and Early Cretaceous ironstone intervals of north Sinai are of variable thicknesses and Fe content. The ironstone bands comprise two, rather distinct types including (a) non-oolitic ironstone horizons formed by concretionary, massive, clayey ochreous, and rhythmic laminated varieties. They represent either paleosols and/or ferruginous mud flat intervals interrupting the cyclic clastic sequences of the host Jurassic deltaic sediments, and (b) oolitic ironstone bands often terminating an intermitted short-lived small-scale shoaling cycles of intertidal regressive falling sea level.

3.2 Upper Cretaceous Ironstones, Laterites and Phosphorite Deposit

The Tethys initiated in Early Cenomanian by high stand sea level, started to close with the development of widespread Cenomanian–Turonian successions (Darwish, 1994; Issawi et al., 1999). This led to the deposition of marine carbonates, marls, and shales toward the north (Halal and Raha formations) and the equivalent paralic sediments of the Galala

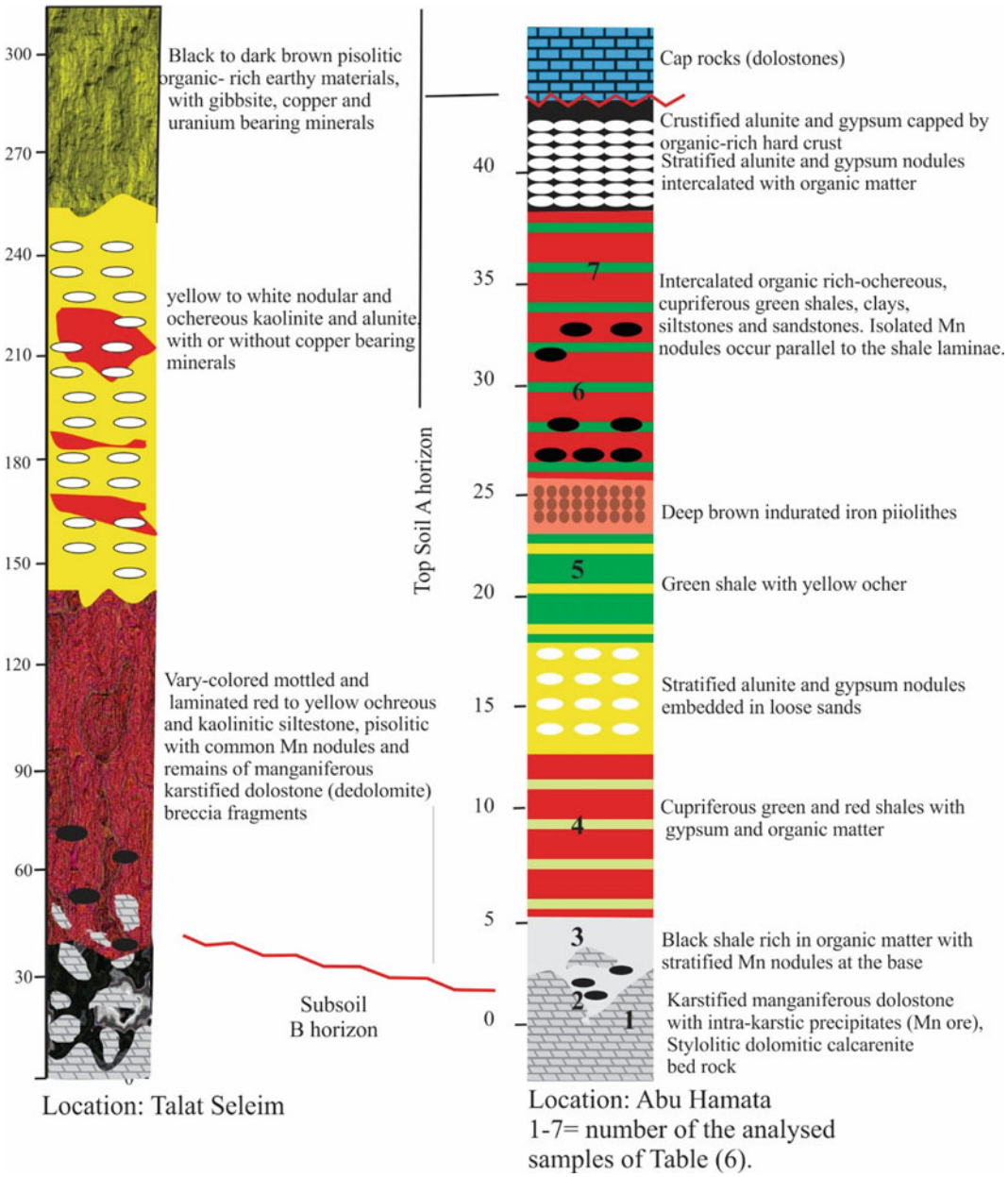

Fig. 11 Fine stratigraphy of the intra-Carboniferous paleo-karst profile and the topsoil sediments of two representative locations, including Talat Salem (after Aita, 1996) and Abu Hamata (after El Sharkawi et al., 1990a)

Formation as well as the Bahariya and El Heiz formations in the central Western Desert (Fig. 12). Further south, the comparable clastics of the Maghrabi Formation (Kharga-Dakhla district) show lesser marine influence. The entrance of Wadi Dara, Gulf of Suez is occupied by late Cenomanian siliciclastics and carbonate rocks, para-conformably overlain by reduced Turonian succession and Miocene evaporites (El Manawi, 2006, personal communication). In this site, the Late Cenomanian rocks of the Galala Formation contain, within its shallow marine middle part, an oolitic ironstone interval of about 18 m thick and 21–46% Fe (Figs. 13 and 14; Table 8). This interval is divided into a series of small-scale prograding parasequence sets of coarsening up pattern, mostly restricted to tidal flat facies. The Cenomanian paralic Bahariya Formation of the Western Desert includes within its lower and upper members ironstone bands and lenses, up to 15–150 cm in thickness, well exposed in El Bhariya Depression or along its surrounding scarps as a result of repeated tectonic pulses of the Late Cretaceous-Early Tertiary "Laramide" tectonic event (Figs. 2 and 14; Table 1). Economic ironstone bands are reported in El Harra mine area. Estuarine Cenomanian clastics of the

Table 5 Manganese ore facies types, environments, sedimentary structures, lithologies, and paragenesis (compiled by El Aref, 2020b and references therein)

Ore types (facies) and environment				Sedimentary structures	Ore lithologies	Ore fabrics	Paragenesis
• Stratiform continental (channel fill) Mn conglomerate, sandstone and mudstone (Fig. 9, Zone D) • Surface slope deposits accumulated through mud flow of braided tributaries with derivation of framework components from nearby contiguous sources				Fining-upward cyclic sequences with erosive bases, lamination and cross-lamination, desiccations, lenticular bedding, scouring and erosive sols	• Mn para-conglomerate • Mn sandstone • Mn mudstone • Red ochers	Mn boulders, gravels, sands and silts: Mn-rich matrix, colloform encrustation and cockade structure, filamentous algae, dendritic leaf-like and cellular patterns	Pyrolusite, romanechite, goethite, hematite, kaolinite, quartz, organic remains
Karstified manganiferous dolostone and mudstone (Drowned karst profile), Fig.9, Zone C	Soil horizons	Topsoil (eluvial) horizon	• Karst lateritization and bouxitization involving eluviation and illuviation processes (pedogenesis) and development of subsoil and topsoil horizons	Alternating multicolored layers of organic-rich alunitic, kaolinitic, gibssitic, cuprefrous and ochreous shales, siltstones and sandstones with abundant Cu, U and V minerals and organic and plant remains (polymorphs), shrinkage cracks, nodular forms, rhizoliths and rhyzoctions			Mn and Fe oxides and hydroxides; Cu, U, V, carbonates, chlorides, silicates, sulfates, phosphates and vanadates; kaolinite, gibbsite, calcite, quartz, jarosite, dolomite, ankarite. Illite, montomorilonite
		Subsoil (illuvial) horizon		Mn conglomerates in earthy matrix, crackle breccia and Mn-rich speleothems, nodules and concretions, collapse breccia, earthy Mn-rich precipitates and encrustation, basal undulated surface of cuspate form dominated by solution sinkholes and small to large-scale solution features (cavities) with collapse breccia and rotten stone fragments, Mn encrustations			
	(Lower horizon) parental (intact) rocks, (up to 9 m thick)		• Lagoonal to swampy manganiferous mudstones and dolostones • Deposition in coastal low energy shallow lagoons, charged with Mn continental sediments • Prevalence of splash meteoric water with continuous uplifting and subsequent karstification	• Stratified stvlolitic manganiferous dolostones • Cyclic alternating beds with ooids and peloids, abundant marine fossils and bioclasts • Thin lamination and desiccation cracks, stratified gypsum and barite nodules, crackle breccia, in-situ brecciation, abundant in-filled solution openings (variable diameters) with collapse breccia and Mn-rich encrustation along cave walls, ceiling and floors, pulverization, mottling, intensive karstification and brecciation toward the overlying horizon	• Laminated and crustified manganiferous mudstone • Mottled ferruginous and manganiferous mudstone • Manganiferous dolostone	• Bedding, lamination and desiccation, stylolitization • In place brecciation and fracturing strata • Mn concretions, pisoliths and glaebules • Reddening • Encrustation, filling cavities and solution opening • Collapsing, cockade structure, boxwork and alveolar structures • Dedolomitization • Leaching and accumulation of Mn-rich earthy materials (soils) • Filamentous algal fabrics	Pyrolusite, manganite. romanechite, fear on dolomite, dedolomite goethite, hematite. Fe sesquioxides, calcite barite, gypsum, kaolinite
• Stratiform pisolitic (oncolitic) ore type (0–5 m thick), (Fig. 9, Zone B) • Near-shore (marginal marine environment, under shoaling storm-generated conditions				• Fairly bedded showing small-scale coarsening-upward arrangement, bioturation, abundant organic matter, pisolitths (oncoids), shrinkage fractures, ripple marks, flaser structure, matrix to grain-supported fabrics, skeletal fragments, fossil molds, isolated Mn-rich spherules and concretions, evaporite nodules	Organic-rich bioturbated manganiferous and/ferruginous mudstones		Pyralusite, geothite, calcite, barite, gypsum, anhydrite, Fe and Mn sesquioxides

Table 6 Identified Cu, U, and rock-forming minerals of the intra-Carboniferous paleo-karst profile (compiled from Abdel Motelib, 1987, 1996; Aita, 1996; El Aref & Abdel Motelib, 2001; El Sharkawi et al., 1990a)

Sulfates	Phosphates	Carbonates	Oxides	Silicates
Jarosite $KFe_3(SiO_4)(OH)_6$, Alunite $KAl_3(SiO_4)_2(OH)_6$, Gypsum $GaSiO_4 \cdot 2H_2O$, Anhydrite $GaSiO_4$ Zippeite, $(UO_2)_2(SO_4)(OH)_24H_2O$ Chalcanthite $CuSO_4 \cdot 5H_2O$ Antlerite $Cu_3(SO_4)(OH)_4$ Barite BaSiO4	Phosphosiderite $FePO_4$, $\cdot 2H_2O$, Bassetite $Fe(UO_2)_2(PO_4)_2 \cdot 8H_2O$, Pseudomalachite $Cu_5(PO_4)_2(OH)_4 \cdot H_2O$ Turquoise $CuAl_6(PO_4)_4(OH)_8 \cdot 5H_2O$	Calcite $CaCO_3$, Dolomite $CaMg(CO3)_2$ Aukerite Ca $(FeMgMn)(CO_3)_2$, Malachite $Cu_2CO_3(OH)_2$ Liebigite $Ca_2U(CO_3)_4 \cdot 10H_2O$	Hematite, Quartz, Hausmanite Mn_3O_4	Chrvsocolla $Cu_2H_2(Si_2O_5)(OH)_4$ Lungite $Cu_4(SO_4)(OH)_6 \cdot H_2O$ Spangolite $Cu_6Al(SO_4)(OH)_{12}$ $Cl \cdot H_2O$ Kaolinite, Illite, Montomorillonite
Hydroxides	Vanadates	Halides	Nitrates	
Gibbsite $A1(OH)_3$, Goethite	Metatyuyamuinite $Ca(UO_2)_2(VO_4)_2 \cdot 35H_2O$	Atachamite $Cu_2Cl(OH)_3$ Paratacamite $Cu_2(OH)_3Cl$ Connellite $Cu_{19}Cl_4(SO)(OH)_{32} \cdot 3H_2O$	Bultgenbachite $Cu_{10}(NO_3)(OH)_{32}Cl_4 \cdot 3H_2O$	

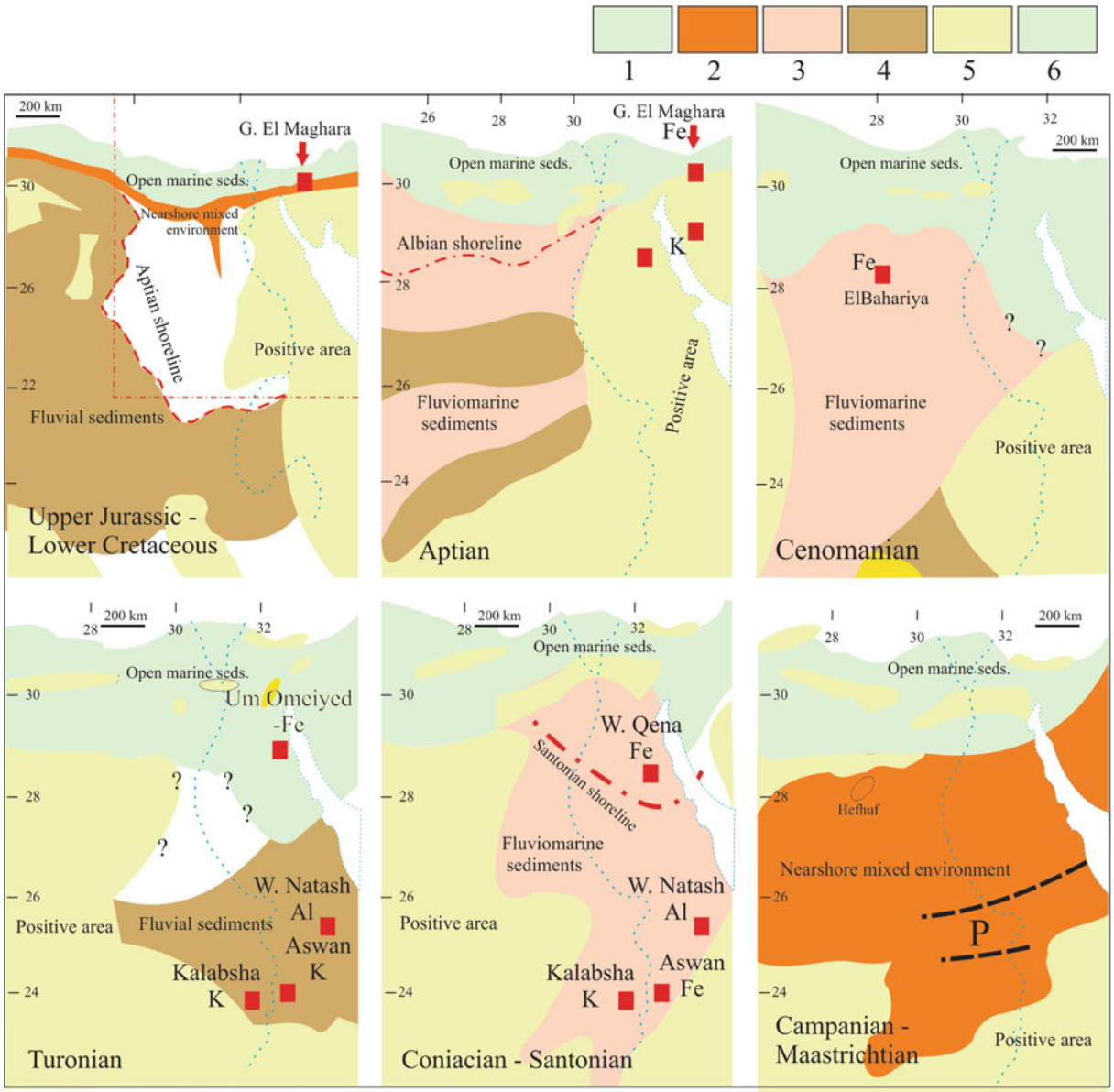

Fig. 12 Paleo-geography of the Mesozoic stages and distribution of the related stratabound and stratiform deposits (compiled and simplified after Klitzsch & Wycisk, 1987; Said, 1990a). 1 = open marine sediments, 2 = near-shore mixed sediments, 3 = fluviomarine sediments, 4 = fluvial sediments, 5 = positive land, Fe = ironstone, K = kaolin laterite, Al = laterite

Bahariya Formation including ironstone bands of up to 1 m thick are recorded to the west of Lake Naser at Gabal Saad (Issawi & Osman, 1993).

3.2.1 Turonian Laterites

A major regressive phase has been established during the Middle Turonian accompanying an important pulse of the "Laramide" movement which was responsible for the elevation for southern Egypt, El Bahariya arc and numerous structures across northern Egypt and Sinai (Fig. 12). Thick marine carbonates related to the Wata Formation were deposited over the structural lows of northern Egypt, while the coeval paralic sediments of the Um Umeiyed Formation were deposited southwards and crop out in central Wadi Qena. Meanwhile, the extreme southern hinterlands were subjected to deep weathering processes inducing lateritization and bauxitization and received simultaneous fluvial deposits. Exposed outcrops of lateritized Pre-Cambrian metamorphic and igneous rocks are widespread east and south of Aswan and in the western part of Kalabsha area near Sinn El Kadabb, southwest Aswan area (Fig. 12). The continental Abu Agag Formation (~ 5–40 m thick) overlies an irregular relief of the extensively lateritized Precambrian rocks. It consists of fining-upward sequences of breaded

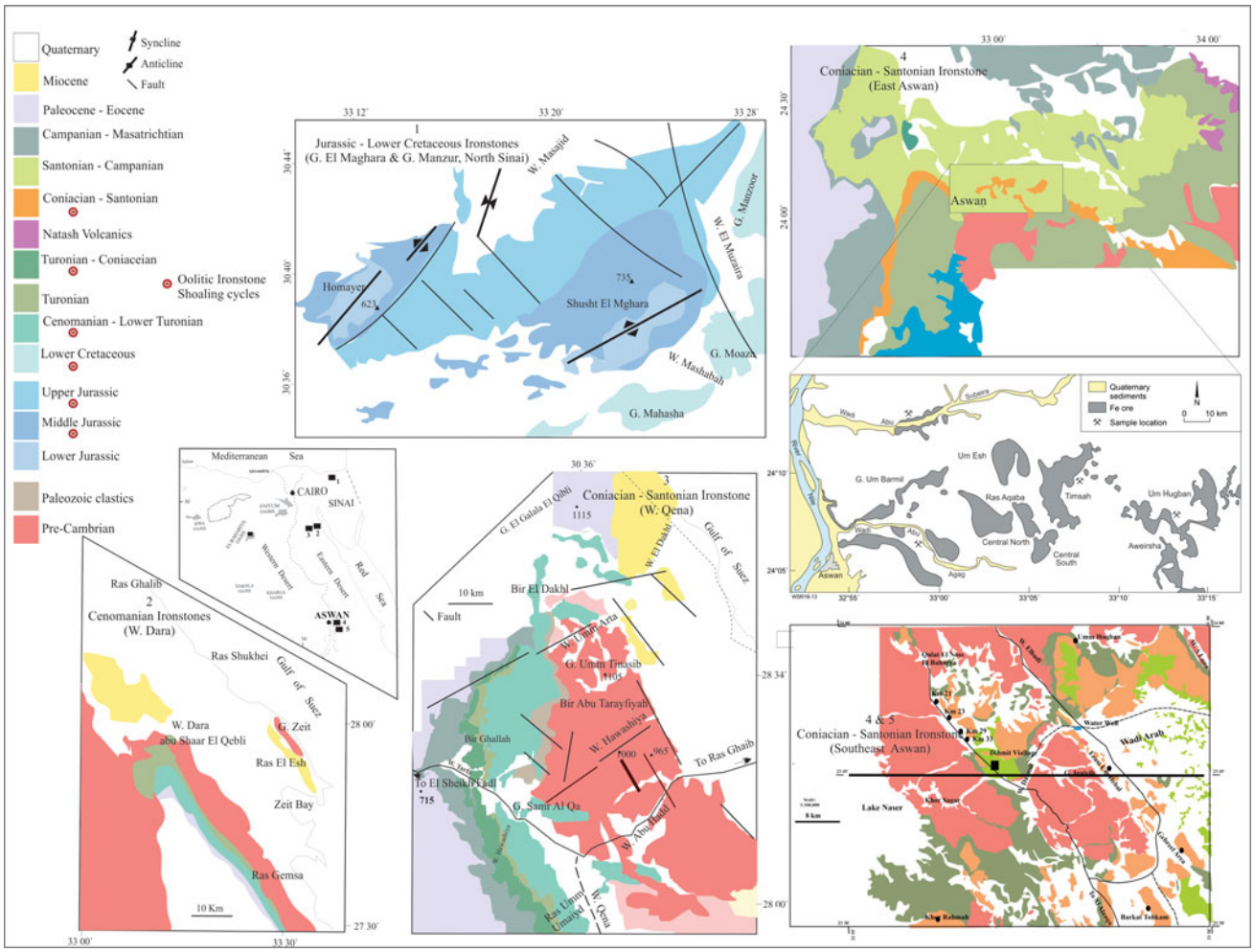

Fig. 13 Simplified geological maps showing the stratigraphic settings and areal distributions of the ironstone hosting sequences (G. El Maghara, W. Dara, W. Qena, and Aswan occurrences), compiled from El Sharkawi et al. (1989); Helba et al. (2003); El Manawi (2006) and IEP (1993–1997)

river environment, including trough cross-bedded conglomerates and sandstones, kaolinite-rich laterite and in situ latosols. Southwest Aswan at Wadi Kalabsha, the probably correlative Kaolin Member of Said and Mansour (1971) is overlain and underlain by the Abu Agag fluvial conglomerates and sandstones. Eastward of Aswan at Wadi Natash (Fig. 13), Abu Agag Formation is intercalated with the Natash volcanic sheets and their lateritic cap. The Turonian Laterite deposits of southern Egypt could be classified into two types according to their relation with the country rocks within which they are found. These types are:

(a) Stratabound autochthonous bauxitic laterites (fossil latosols) of two different stratigraphic positions, including latosol capping Pre-Cambrian granites, schist's and migmatites and truncated by Abu Agag fluvial clastics, and laterites capping Cretaceous volcanic rocks and also truncated by the Abu Agag clastics. The in situ latosol profiles comprise an upper iron-rich pisolitic crust, 20–50 cm thick, with or without silcrete intercalations; a middle bleaching (mottled) horizon of up to 10 m in thickness rich in hydro-mica and nodular kaolinite, and a lower argillaceous lithomarge (saprolite) horizon (5–20 m thick) consisting of kaolinitized rock fragments and mineral grains setting in kaolinite-rich matrix. These constituents grade downward into weathered parent rocks. Gibbsite, boehmite, meghemite, and montmorillonite are also recorded in these laterite profiles (Said et al., 1967), and

(b) Stratiform allochthonous kaolin-rich laterites, locally bauxitic, intercalated within the Abu Agag fluvial sediments in the form of either thick (up to 9 m) succession as in W. Kalabsha or accumulated within the troughs of the cross-bedded fluvial clastics. Ferruginous kolinitic

paleosol intervals often terminate the fining-upward sequences of the host Abu Agag sediments. In situ second bauxitization of some of the laterite intervals resulted into the formation of bauxite bearing latosol of different thicknesses (Germann et al., 1987).

3.2.2 Coniacian-Santonian Oolitic Ironstones

The paleo-geographic patterns of the Coniacian-Santonian shorelines were obviously controlled by two main factors: (a) the continuation of the Late Cretaceous-Early Tertiary "Laramide" tectonic movement and (b) the southward transgression of the shallow Coniacian-Santonian Sea which extended until northern Sudan. Genuine marine sediments laid down in the structural lows of northern Egypt and the Gulf of Suez (Fig. 12). Meanwhile, near-shore paralic sediments including stratiform ironstone bands dominated within the restricted Coniacian-Santonian basin. These sediments crop out at central Wadi Qena (Hawashiya Formation, Figs. 13 and 14; Table 8) and at the vicinity of Aswan (Timsah Formation, Figs. 13 and 14). In north Wadi Qena, microglaebular ooidal ironstones occur within the Coniacian transgressive succession of the Hawashiya Formation, delineating basal transgressive facies and terminating shallower regressive assemblages (Figs. 13 and 14; Table 8). According to Helba el al. (2003), the ironstone development is intimately related to the duration of specific sedimentary dynamics, which reflect interaction between sediment supply and hydrodynamic regime. The majority of the welded ferriferous framework components are related to in situ growth from glauconite in sands and muds that are exposed to lateritic weathering during periods of sea level fall (Helba et al., 2003).

The Coniacian-Santonian Aswan ironstones constitute the third shallowing-upward cycle of the Temsah Formation (Figs. 12, 13 and 14; Table 8). The shallowing cycle, 1–3 m in thickness, starts in the base with muddy ironstone followed upwardly by Fe-rich oolitic ironstone band, representing gradual migration of tidal Fe ooid bar on basal

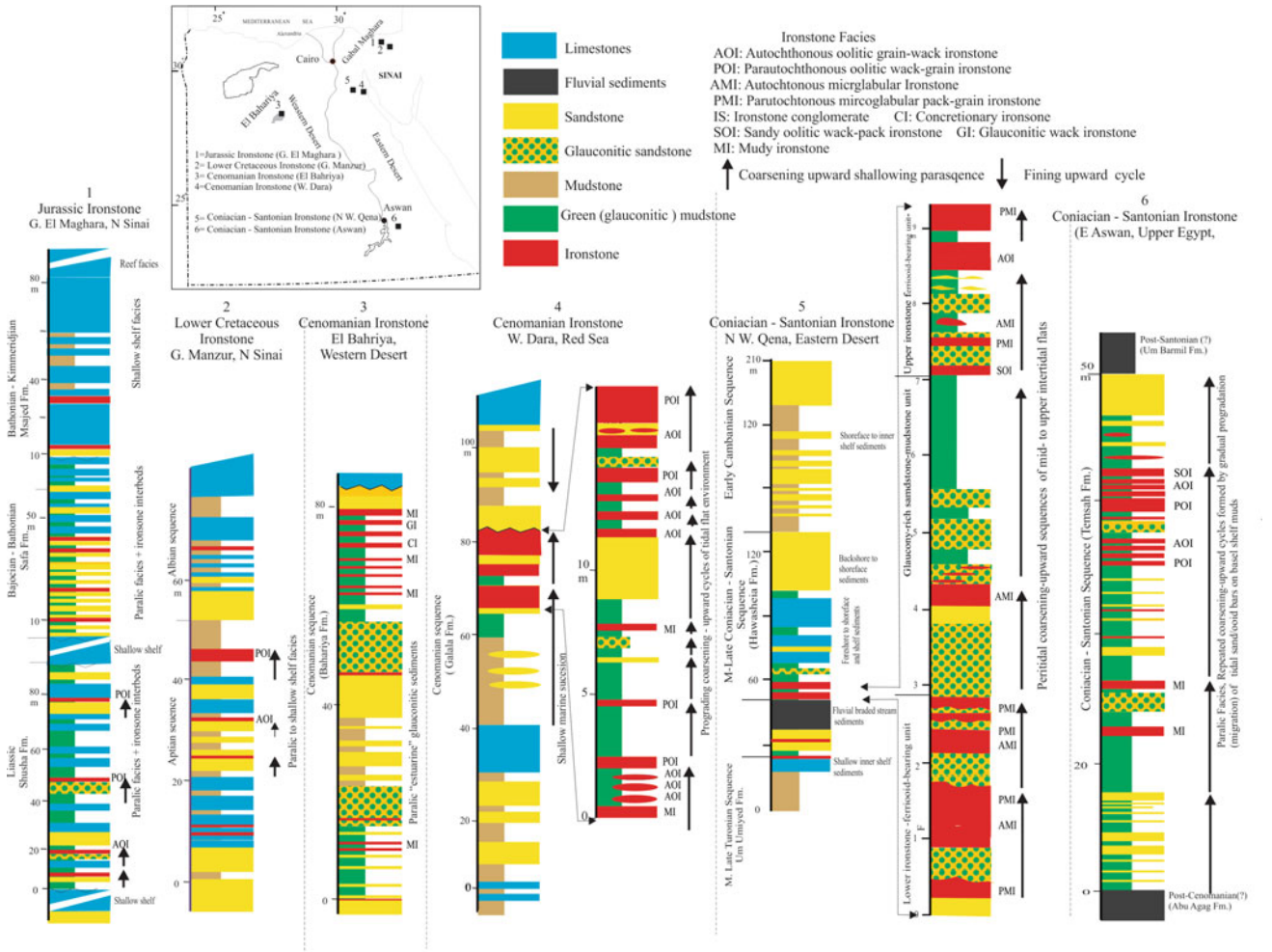

Fig. 14 Stratigraphic settings, facies, and environments of the Egyptian oolitic Mesozoic ironstones. 1 and 2 (El Sharkawi et al., 1989), 3 (IEP, 1993–1997), 4 (El Manawi, 2006), 5 (Helba et al., 2003), 6 (El Sharkawi et al., 1999)

Table 7 Major and trace element content of Abu Hamata paleo-karst profile of Fig. 11, after El Sharkawi et al. (1990a)

	SiO_2	TiO_2	$A_{12}O_3$	Fe_2O_3	MnO	MgO	CaO	K_2O	Na_2O	P_2O_5	LoI	Total
7	57.44	1.18	15.00	6.99	0.02	0.79	0.25	3.17	0.10	0.09	14.21	99.24
6	49.96	0.82	12.82	12.04	2.63	8.63	0.82	2.64	0.42	0.17	6.76	97.76
5	50.27	0.90	13.38	23.34	0.07	1.70	0.10	2.78	0.35	0.10	3.81	96.80
4	47.37	1.48	19.76	8.87	0.45	4.38	0.45	5.43	1.01	0.09	7.30	96.59
3	55.69	1.09	18.19	11.93	0.05	2.31	0.58	3.96	0.45	0.42	5.08	99.75
2	7.34	0.17	0.36	2.93	2.19	14.05	31.81	0.35	0.01	0.01	40.35	99.59
1	2.77	0.08	0.24	1.31	0.14	19.75	29.92	0.19	0.01	0.01	45.06	99.48
	Rb	Ba	Pb	Sr	La	Ce	Nd	Y	Th	Zr	Nb	Zn
7	49	74	135	143	92	155	66	68	29	524	72	58
6	83	1282	69	192	84	176	75	72	16	412	50	423
5	89	76	146	200	108	220	102	69	12	431	50	498
4	171	105	221	126	155	241	133	82	27	715	84	1020
3	128	93	31	179	127	242	162	115	21	524	69	446
2	22	1610	172	88	259	207	342	231	1	110	15	567
1	–	125	101	35	–	–	–	–	–	–	–	61
	Cu	Co	Ni	Sc	V	Cr	Ga	Code (sample locations in Fig. 11)				
7	151	7	17	15	350	346	26	7 = green shale				
6	476	35	97	13	555	614	20	6 = cupriferous green shale				
5	438	44	58	16	1480	1310	19	5 = ferruginous shale				
4	178	42	328	16	1430	1140	29	4 = green shale				
3	470	23	93	17	193	625	28	3 = black shale				
2	74	61	291	14	286	544	9	2 = dedolomite (subsoil)				
1	110	–	–	–	10	9	–	1 = bed rock				

shallow shelf mud (Fig. 14, El Sharkawi et al., 1999). The framework component of the oolitic ironstone bands are represented mainly by mechanically accreted Fe ooids, with or without sand grains. The ooids are formed by well or ill-defined concentric laminae of hematite, chamosite, goethite and Fe oxyhidroxides, kaolinite, calcite and ultra-fine fluorapatite having variable Fe content (Fig. 15). According to, the high phosphorous content of Aswan ironstone (up to 3 wt%) is related to the presence of disseminated aluminum phosphate-sulfate (APS) minerals within the ferriferous ooids and the matrix (Salama, 2014). However, Omran (2015) and Omran et al. (2014, 2015) succeeded in removing

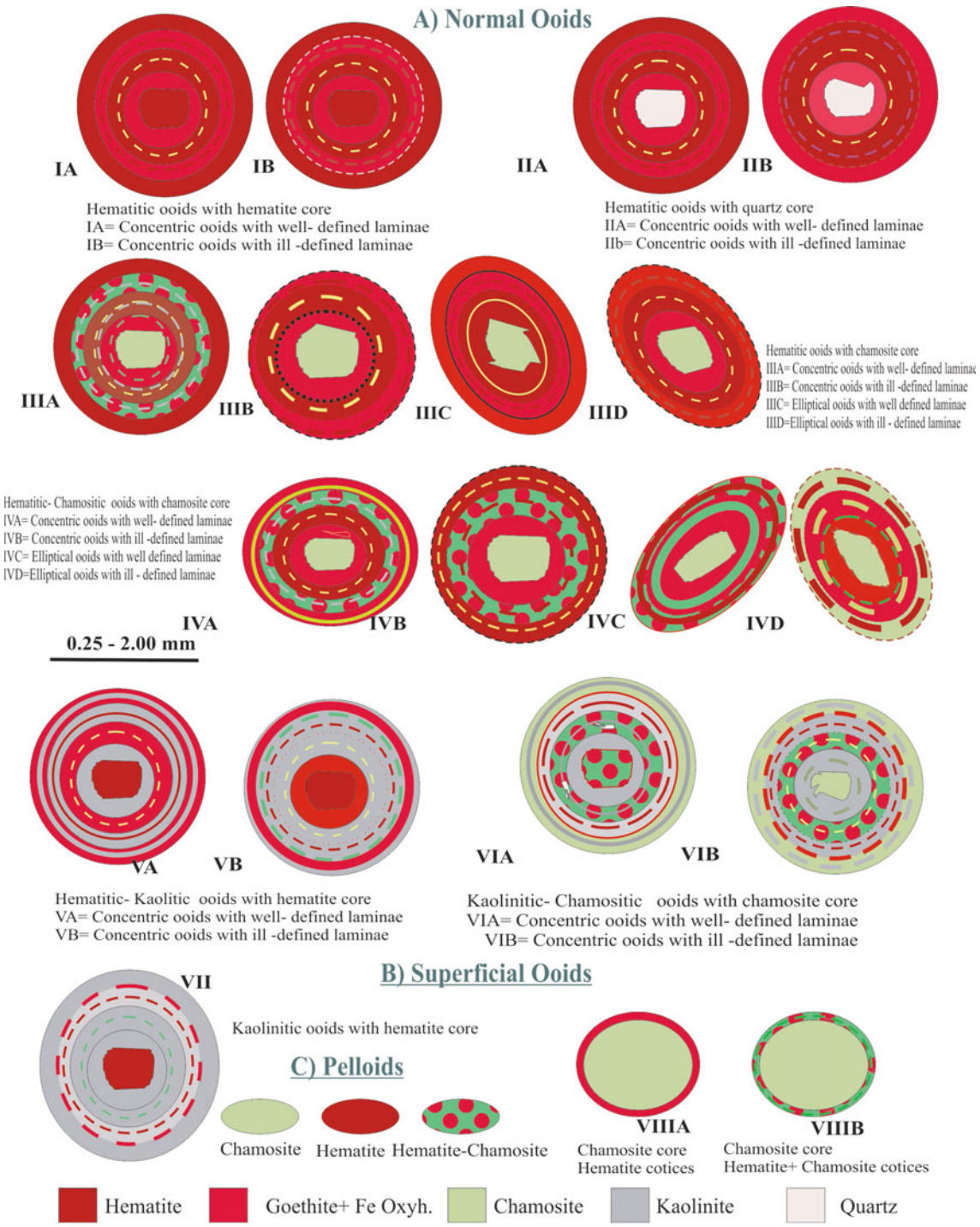

Fig. 15 Internal geometry and ooids and peloids composition Aswan Ironstone (CMRDI, 1998)

phosphorous from this ore type by combined microwave and ultrasound treatments. In addition to that, promising upgrading results are concluded by Yahiya (2007). The probable regional southward and south-eastward extensions of Aswan oolitic ironstones, particularly along Wadi Garrara-Gabal Abraq graben and Aswan-Allaqi sector, (until lat. 22°), are considered as a good target for further ore exploration (IEP Iron Exploration Project, 1993–1997; El Aref, 1999b).

3.2.3 Campanian–Maastrichtian Stratiform Phosphorite Deposit

The early Campanian–Maastrichtian sea transgression led to the deposition of wide carbonate/clastic facies, containing great reserves of phosphorite deposits (Fig. 12). The economic phosphate strata are confined to the Campanian–Maastrichtian phosphate bearing Duwi Group of Glenn and Arthur (1990). The Duwi Group, up to 145 m thick, is best exposed in a generally E-W trending belt extending along the middle latitude of Egypt (Figs. 1 and 12). It overlies non-marine, varicolored shales (Quseir Formation) and is conformably overlain by gray, laminated, foraminiferal-rich marine shales (Dakhla Formation). Within the Duwi Group, two main depositional realms are identified by Glenn and Arthur (1990): (a) a shallow hemi-pelagic environment responsible for the formation of organic-rich shales, bio-siliceous sediments and phosphorites and (b) a relatively high energy depositional regime. The formation of the phosphorites is attributed to current winnowing and concentration in reducing environment, associated with the deposition of shales and biosilicious sediments (Glenn & Arthur, 1990). In some sites, the phosphate ore shows abnormal concentration of trace elements, REEs, and uranium. The U content ranges between 20 and 180 ppm, averaging 58 ppm (El Kammar, 2020). El Kammar (2020) directed to utilize the rare earth elements (REE) as additional products from the phosphoric acid industry.

4 Cenozoic Stratabound Ore Deposits

4.1 Cenezoic Framework and Related Ore Deposits

The Cenozoic evolution witnessed global sea level changes and crustal deformations (Table 1), involving: (a) the culmination of the Early Tertiary "Syrian Arc" or "Laramide" movement, (b) Oligo-Miocene volcanic activity, and (c) the initiation and development of the Red Sea rift system. Humid and warm conditions dominated most of the Tertiary, while arid episodes were of short durations. A relatively long interval of aridity was exclusively a Late Pleistocene feature (McCauley et al., 1982; Said, 1990a). Late Cretaceous-Early Tertiary worldwide rising of sea level resulted in the submergence of most of Egypt by the Tethyan Epicontenental Sea, depositing the Dakhla shales, chalk formations, and the Esna shales. The southward migration of the Early Eocene paleo-shoreline continued until north Sudan. According to Issawi et al (1999), emergence of the Egyptian land took place from south to north at the close of the Late Eocene, accompanied by a major northward regressive phase of the paleo-shorelines (Table 1; Fig. 16). During the Middle and Late Eocene time span, further northward retreat of the shoreline took place (Table 1; Fig. 16). The Middle Eocene shoreline was approximately along south Minea-El Bahariya latitudes (Table 1; Fig. 16). The Early Cenozoic consequent streams (Gilf system of Issawi & McCauley, 1992) followed this phase of sea retreat and resulted in the initial stripping of the emerged Lower Tertiary, Mesozoic, and Paleozoic rock successions to the south. The denudation of these rocks was accelerated by karst processes (El Aref et al., 1987; Issawi & McCauley, 1993). A late Eocene delta was developed in Fayum basin, where the deltaic sediments of Qasr El Sagha Formation were laid down. The Oligocene shoreline was confined to the north, shelf marine sediments dominated in north Egypt, while fluvial sediments were deposited in the Suez-Cairo-north Fayum land stretch and El Bahr area (northeast El Bahariya Depression). During the Neogene, two main depositional regimes prevailed (Table 1), involving: (a) continental and shallow marine environments covering the extreme northern part of Egypt, accompanying advanced northward sea retreats, and (b) rift-related continental and coastal environments corresponding to the Red Sea rift dynamic (Table 1). The northward retreat of the Tethyan paleo-shorelines and syn-rift uplifting phases left behind vast areas of exposed carbonates of older ages, that continued to be exposed to subsequent phases of paleo-karstification processes during post-Eocene-Quaternary humid rainy periods. This is what led to the gradual lowering of the carbonate relief, ultimately into the exposing and denudation of older fossilized paleo-karst surfaces and the related cave systems and formation of the present-day karst morphogenetic carbonate landscape.

Two groups of Cenozoic stratabound and stratiform ore deposits of different paleo-geographic positions, stratigraphic setups, and paleo-environments are distinguished and deeply examined. These are: (a) Paleogene stratabound deposits and (b) Neogene rift-related deposits.

4.2 Paleogene Stratabound Deposits

These deposits encompass varieties of unconformity bounded fossilized oolitic-oncolitic ironstones and iron laterite, iron-rich lateritic blankets (surficial ferricrete duricrust) as

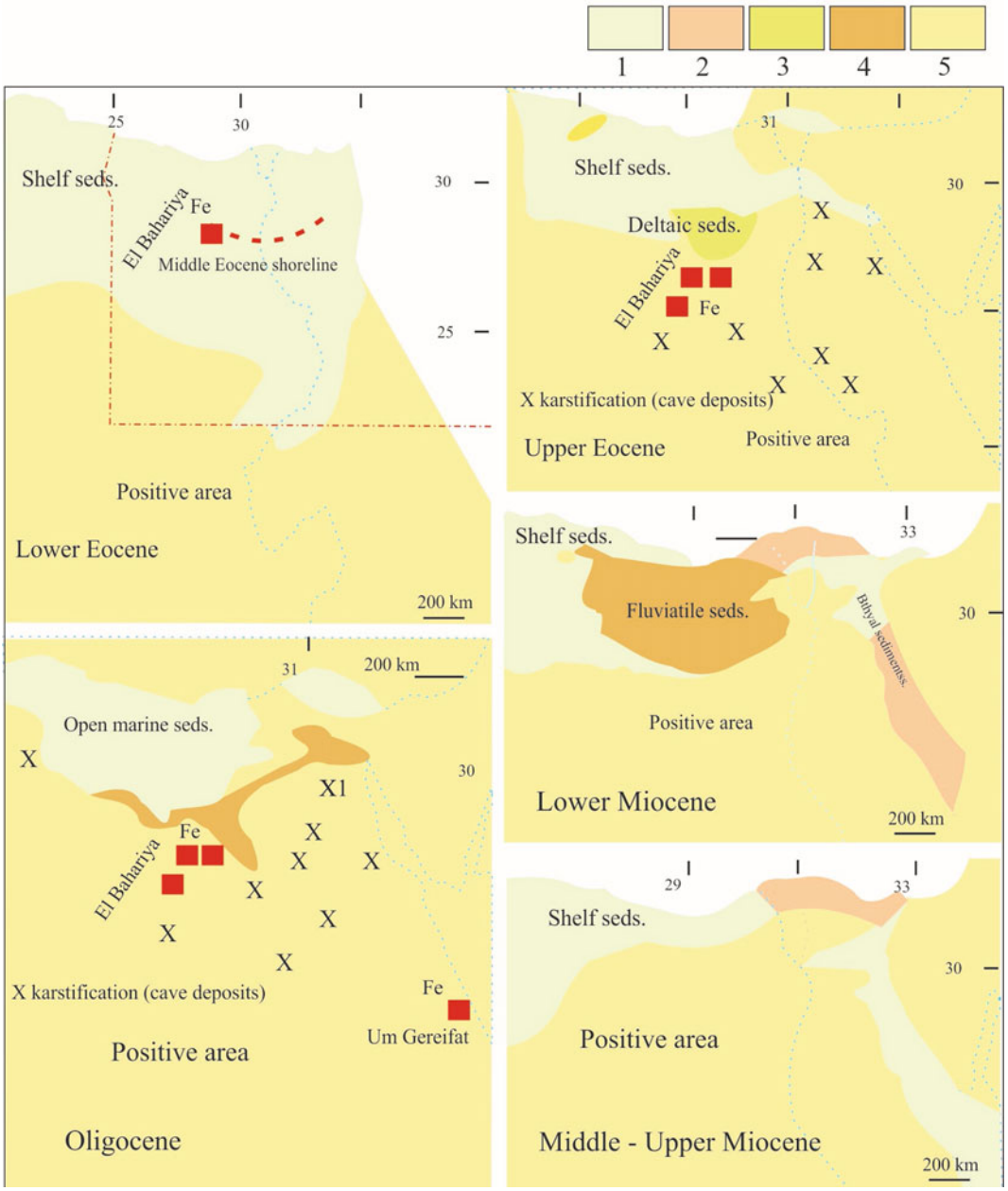

Fig. 16 Paleo-geography of the Cenozoic series (compiled from Klitzsch & Wycisk, 1987; Said, 1990b and simplified by El Aref, 1996). 1 = marine sediments, 2 = bethel sediments, 3 = deltaic sediments, 4 = fluviatile sediments, 5 = positive land, Fe = iron deposits

well as karst precipitates and recrystallized carbonates ("Egyptian Alabaster" and the associated red-matrix breccia).

4.2.1 Lutetian-Bartonian Stratabound Oolitic-Oncolitic Iron Ore (El Bhariya Depression, Western Desert)

El Bahariya district (Fig. 17) is of special interest because it contains exploitable large reserves of middle Eocene iron ores (Table 9. This district represents one of the main outcrops of Cretaceous rocks in North Western Desert, the other outcrop is at Gabal Abu Roash west of Cairo. These two localities display the highest push-up structural domains aligned along a giant tectonic Line trending in ENE direction of the Syrian Arc System or "Laramide" movement. The associated structural elements are related to a wrenching stress type of regime as concluded by Sehim (1993) and Moustafa et al. (2003). In the Early Lutetian, sea drowns the Bahariya paleo-high, which was subjected to denudation since Late Cretaceous time. A general N to NE gentle

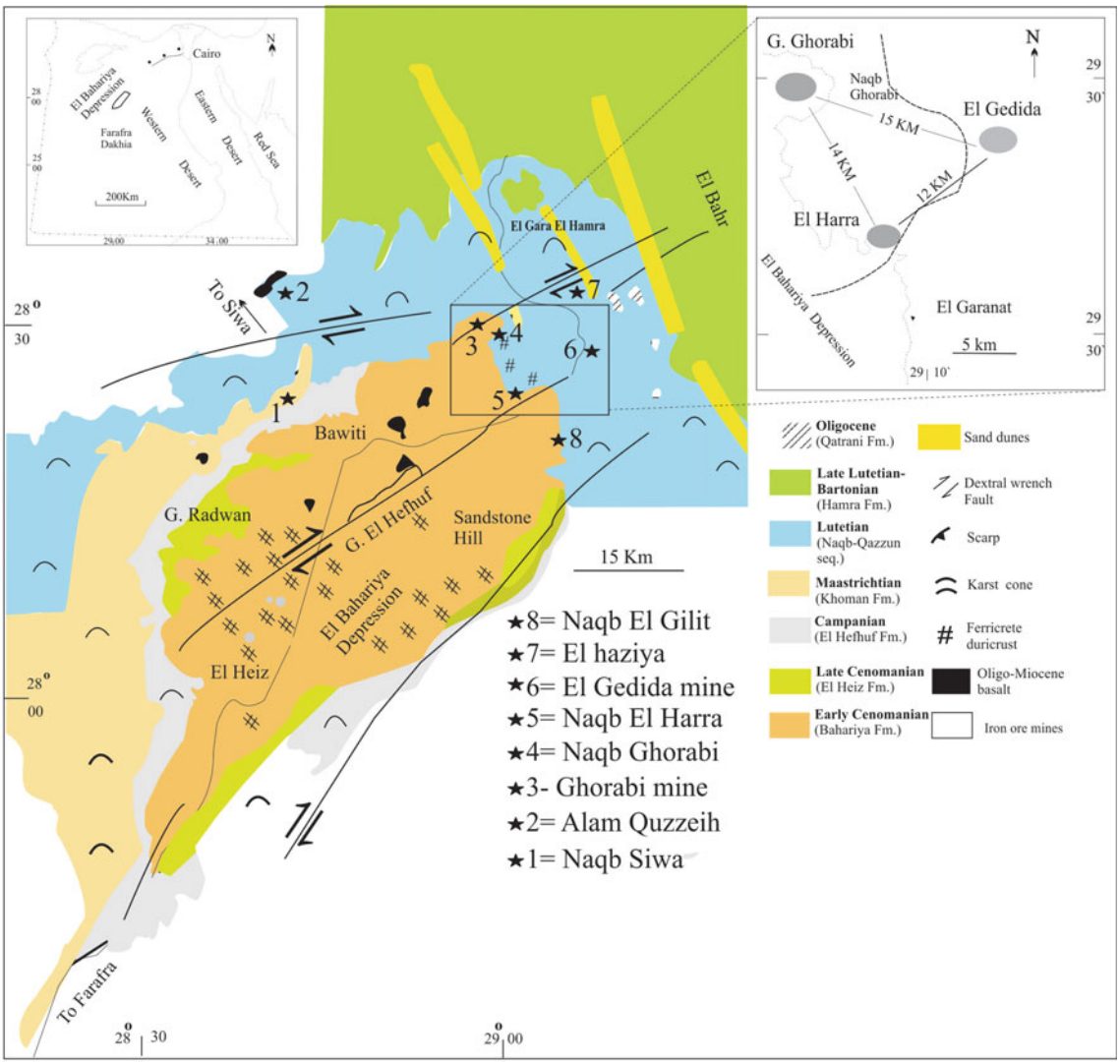

Fig. 17 Simplified geological and geomorphological map of El Bahariya Depression and locations of El Bahariye Fe mine areas and El Heiz duricrusted hills (modified by El Aref et al., 1999a after Hermina et al., 1989, detailed structural elements are shown in Sehim, 1993)

sloping ramp was developed, containing isolated submarine swells and islands in the northeastern plateau of the depression, namely El Gedida (6.5 km^2), El Harra (2.9 km^2), and Ghorabie (3.5 km^2) submarine swells (El Aref et al., 2001, 2006a, Fig. 17). The Cenomanian Bahariya Formation constitutes the floor of the depression and most of the scarp faces, and locally crops out on the northeastern plateau surface as minor fault blocks (e.g. El Gedida, El Harra and Ghorabi mine areas, Table 9). Along the ramp, Lutetioan fossiliferous carbonates (Naqb and Qazun formations) cover different Cretaceous rock units. The northward retreat of the Tethyan paleo-shoreline which was accompanied by the culmination of the Syrian arc system led to the uplifting of the Cretaceous strata in El Bahariya region. This is evidenced by the development of lateritic iron deposits demarcating the Cenomanian-Eocene unconformity surface (e.g. the basal part of El Harra ore section, ore type 2 of Table 10). The Facies assemblages of the Lutetian ramp carbonate succession are accreted in three distinct depositional belts, comprising: (a) back-bank/pritiadal belt, (b) bank/shoal belt, and (c) fore-bank/open marine belt (El Aref et al., 2001), often disrupted by several depositional breaks augmented by paleo-karstification processes. Upon the submarine swells (mine areas), the Eocene carbonate succession entirely changes into a very condensed section of oncolitic-oolitic and nummulitic ironstone facies of shallowing–upward pattern (Table 10; Figs. 18, 19 and 20).

As shown in Table 10, the condensed iron ore succession is bounded between two unconformities (sequence boundaries), namely the Lower Cretaceous–Middle Eocene boundary and the upper Eocene–Oligocene boundary. The

Table 8 Main geological, stratigraphic, geometric, mineralogical, and chemical characteristics of the Egyptian Mesozoic ironstones (IS) and their economic potentialities (compiled and simplified from El Aref et al., 1999b; El Manawi, 2006; El Sharkawi et al., 1989, 1999; Helba et al., 2003)

Age	Jurrasic—Early Cretaceous G. El Maghara environ, N. Sinai			Late Cretaceous	
Location	G. El Maghara Jurassic	G. Manzur Early Cretaceous	W. Dara cenomanian	W. Qena Coniacian	Aswan Coniacian-Santonian
References	El Sharkawi et al. (1989)		El Manawi (2006)	Helba et al. (2003)	El Sharkawi et al. (1999) El Aref et al. (1999b)
Host rock units	Shallow marine marginal facies of the Tethyan paleo-shore lines represented by of the following transgressive units				
	Jurassic Shusha (Late Triassic), Safa (Bathonian) and Masajid (Bathonian-Kemmeridjin) formations	Aptian-Albian G. Manzur formation	Late Cenomanian Galala formation (∼ 100 m thick)	Coniacian Hawshiya formation (∼ 178 m)	Coniacian-Santonian Temsah formation (∼ 40 m thick)
Host rock environment	Shallow marine tidal flat marginal facies				
IS bearing interval (succession)	Up to 5 m thick		Up to 18 m thick	Up to 10 m thick	6–8 m thick
	Deposition during repeated shoaling cycles				
Fe % content	17–42% Fe		21–46% Fe		25–75 % Fe (exploitable, ∼ 43% Fe)
Congruence: (stratified bands)	Up to 4 m thick of concretionary IS, massive IS, clayey IS, banded IS, laminated IS, oolitic IS		5 cm–2 m thick	5–40 cm thick	0.5–2 m thick
	Non-oolitic IS (mudy ISs, sandy ISs), oolitic IS, IS conglomerates				
Geometrical arrangement	Small-scale (short-lived) shoaling-upward cycles			Large-scale long-lived shoaling-upward cycles	
Framework components	Variable proportions of welded ferriferous allochems of micro-nodules, coated grains, ooids, micro-glaebules skeletal particles, rock fragments, quartz and glauconitic grains, pyrite				

Table 9 Summary of the estimated ore reserves of El Gedida, Ghorabi, Nasser, and El Harra mine areas (Technical and internal reports of EGSMA (1969–1971), ISCo Annual Internal Reports (1987–1977), IEP (1993–1997), El Aref, 1999)

Area	Area (km^2)	Overb. thickness (av., m)	Iron ore thickness (av., m)	Cutoff grade Fe %	Reserves (m.t.)-by			
					EGSMA (1969–1971)	UEC (1976)	ISCo (1987–1977)	IEP (1993–1997)
Ghorabi	2.308	0.1–2.0	11.1	40%	55,528,840	56,971,689		
Nasser	1.203	0.1–20.0	12.68	30% (25%)	28,990,760	26,023,281		
Nasser (2) (new discovery by ISCo. 1989)				30% 40%			10,044,356 7,856,000	
El Harra	2.9	5.90	8.0	30%	53,744,291	61,226,230		
NE-EI Harra (new discovery by IEP 1997)	2.4			40%				16,302,809 (40% Fe) 22,937,730 (Fe%?)
El Gedida	6.464	7.20	10.52	40%	117,000,000	123,718,000	148,640,358 (re-evaluation)	
South El Gedida (new discovery by IEP 1995)	0.5							12,650,497 (geological reserve)
Additional reserves							34,926,714 (Nasser 2 + re-evaluation of El Gedida)	35,588,227 (NE-EI Harra+ S. El Gedida)

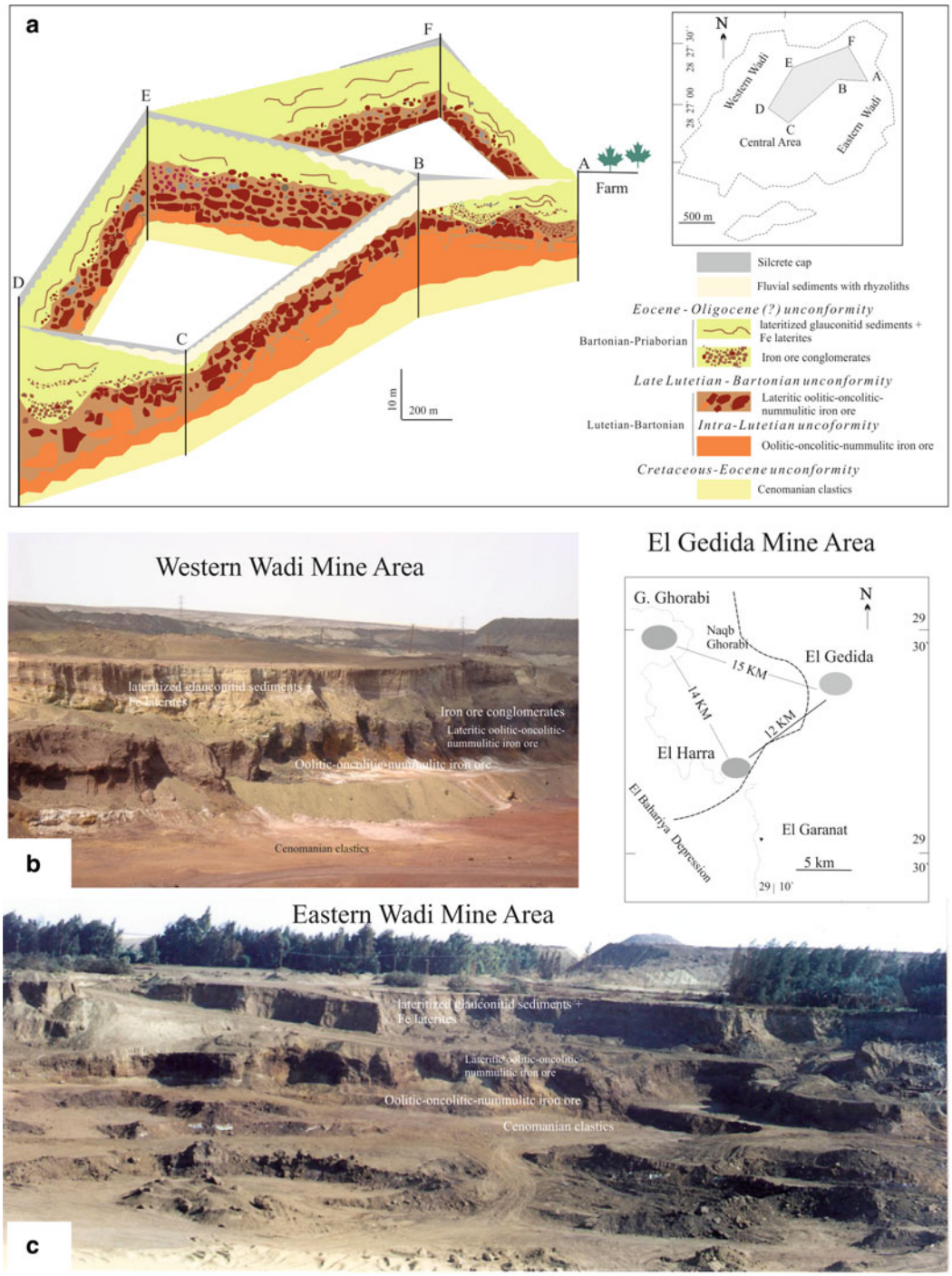

Fig. 18 **a** = Panel diagram showing the stratigraphic setting, lateral extension, and thickness variation of the different ironstone types of El Gedida mine area (IEP, 1993–1997). **b** and **c** = Panoramic field photographs showing the stratigraphic settings of the different ironstone types of the Eastern and Western Wadi sectors of El Gedida mine

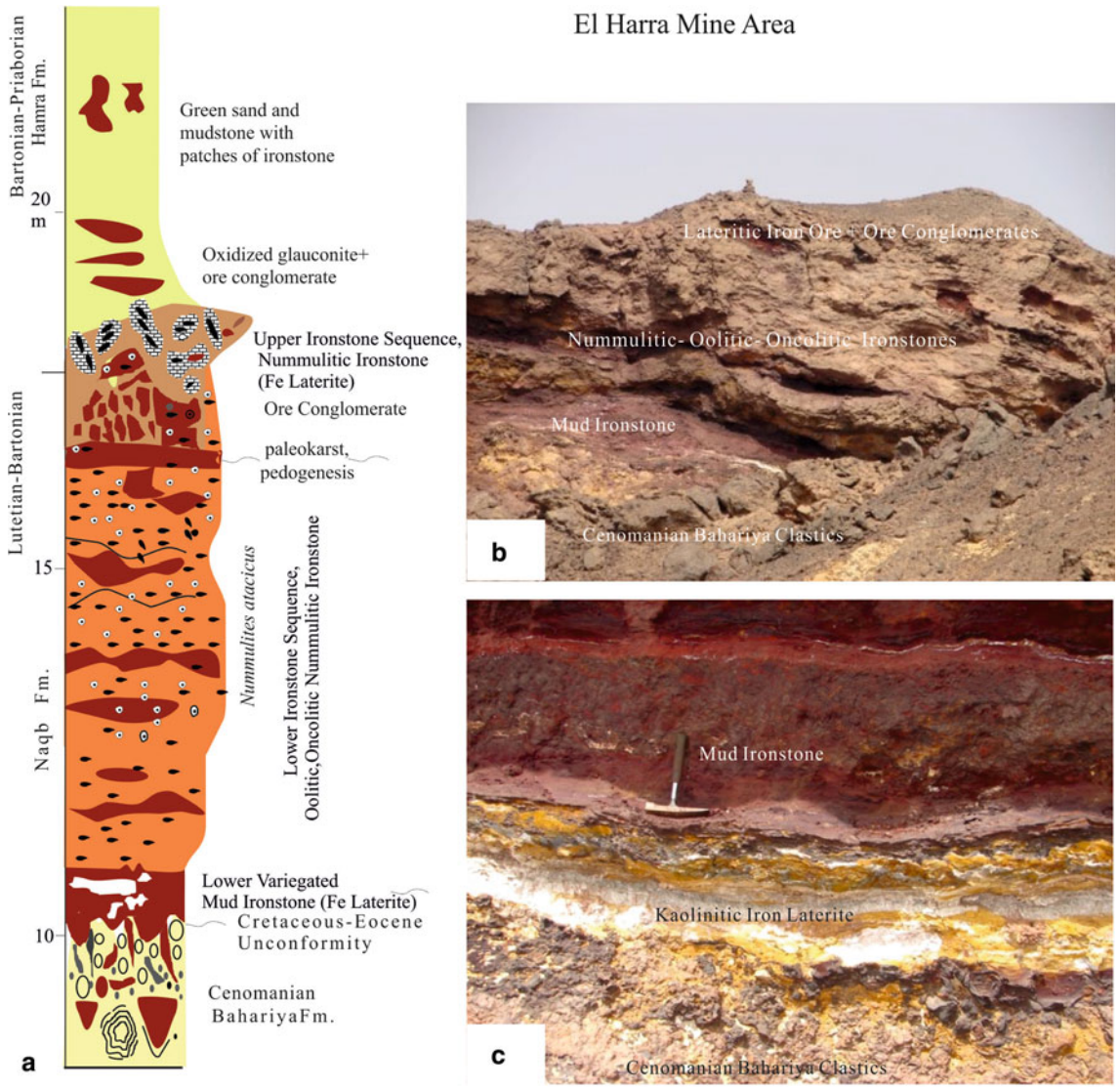

Fig. 19 **a** = Fine lithostratigraphy of the Lutetian ironstones at the upstream of Wadi El Harra mine area (Helba et al., 2001). **b** = Close-up view of the kaolinitic iron laterite developed along the Cenomanian-Lutetian contact, El Harra mine area. **c** = Field photograph showing the ironstone succession of El Harra mine area and the related main ironstone facies

ore succession includes the following vertically stacked ore facies types, arranged chronologically as follows:

(1) Stratiform ironstone bands and concretions encountered within the upper storm-influenced shallow shelf sediments of the Cenomanian sequence (ore type 1, Table 10). Most of these bands contain relics of oxidized glauconite and quartz grains floating in earthy goethite and hematite matrix mixed with amorphous oxyhydroxids. Such bands and concretions reach workable dimension and thickness in Nasser (north Ghorabi) and El Harra mine areas.

(2) Stratabound iron and manganese-rich laterite hosting kaolinite, alunite, and gibbsite nodules, developed along the Cenomanian–Lutetian boundary in El Harra and El Gedida mine areas (ore type 2, Table 10).

(3) Stratiform lateritized oolilitic-oncolitic and nummulitic ironstone sequences of shallow marine environment superimposed by lateralization processes (ore type 3, Table 10).

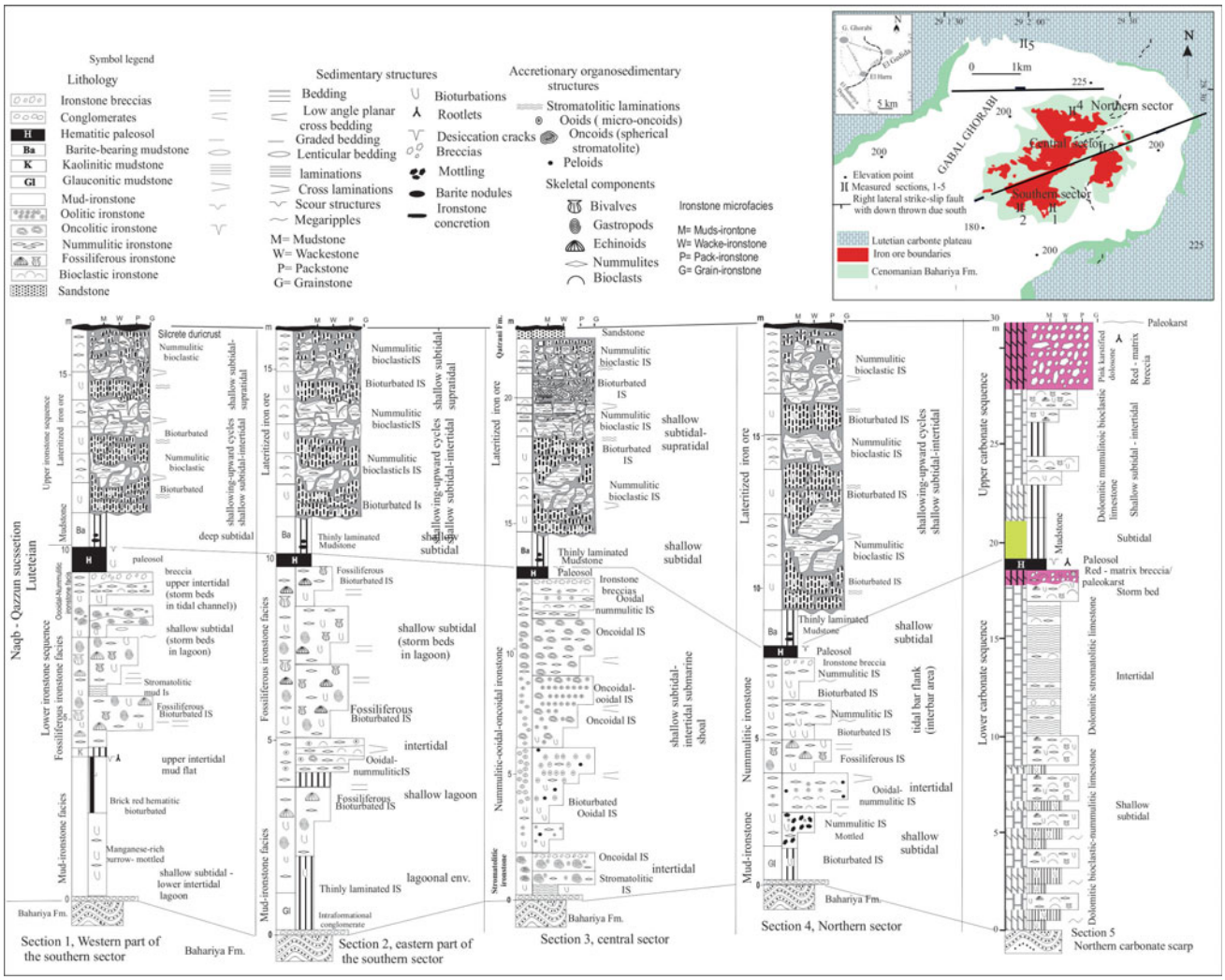

Fig. 20 Stratigraphic sections showing the distribution of the different ironstone units and the related facies of the different sectors of Gabal Ghorabi area (after El Aref et al., 2006a)

(4) Stratiform channel fill ore conglomerates with abundant melon-shaped concretions of silicified limestone and chert enclosing abundant molds of *Nummulites gizehensis,* truncating the Lutetian lateritized oolitic-oncolitic-nummulitic ironstones (ore type 4, Table 10).
(5) Bartonian iron laterite developed during intermitted lateritization of the Bartonian glauconitic sediments (ore type 5, Table 10) well-represented in El Gedida mine area (El Sharkawi & Khalil, 1977).

Stratigraphic Architecture and Facies Hierarchy of the Oolitic–Oncolytic-Nummulitic Ironstone

The encompassed Lutetian oolitic-oncolitic-nummulitic ironstone succession is underlain by the Cenomanian paleo-highs and or the Cretaceous-Eocene laterite deposits and overlain by channel fill iron conglomerates, Bartonian glauconitic succession, fluvial sediments, and/or silcrete hard cap (Figs. 18, 19 and 20). The main ironstone facies assemblage comprises two main sequences separated by thin red veneer of lateritic paleosol (Figs. 18, 19 and 20; Table 11). The lower sequence starts with tidal flat/lagoonal mud-ironstones with minor siliciclastic mudstones, representing deposition from suspension in low energy depositional environment (Figs. 19 and 20). These pass upward to shoals/mega-rippled yellow oncolytic-oolitic-nummulitic, grain-to pack-ironstone peritidal facies association, and indicating deposition under tidal and/or storm-generated shoaling-upward conditions during periods of sea level fall. The oncolitic-oolitic-nummulitic ore type constitutes the thickest ore type in El Gedida mine (up to 22 m thick, Fig. 18). In Ghorabi mine area (Fig. 20), the upper ironstone sequence begins with the deposition of shallow subtidal

Table 10 Upper Cretaceous and Tertiary stratigraphic units of the northern part of El Bahariya Depression and the related stratigraphic gaps and ironstone types (after El Aref et al., 1999a, 1999b)

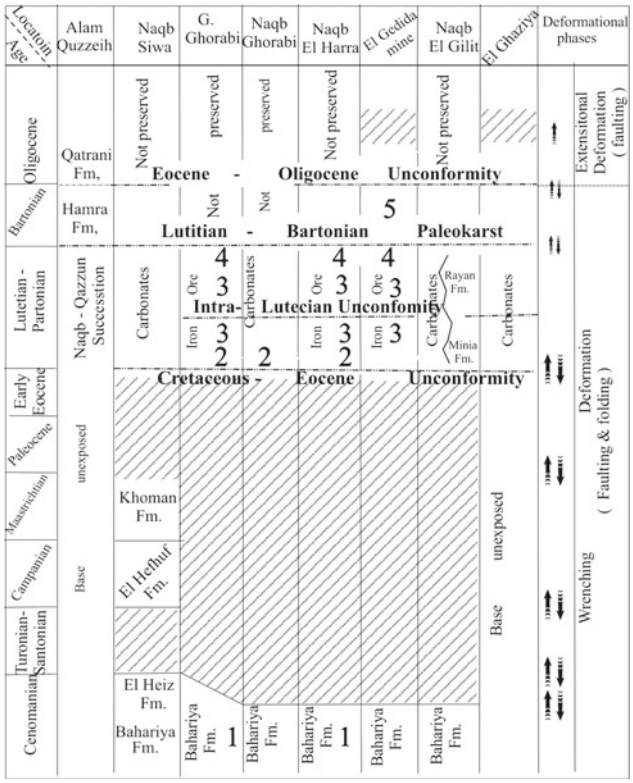

Ironstone types: 1 = Cenomanian ironstone, 2 = Cretaceous-Eocene ferruginous latosol, 3 = Lutetian oolitic-oncolitic ironstone, 4 = ore conglomerates, 5 = Bartonian glauconitic Fe laterite

green mudstone facies of new marine transgression followed by peritidal shallowing-upward cycles of ironstones terminated by supratidal stratiform barite (Fig. 20). Each cycle begins by shallow subtidal mud-ironstones grading upward into shallow subtidal-intertidal nummulitic-bioclastic ironstones. The facies hierarchy of these ironstone sequences, their vertical arrangement and lateral variation changes into the coeval shallow subtidal-intertidal carbonate facies are well recognized and identified in Ghorabi mine area (Fig. 20; Table 11). The upper ironstone sequence is intensively lateritized forming iron ore laterite. The superimposed subaerial weathering complicated the diagenetic history and in many cases may partially to completely obliterate the original marine fabrics and textures of the upper ironstone sequence (Figs. 18, 19 and 20; Table 11).

Petrographically, the Lutetian oolitic-oncolytic-nummulitic ironstones comprise varieties of grain- and mud-supported microfacies, which are defined relying on the type and content of ferriferous allochems as well as depositional fabrics and structures. The matrix of these facies consists mainly of earthy iron oxides and hydroxides, ferrihydrite, amorphous iron oxyhydroxide, sooty manganese-rich materials, phosphoric clays, ultra-fine kaolinite particles as well as sandy to silty sized quartz and glauconite grains. The cement is formed mainly of iron oxides and hydroxides and less abundant manganese oxides and hydroxides, barite, dolomite, calcite, siderite, quartz, gypsum, and halite. The recorded ferriferous allochems are classified into three main categories, including (a) ferruginized skeletal particles (tests and molds of nummulites, alveolinids, with body fossils of gastropods, bivalves, echinoderms, and benthic algae as well as microbial remains, (b) ferruginous coated grains and ooids (biogenically encrusted or microbial-mediated grains such as ferriferous oncoids and ooids, ferriferous cortoids and ferriferous concretionary glaebules, and (c) ferriferous peloids and intraclasts. The development of the various microbial-mediated structures (stromatolites, oncoids, and ooids) is attributed to biogenic accretion mechanism (El Aref et al. 1999b, 1999b, 2006b and Helba et al. (2001). The biogenic accretion was responsible for the accumulation and early cementation of the original precipitates, i.e. amorphous Fe oxyhydroxides. The ferruginous microbialite morpho-structures are classified into three main morpho-types (Fig. 21), including (1) Ferruginous

Table 11 Distribution of ironstone facies and microfacies of the ironstone sequences of Gabal Ghorabi mine area and their lateral variation into the equivalent Lutetian carbonate facies (Salama, 2006)

	Southern sector		Central sector			Northern sector		Eastern scarp	Northern scarp
Upper ironstone sequence	Stratabound karst (lateritized) iron ore, karst-related barite deposits karst carbonate breccias and terra rossa sediments								
	Stratiform barite layers Nummulitic-bioclastic wacke-/pack-ironstone Bioturbated mud-ironstone Stratiform barite layers Nummulitic-bioclastic wacke-/pack-ironstone Bioturbated mud-ironstone Nummulitic-bioclastic wacke-/pack-ironstone Bioturbated mud-ironstone							Nummulitic-bioclastic wackestone/packstone Lime mudstone Nummulitic-bioclastic wackestone/packstone Lime mudstone Nummulitic-bioclastic wackestone/packstone Stromatolitic wackestone Lime mudstone	
	Green mudstone facies containing barite nodules								
Lower ironstone sequence	Red hematitic paleosol and collapse ironstone breccias							Terra rossa sediments	
		Ooidal-nummulitic grain-ironstone	Nummulitic-ooidal-oncoidal ironstone	Ooidal-nummulitic	Grain-ironstone	Nummulitic	Nummulitic wacke-ironstone	Glauconitic mud-ironstones	Fossiliferous float-/rudstone
		Mud-ironstone			Pack-ironstone				
		Oncoidalfoat-/rud-ironstone		Oncoidal	Pack-/grain-ironstone		Mud-ironstone		
		Mud-ironstone			Wacke-ironstone				Stromatolitic limestone (wackestone)
		Wacke-/pack-ironstone		Oncoidal-ooidal	Pack-/grain-ironstone		Pack-ironstone		
		Stromatolitic mud-ironstone			Wacke-ironstone				
		Float-/rud-ironstone		Oncoidal	Rud-ironstone		Wacke-ironstone		Five repeated shallowing-upward cycles: each of which begins by bioturbated nummulitic mud-/wacke stones and terminated by bioclastic-nummulitic packstones
		Mud-ironstone			Float-ironstone		Wacke-/pack-fossiliferous ironstone		
	Mudstone			Ooidal	Pack-/grain-ironstone		Fossiliferous mud-ironstone		
	Mud-ironstone	Brick red hematitic mud-ironstone			Mud-/wacke-ironstone		Ooidal pack-/grain-ironstone		
		Burrow-mottled mud-ironstone	Stromatolitic ironstone	Oncoidalrud-ironstone			Wacke-ironstone		
				Stromatolitic mud-ironstone			Mud-ironstone		

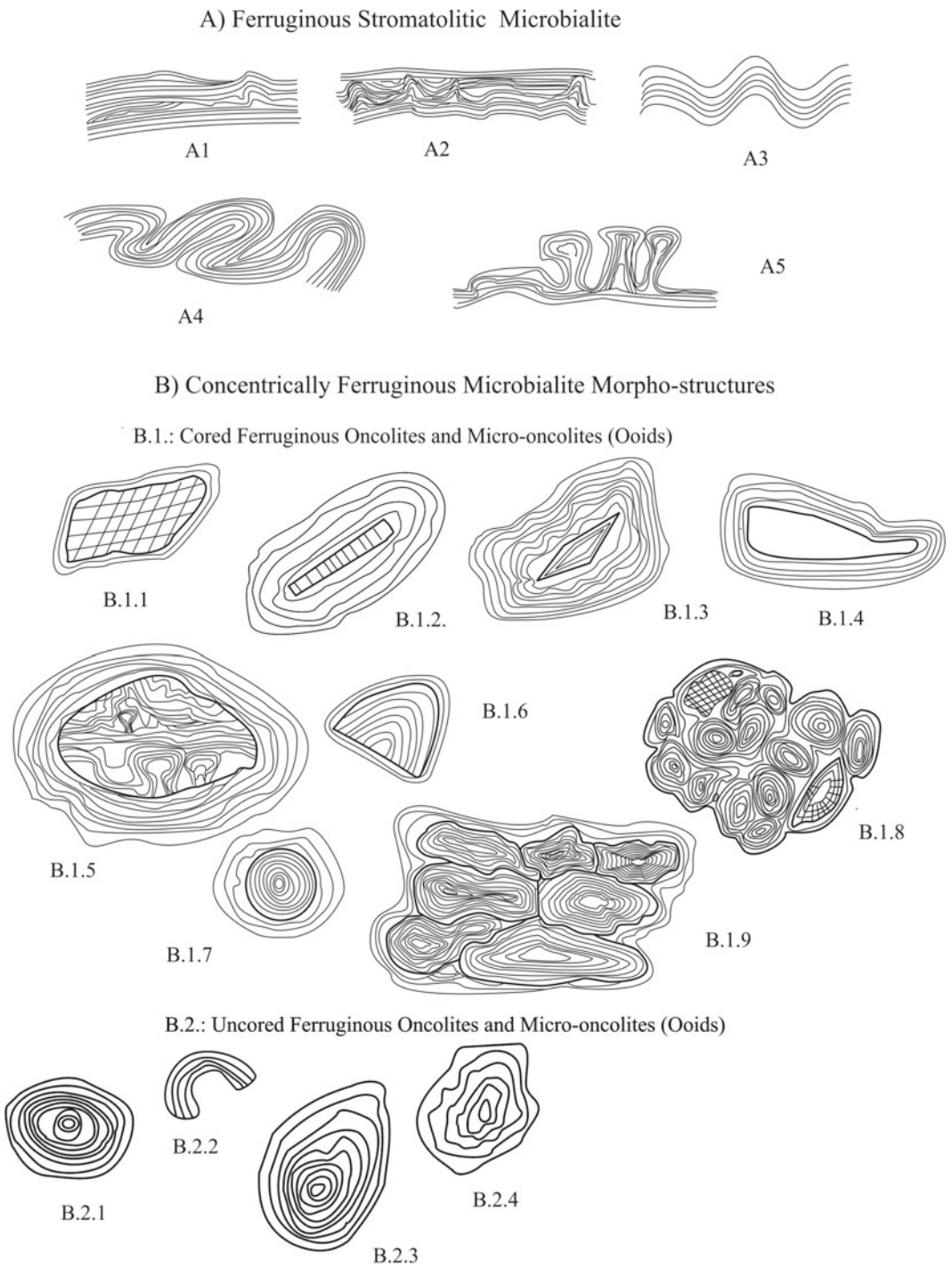

Fig. 21 Schematic illustrations of the recognized ferruginous microbialite morpho-structures of the Luteteian ironstones, not to scale (El Aref et al., 2006b). Types (A1–A4): biostromal (stratiform) stromatolitic buildups, Type A5: digitate stromatolites, Types (B1.1–B1.9): cored oncolites and micro-oncoids (ooids) with cores of: nonskeletal particles (Types B1.1–B1.3); mud ironstone clasts (Type B1.4); sromatolitic mat chips and fragments (Type B1.5); intact and/or segments of ferruginous ooids and peloids (Types B1.6 and B1.7); and groups of ferruginous ooids and oncoids Types (B1.8 and B1.9). Types (B2.1–B2.4): uncored ferriferous oncoids and micro-oncoids. Types (B2.1 and B2.2) are oncoids of spherical to ellipsoidal shapes having plastically deformed or spastolithic forms (Type B2.2); Types B2.3 and B2.4 are oncoids with internal convex outward discontinuous, wavy to slightly crenulated laminae

stromatolitic microbialites (Fig. 22a, b), (2) ferruginous concentrically laminated microbialites (ferruginous oncoids, micro-oncoids and ooids, and (3) ferruginous peloids. The internal structure of the ferruginous stromatolites and microbially coated grains consists of cyclic microbial and Fe oxyhydroxide laminae. The microbial laminae consist of fossilized neutrophilic filamentous iron-oxidizing bacteria (Salama et al., 2013, Fig. 22c).

The lateritization processes acted upon the upper ironstone sequence led to the development of solution openings, passages and cavities and angular rubble to boulder-sized collapse breccia's of ooidal and nummulitic ironstones (Figs. 18, 19, 20 and 22d–f). The solution features are mostly filled by chemical and biogenic products. Their internal walls are often lined by crustified banded yellow amorphous iron oxyhydroxides and brown radial goethite

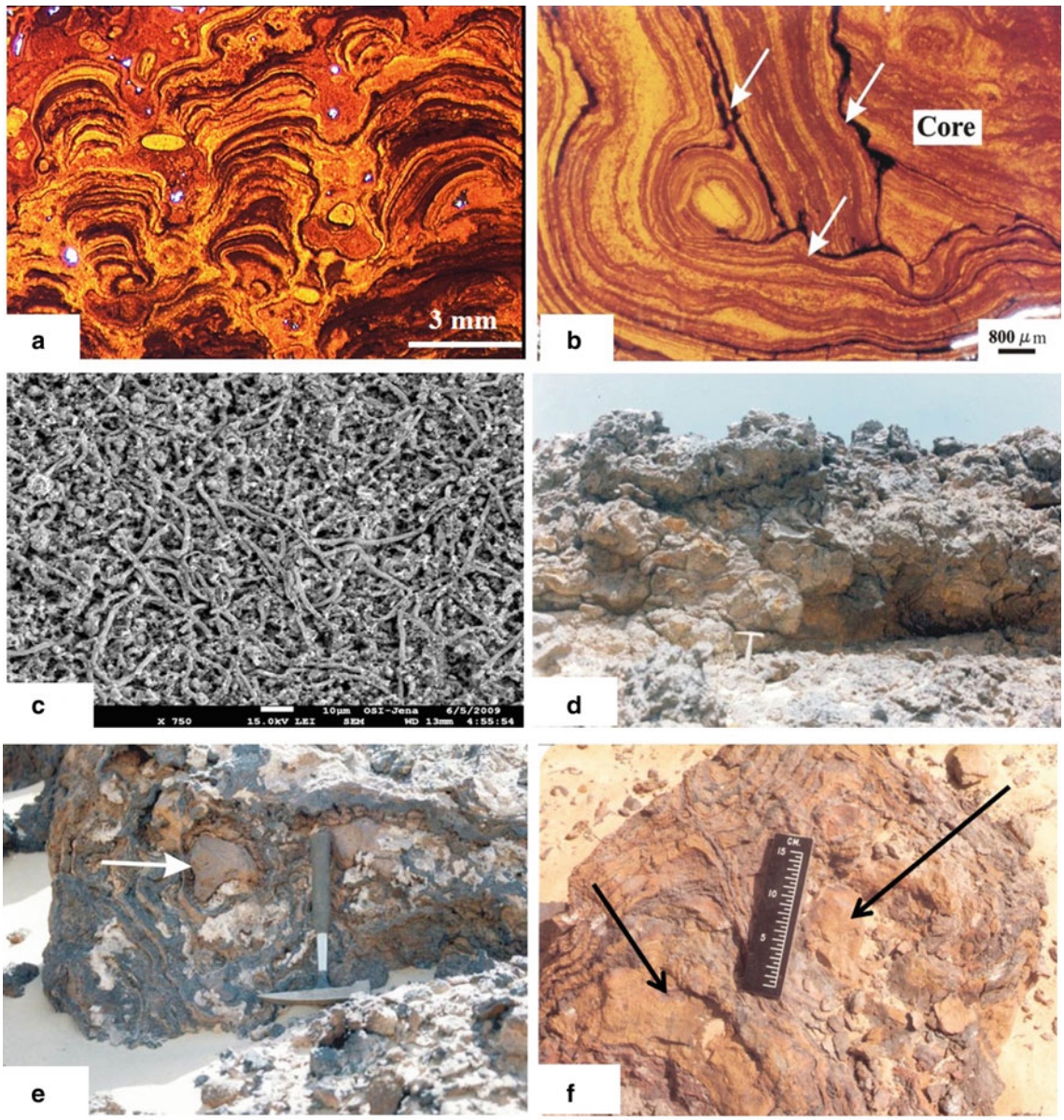

Fig. 22 **a** = Transmitted light photomicrograph of micro-columnar and micro-domal ferruginous stromatolites. **b** = Transmitted light photograph of Large ferriferous oncoids with inner core made up of stromatolitic fragment and outer multiphase encrustations separated by micro-erosional surfaces (arrows). **c** = SEM photomicrograph shows microbial ferruginous laminae consisting entirely of leptothrix-like bacteria (Salama et al., 2012). **d** = An outcrop of the upper lateritic Fe sequence dominated by collapsed ironstone boulders setting in soily matrix. **e** and **f** = Cockade structures of the upper Fe laterite sequence showing crustified colloform goethite cementing omcolitic ironstone fragments (arrows)

crystals of colloform outlines. Cockade structure of crustified colloform goethite enveloping ironstone breccia fragments is very common.

The mineralogy and geochemical characteristics of the different marine ironstones and the related lateritic products are intensively investigated by Salama et al. (2012, 2013, 2014, 2015) and Valerian Ciobotă et al. (2011), using a Jeol JSM-7001 field emission scanning electron microscope, applied Mössbauer spectroscope, SEM, XPS, XRD, FTIR and ICP-OES methods, thermoanalyses (DTA-TGA) and isotope measurements. The lagoonal ironstone facies association consists mainly of goethite, hematite, todorokite, psilomelane, pyrolusite, birnessite, aurorite and manjiroite, and authigenic kaolinite and illite together with detrital minerals (quartz, rutile, and feldspars). The peritidal microbially mediated ironstone facies association consists mainly of goethite, psilomelane, pyrolusite, apatite, quartz, and jarosite with organic materials such as proteinaceous compounds, lipids, cellulose, and carotenoids are detected in the cortices of the ferruginous ooids and oncoids. The iron laterite consists mainly of crustified colloform goethite, hematite and psilomelane, alunite, kaoinite, gibbsite, palygorskite, and halloysite.

Sedimentary Processes, Diagenesis, and Supergenesis

As it has been concluded by the above-mentioned publications, the original precursor materials include iron-rich kaolinitic clays and amorphous iron oxyhydroxides (ferrihydrite) with less frequent oxidized glauconite peloids and sandstone rock fragments. The iron compounds were transported as an organic-rich colloidal suspension from the Cenomanian paleo-highs by rivers to the depositional system. The depositional processes include:

(a) Deposition of detrital Fe-rich glauconitic and kaolinitic clays and yellow amorphous Fe oxyhydroxides in areas of variable water depths, Eh, pH, and organic matter content with or without manganese enrichment in some horizons depends on the behavior of the manganese and iron in the solution during the depositional and diagenetic processes,
(b) Growth of stromatolitic (microbial) buildup and formation of in situ Fe oncoids and ooids (Fig. 22a–c) in a quiet water condition intermittent with short agitated periods of storm waves. The detailed composition of the accreted microbialites, the precipitation, and accretion mechanism of the different various microbial forms as well as the ferruginization processes of the associated skeletal particles during the marine deposition, subsequent diagenesis, and subaerial processes are discussed in detail by Mesaed et al (2005), Helba et al. (2001), Salama (2006, 2010) and Salama et al., 2012, 2013, 2014, 2015). According to Salama et al. (2013), the microbialites consist of cyclic alternations of microbial and iron oxyhydroxide laminae formed by neutrophilic iron-oxidizing bacteria at the interface between ascending acidic Fe (II)-rich groundwater and marine water. The microbial laminae consist mainly of fossilized filamentous iron-oxidizing bacteria, most similar to the modern Leptothrix species, which indicate microbial precipitation of amorphous iron oxyhydroxides around the bacterial surfaces, crystallized during early diagenesis into nano-crystalline goethite. Acidic groundwater may have induced syn- and post-depositional alteration by oxidation of sulfides (primarily pyrite) hosted in the underlying Cenomanian Bahariya Formation. Iron sulfates and oxides were precipitated by another generation of acidophilic iron-oxidizing bacteria (Salama et al., 2013), and
(c) Reworking and distribution of shells and shell fragments and their admixing with the other biogenic Fe components in storm-dominated condition during shallowing regimes.

- **Early diagenesis**

The early diagenetic processes include:

(a) Organic matter degradation by benthic microbes mainly cyanobacteria, which create a weakly reducing (post-oxic) diagenetic environment of low pH and Eh,
(b) releasing of Fe, Mn, silica, and other residual elements and their re-concentration in the interstitial pore water as a result of lowering in pH and Eh,
(c) Matrix pelletization and growing of in situ peloids and ooids. In situ ferriferous peloids and ooids are formed as organic-rich windows within the matrix components due to the inhomogeneous distribution of the organic matter with the precursor materials,
(d) Dissolution and replacement of the original calcareous wall structures of the skeletal particles and the formation of intra- and inter-skeletal porosities. The calcareous skeletal particles and bioclastic debris are also subjected to early weakly reducing diagenetic changes within the semi-confined micro-cavities of the foraminiferal tests and bioclastic debris. This may facilitate dissolution of the original calcareous wall structures leaving ferruginized fossil molds and casts, and
(e) Growing of barite nodules.

- **Late diagenesis**

During the late diagenetic stage, the amorphous to poorly crystalline iron oxyhydroxides (ferrihydrites) together with the in situ formed early diagenetic ferriferous ooids and peloids as well as the ferruginized skeletal particles undergo diagenetic dehydration and recrystallization. During these processes, the unstable yellow to reddish brown ferrihydrite phase is directly transformed into varicolored stable phases of well crystalline goethite and/or hematite of different morphological forms. The recrystallization processes begin within the interstitial iron oxyhydroxides matrix and extend outwards into the enclosing ferriferous grains consequently until the hematitization of the original components. Silicic acids are released into the interstitial pore solution during the early post-oxic diagenetic stage as a silica-like gel phase. During the subsequent stages of dehydration, the silica gel phase recrystallized into cryptocrystalline and microcrystalline quartz, this was followed by late siderite, calcite, barite, and halite cements.

- **Subaerial lateritization (supergenesis or telogenesis)**

The superimposed subaerial lateritization complicates the diagenetic history of the ironstones and partially to completely obliterates their original marine fabrics and textures (Fig. 22d). Crustified colloform layers of goethite, hematite, and pyrolusite form megascopic reniform textures, spherules, and/or bundle-like or flower-like textures. The collapsed ironstone breccia fragments are embedded in illuviated iron oxyhydroxides and often cemented by layers of colloform goethite, forming cockade structures (Fig. 22e, f). The ferriferous ooids and ferruginized skeletal particles are cemented by meniscus goethite vadose cement. Other pedogenic features are also displayed by coating of ferriferous ooids and peloids by amorphous iron oxyhydroxides and goethite cutans, the presence of well-developed grain bridges and sinuous fenestrae forming alveolar textures, as well as the presence of root mold porosities. The formation of sulfate, nitrate, carbonate, and silicate minerals in solution openings may indicate more recent alteration under arid climatic conditions.

Genetic Considerations and Recommendations

Summing up, the original Lutetian ironstones (iron ores) had been accumulated on submarine swells (the wrench-related Cenomanian swells) under well-aerated and intermittent agitated and quiet water conditions. Hence, the paleo-topographic evolution during the post-Cenomanian and Eocene time span resulted in the drastic variations in both facies and thickness of these ironstones. The humid paleo-climate during the Cretaceous-Eocene time and the paleo-geographic distribution pattern of the paleo-Tethyan shoreline are other essential genetic parameters in the formation of these ironstones. The main genetic parameters responsible of the formation of these iron ores can be summarized as follows:

1. paleo-topography of the glauconitic Cenomanian paleo-highs,
2. paleo-climatic evolution,
3. paleo-geographic distribution pattern of the Tethyan shoreline,
4. paleo-environments of the ramp carbonates and the equivalent ironstone facies
5. syn-sedimentary supply of amorphous iron,
6. sedimentation and biogenic microbialite accretion of iron oxide, in situ reworking and local transportation, via mega ripple migration,
7. shallow marine and subaerial paleo-environments with marine diagenetic modifications,
8. intermittent phase of uplifting and lateritization responsible for the modification of the original marine ironstone facies association and redisposition of iron as cavity filling or laterite products,
9. authigenesis of iron and manganese oxides, silica, and sulfates.

4.2.2 Fe-Rich Lateritic Blankets (Surficial Ferricrete Duricrust)

In order to complete the perception of the geomorphological history of El Bahariya region, special importance must be focused on the developed El Heiz ferricrete high-laying duricrust of El Bahariya Depression (Figs. 17 and 23a-d, El Aref & Lotfy, 1989; Sokker, 1991; El Aref et al., 1991, 1992), touristically known as El Heiz black desert natural protected area. It shows the extent of the lateritization and karstification of the uplifted hinterlands of El Bahariya, since the regression of the Eocene sea. The high-lying ferricrete duricrust forms a clear black morphologic marker of fairly constant altitude, ranging from extensive sheet as in Gabal Radwan and Sandstone hills until discrete lenticular or rounded masses within the depression, capping the summits of isolated cone hills, inselbergs, and flat-toped tablelands of different clastic and carbonate stratigraphic units (Fig. 23). It represents remnants of an old erosion surface of old erosion cycle and was formed by general lowering of the landscape over long period of humid paleo-climate. The ferricrete profile, 6–16 m thick, consists of three main gradational horizons corresponding to the typical laterite profile (Fig. 23), including (a) an upper hard cap, (b) a middle varicolored (illuvial) horizon, and (c) a lower horizon of

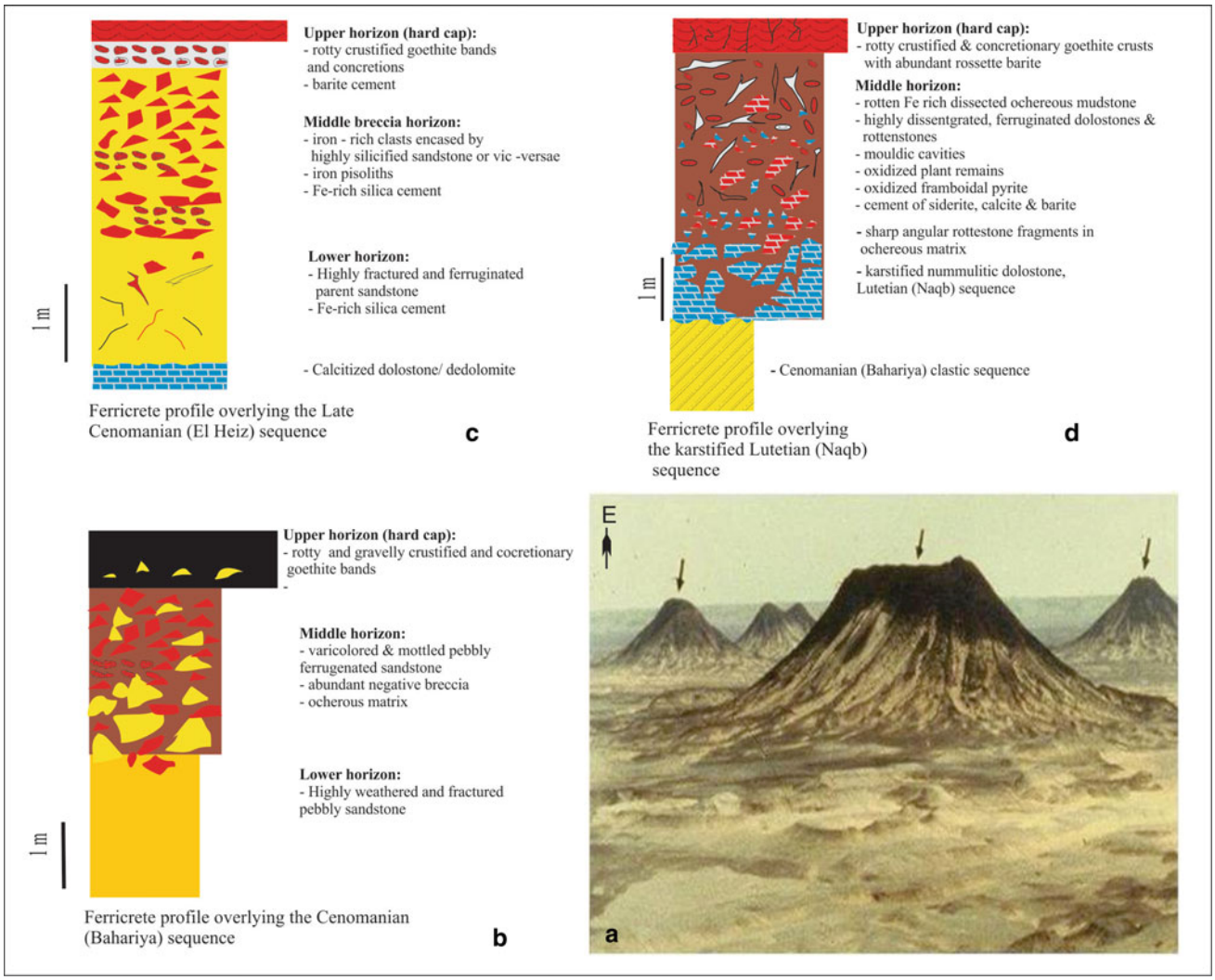

Fig. 23 El Heiz high-lying ferricrete duricrust, El Heiz black desert Protected area, El Bahariya depression, Western Desert. **a** = field view showing the high-lying ferricrete duricrust (arrows) capping isolated cone hills, **b** = ferricrete profile overlying Cenomanian clastics, **c** = ferricrete profile overlying Cenomanian dolostone, **d** = ferricrete profile overlying Lutetian dolostone. Simplified after El Aref et al., (1991, 1992)

weathered rocks. Subsequent weathering and paleo-karstification cycles with etchplanation and pedimentation processes, (post-Eocene-Quaternary) affected the high-lying paleo-peneplained surface and the surrounding carbonate plateau. These processes led to continuous stripping of regolith's, incision and deepening of rivers, gradual consumption of the interfluves, gradual slope, and scarp retreat until the complete excavation of the depression and development of remnants of duricrusted cone hills of black appearance (Fig. 23c). Hence, the landform evolution of El Bahariya region and the related development of lateritic deposits indicate that the whole region was subjected to multiple erosion cycles under humid conditions (lateritization and karstification) affected the exposed carbonates and clastics of the hinterlands, since the Middle Eocene northward sea retreat.

4.2.3 Fossil Pre-rift (Post-Eocene-Pre-early Oligocene?) Alumino-Ferruginous Latosol

Another proof of continuous weathering of the hinterlands is manifested by well-developed alumino-ferruginous latosol of Um Gerefat mine, Red Sea coast (El Aref, 1993a, 2020a). It demarcates a pre-rift paleo-erosion surface acted upon Pre-Cambrian granite and was later truncated by the proto-rift Late Oligocene-Early Miocene fanglomerates of the Ranga Formation (Fig. 24a). The latosol profile comprises three main horizons representing a series of weathering degrees grading from slightly weathered Pre-Cambrian

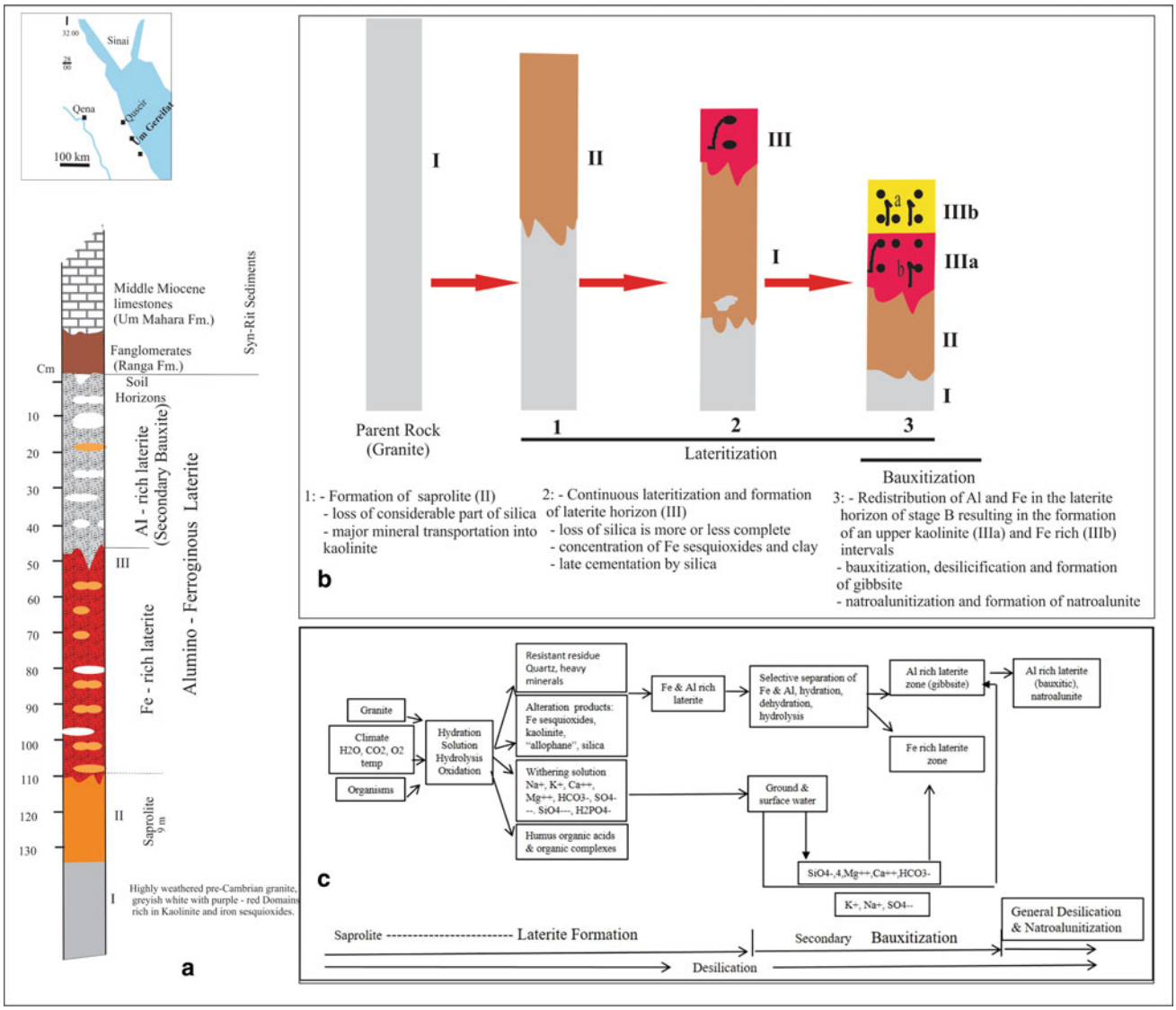

Fig. 24 **a** = Vertical lithostratigraphic profile of Um Gherifat alumino-ferruginous latosol, Red Sea Zone. **b** and **c** = Shematic illustrations of the concluded stages of lateritization, secondary bauxitization and natroalunitization processes and formation of Um Gherifat lateritic iron deposits, Red Sea Zone (after El Aref, 1993a)

granite into saprolite and Al and Fe–rich laterite (Fig. 24a). The saprolite horizon is composed of thoroughly decomposed and disintegrated granitic minerals being enriched in kaolinite mixed with Fe sesquioxides. The top laterite horizon (up to 1.4 m thick) is obviously divided into a lower Fe-rich ochreous zone and an upper Al-rich argillite (bauxitic) zone (Fig. 24a). The lower zone (up to 60 cm thick and of about 35% Fe) is formed of alternating continuous and discontinuous nodular layers and laminae of reddish to yellow ochres and brick red mudstones, showing abundant pelitomorphic to microgranular textures, lenticular to patchy segregations of earthy goethite and kaolinite, massive glaebules, clay aggregates, intra-formational contortions, desiccations, spastoids, circum granular cracks, vertically arranged goethite concretions, goethite coatings and diffuse concentric layers of earthy goethite together with root molds and root hairs, and microcellular and alveolar textures. The uppermost yellowish to yellowish brown Al-rich zone (15–21% Al) is bauxitic in nature being composed entirely of nodular kaolinite and gibbsite with less abundant amorphous "allophane," natrualunite, goethite, and hematite. Worm burrows, tubular voids, shrinkage cracks, and load casts are very common in this zone. The extensive petrographic and geochemical investigations conducted by El Aref (1993a) led to recognition of the processes involved during the lateritization, bauxitization, natural unitization, and development of this laterite ore (Fig. 24b, c). The geologic setting of this latosol type encourages more intensive

explorations for similar deposits along the Pre-Cambrian-Phanerozoic unconformity surface in the eastern desert and Sinai.

4.2.4 Karst Economic Carbonate Stones (Karst Cave Fills, "Egyptian Alabaster")

Carbonate rocks cover about 54% of Egypt's area (Fig. 25) and represent extremely valuable raw materials for construction, cement manufacture, chemical, filler and paper industries, crushed rock aggregates and building and ornamental stones (The Guide Investment Map For Limestone Ore In Egypt, 2004–2006). The most important of which are the famous historical ornamental calcium carbonate stone, commercially known as "Egyptian Alabaster," which is extensively used since Early Dynastic times as pavements, wall lining, sacramental kingdom shrines, statuettes as well as small vessels, canopic jars, bowls and dishes, among other uses. The different exposed Egyptian Phanerozoic carbonate sequences are obviously punctuated by fossilized paleo-karst surfaces of different magnitudes, demarcating periods of carbonate rock exposing subjected to paleo-karstification processes, most probably contemporaneous with the northward retreat of the Tethyan paleo-shore lines (Table 1; Fig. 26). The recognition and verification of these paleo-karst surfaces are based on: (a) very systematic field observations with high-resolution stratigraphic measurements and careful delimitation of the underlying and overlying contacts and biozon facies association, with emphasis on outcrop, hand specimen, microscopic, and crypto-microscopic examinations, following up the depositional, marine digenesis, and subaerial telogenesis or supergenesis. (b) geochemical examinations and textural (chemical and or biogenic) evolution of the marine and freshwater textures, (c) isotope measurements to differentiate between marine and freshwater cements, and (d) quantitative morphometric identification of the Egyptian surface karst-related landforms at various scales and resolutions using field, remotely sensed data and geographic information utilities.

The economic potentiality of the recognized paleo-karst systems is accentuated by the concentration of some potential ore deposits as it has been explained in sections 3, 4, and 5 besides the "Egyptian Alabaster." In addition to these resources, karst reservoirs also host underground storage of water (e.g. the great Farafra and Siwa karst aquifers), subsurface oils and gases. Surface karst landforms form attracted geomorphic sites or geo-parks of great knowledge and cultural values. The "Egyptian Alabaster" is a karst product consisting of re-precipitated calcite intimately associated with red soils and collapse breccias. These karst precipitates comprise a well develop

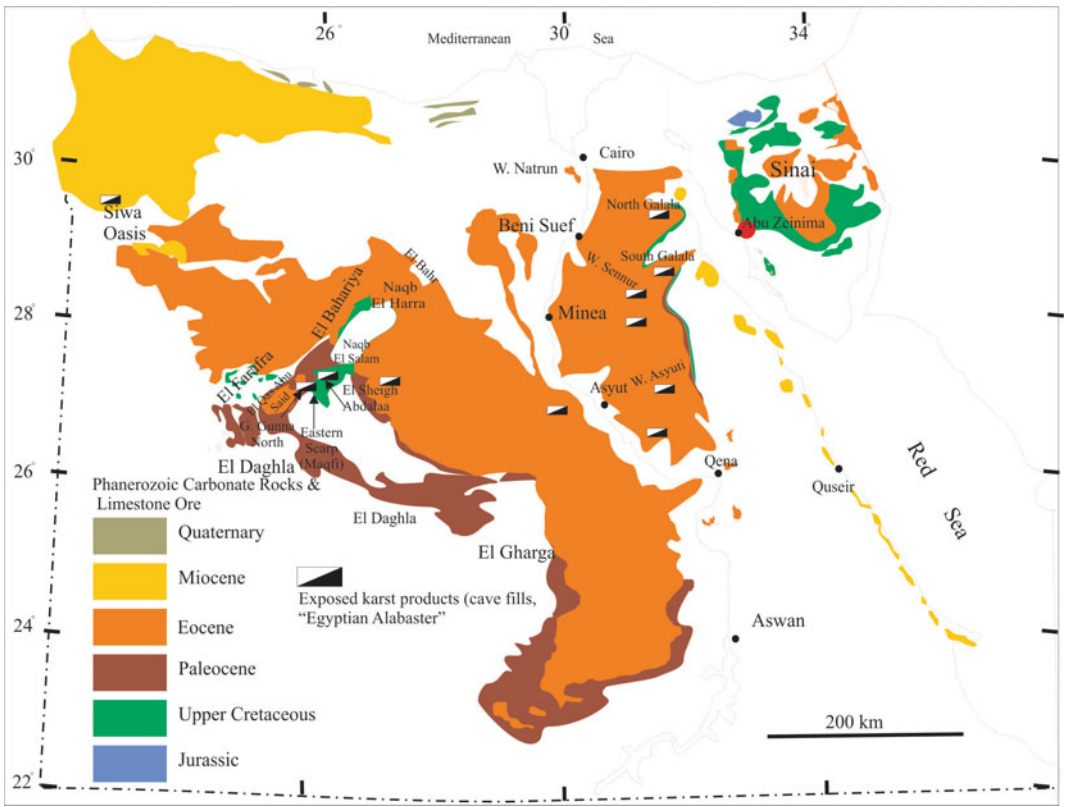

Fig. 25 Paleozoic carbonate rocks of Egypt and distribution of the exposed karst cave fills ("Egyptian Alabaster")

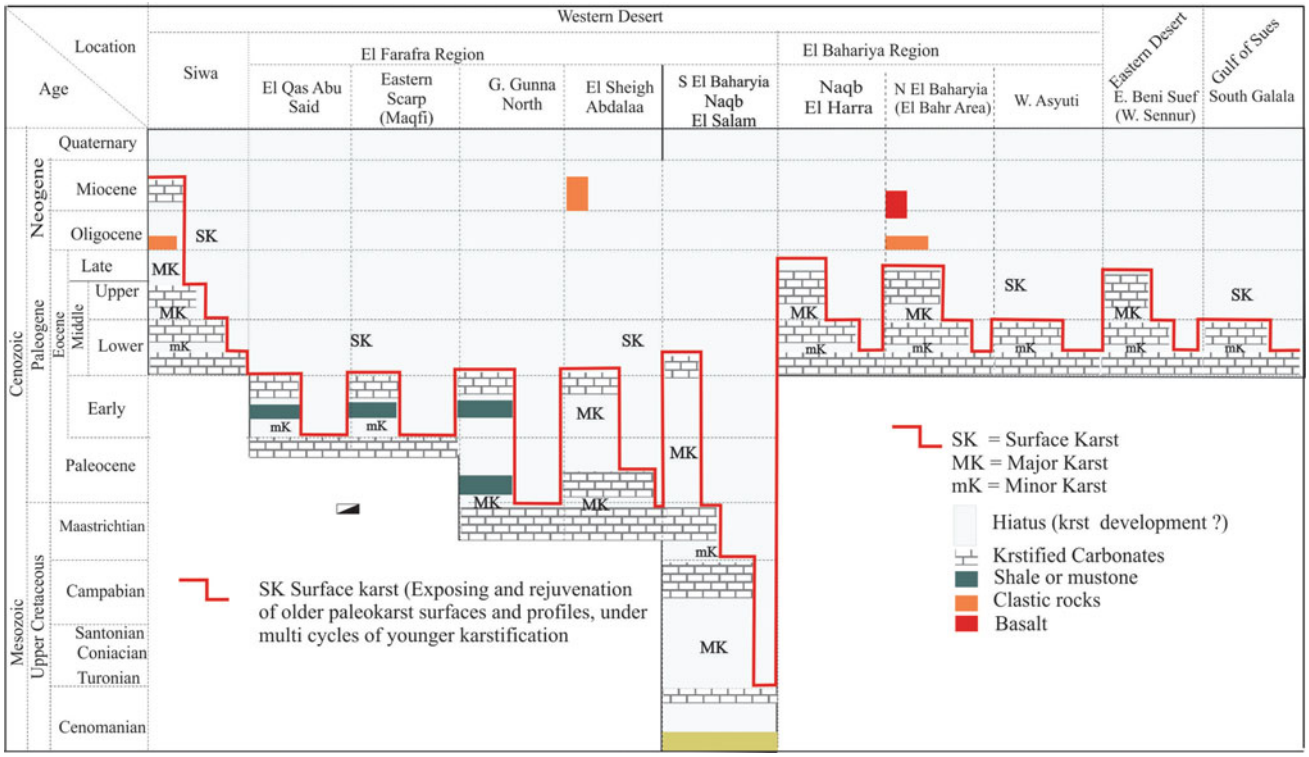

Fig. 26 Intra-, inter-formational, and surface paleo-karst surfaces of the Western and Eastern Deserts and Gulf of Suez (modified after El Aref et al. 2017a, 2017b)

paleo-karst profiles (e.g. Fig. 27) that formed along paleo-karst processes acted upon Cretaceous-Neogene carbonates, since Upper Cretaceous and until the last rainy periods of the Quaternary (Figs. 26, 27, 28, 29 and 30) and completely or partially fill solution openings and caves of variable scales. The re-precipitated cave calcite (flowstones) form crustified rhythmic botryoidal layers and stomatolitic laminae depositing on the internal walls and ceilings of caves and solution passages (Fig. 28a and b) or all around collapse breccia fragments forming cockade structure (Fig. 28c and d). The re-precipitated crustified calcite layers together with the collapse breccia fragments and red soils also form wide decorative textures such as crackle breccia, mosaic breccia, clast, and red matrix-supported chaotic breccia. Calcite crystals also form stalactites and stalagmites, spheriolites, geoids, cave pearls, and hopper structure. Unroofed karst carbonate fills and the associated red soil products hosted in different carbonate sequences of different ages (Upper Cretaceous-Miocene) are widespread as remarkable small exposures all over the Western and Eastern Desert (Figs. 25 and 28e, f). This confirms the findings of Halliday (2003) proving that potentially karstified rocks form the surface of much of Egypt and northern Libya.

The intensive field investigations on the Egyptian carbonate outcrops enable the recognition of the following types of paleo-karst surfaces (El Aref, 2000, El Aref et al. 2017a, 2017b and Fig. 26):

1. Drowned (fossilized or buried) paleo-karst surfaces, including
   (a) Inter-formational fossilized paleo-karst surfaces displaying break in sedimentation or great hiatus developed during periods of relatively long-lived exposure of carbonate sequences (paleo-highs) subjected to intensive karstifications.
   (b) Inter-formational and Intra-formational fossilized paleo-karst intervals displaying break of sedimentation and karstification during relatively short periods of exposure.
   (c) Fossilized depositional paleo-karst surfaces terminating meter-scale shoaling cycles.
2. Surface karst, responsible for the development of the present-day geomorphological karst landscape, characterizing the carbonate rock sequences all over the Egyptian Sahara, as well as progressive destruction and denudation of the outcropped fossilized paleo-karst features and the related deposits.

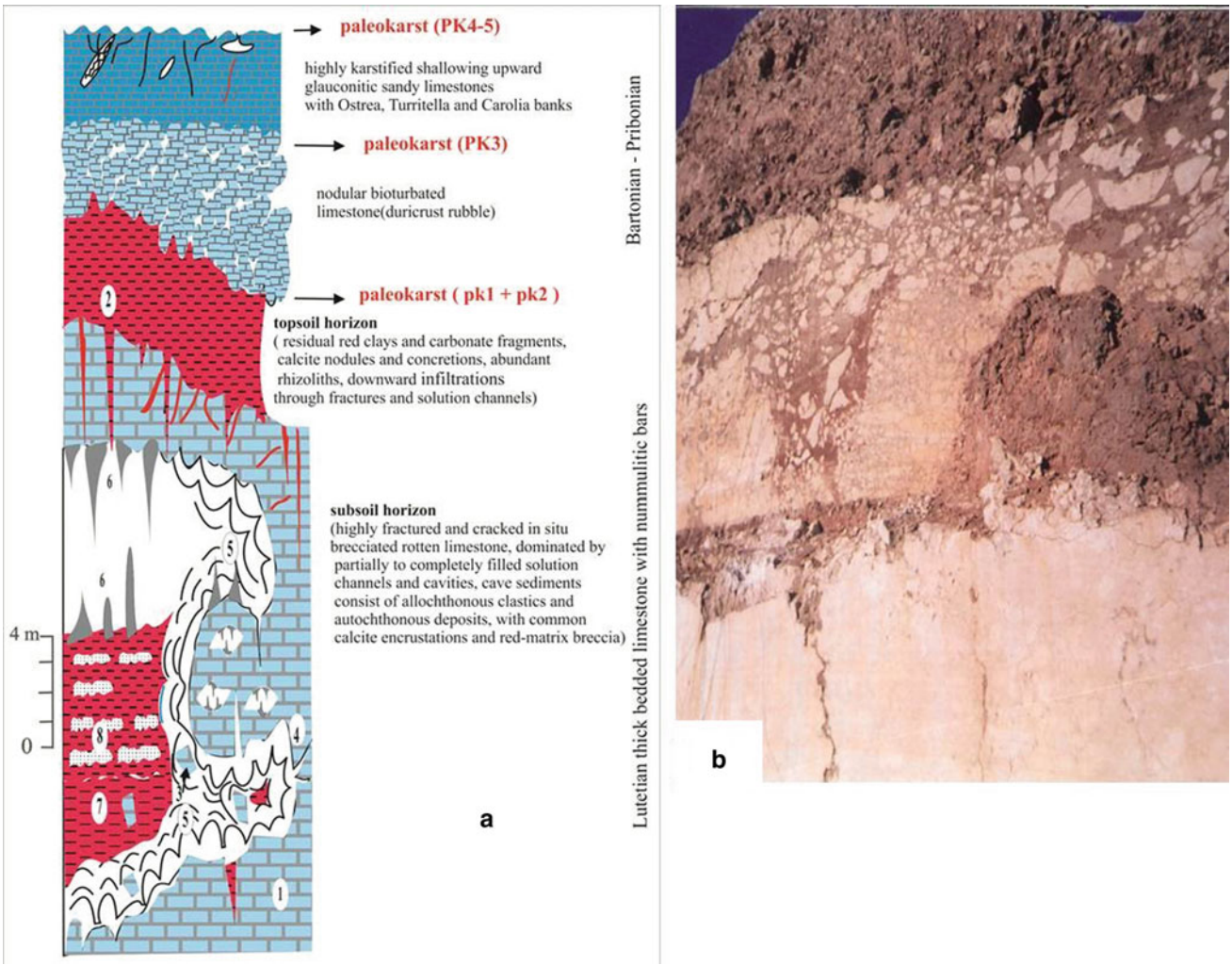

Fig. 27 **a** = Fossilized paleo-karst surfaces and related facies of Wadi Sannur karst region (Gharieb, 1998). 1 = host rocks, karstified limestone, 2 = fossilized sinkholes, 3 = collapse breccia, 4 = crackle breccia, 5 = crustified calcite, 6 = stalactites and stalagmites, 7 = laminated red soil, 8 = concretionary soil. **b** = An outcrop of representative intra-Eocene paleo-karst profile of south Galala, Gulf of Suez, showing the upper red soil, the middle breccia, and the lower karstified rock horizons

The recognized paleo-karst surfaces of the exposed Upper Cretaceous-Miocene carbonate sequences are shown in Fig. 26 and include:

I. Inter-formational fossilized major sequence boundaries (MK, Fig. 26), among which are:
   i. Cretaceous-paleocene (K/P) paleo-karst boundary,
   ii. Cenomanian-Middle Eocene unconformity,
   iii. Intra-Middle Eocene paleo-karst boundary,
   iv. Middle to late Eocene-Oligocene paleo-karst boundary.
II. Inter- and Intra-formational minor paleo-karst intervals (mK, Fig. 26).
III. Intra-formational fossilized (depositional) micropaleo-karst surfaces (mk, Fig. 26), and
IV. Surface paleo-karst (SK, Fig. 26).

Post-Eocene-Quaternary (?) karstification processes are clearly manifested by the continuous lowering and back wearing of the landscape of the exposed Cretaceous- Miocene carbonates through successive processes of karstification, and gradual unroofing, destruction and rejuvenation of the naked paleo-features and related karst products, including the "Egyptian Alabaster" (Fig. 28e and f). Intra- and post-Miocene karst events are reviewed in section (5). The karst-related red soils contain small vertebrate fossils of Late Miocene age (Gunnell et al., 2016; Mein & Pickford, 2010;

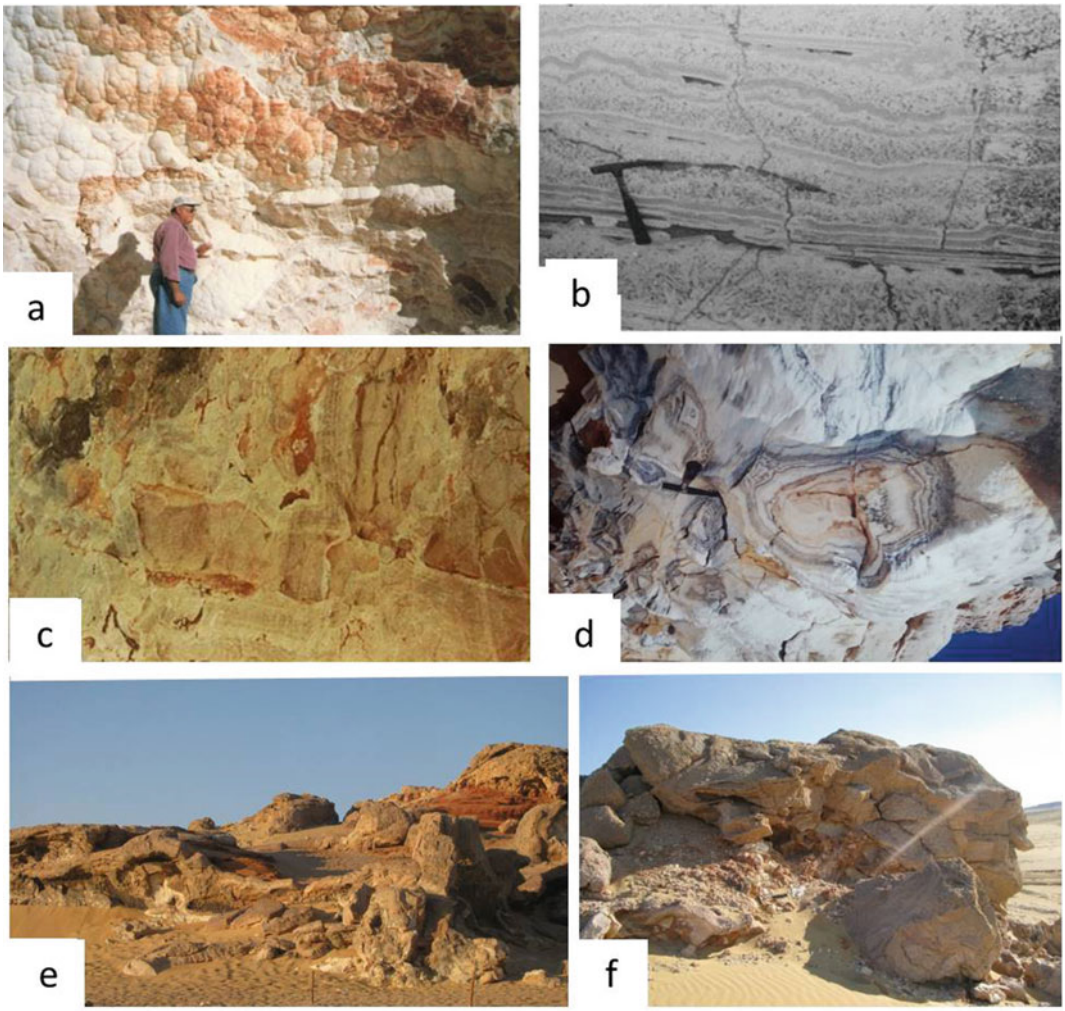

Fig. 28 **a** = Cave deposits entirely formed by crustified colloform calcite ("Egyptian Alabaster"). **b** = Polished slap of the "Egyptian Alabaster" consisting of successive stromatolitic calcite laminae. **c** and **d** = Cockade structures formed of crustified calcite layers deposited all around collapse breccia fragments (cave fill, "Egyptian Alabaster"). **e** = Partially unroofed elliptical cave filled by alternating layers of crustified calcite and red soil precipitates, El Sheigh Ab Dallah denuded paleo-karst, White Desert Protected Area, Western Desert. **f** = Residual mound of unroofed cave deposits being composed of red-matrix breccia enveloped by crustified calcite layers, El Bahariya-Farafra karst Territory

Pickford et al., 2006).Younger karstification processes are recorded along the Mediterranean coast (Halliday, 2003). The exposed karstified carbonates (e.g. Figs. 26 and 29a and b) are dominated by input, output, and residual polygonal karst landforms of allogenic and autogenic recharge areas, expressed by karst depressions (poljes, uvalas, sinkholes, dolines), Karren, tower, pinnacle, cone and cockpits, allogenic and blind rivers, sinking streams and degraded and rejuvenated karst systems, leaving behind remnants of cave fill precipitates (e.g. Figure 28e and f). The gradual lowering and back wearing of the present karst landscape could be reached by determining the paleo-erosion (paleo-karst) surfaces and related. Each of which is of consistent altitude range and demarcate certain paleo-erosion level resulted from an old erosion cycle (e.g. S1–S4 paleo-surfaces of Fig. 29c). The relatively old surfaces are topographically inverted through subsequent etchplanation and pedimentation processes involving destruction and stripping of the high-lying duricrusts, lateritic deposits and karst regolith's and the exposure of the bedrock forms; incision of valleys; slope and scarp retreat; gradual consuming of the residual hills, pedimentation and pavementation and development of younger exposed karst surface (S1–S4, Fig. 29c). East of the River Nile, The karst products including the "Egyptian Alabaster" are usually confined within vertical staked (amalgamated) paleo-karst surfaces and often truncated by younger post-Eocene karst event as well-expressed in Wadi Sannur area (Fig. 30). The detected main hiatus displayed by intra-Eocene fossilized paleo-karst surfaces, most probably coeval to those of the Western Desert. These are: (a) top

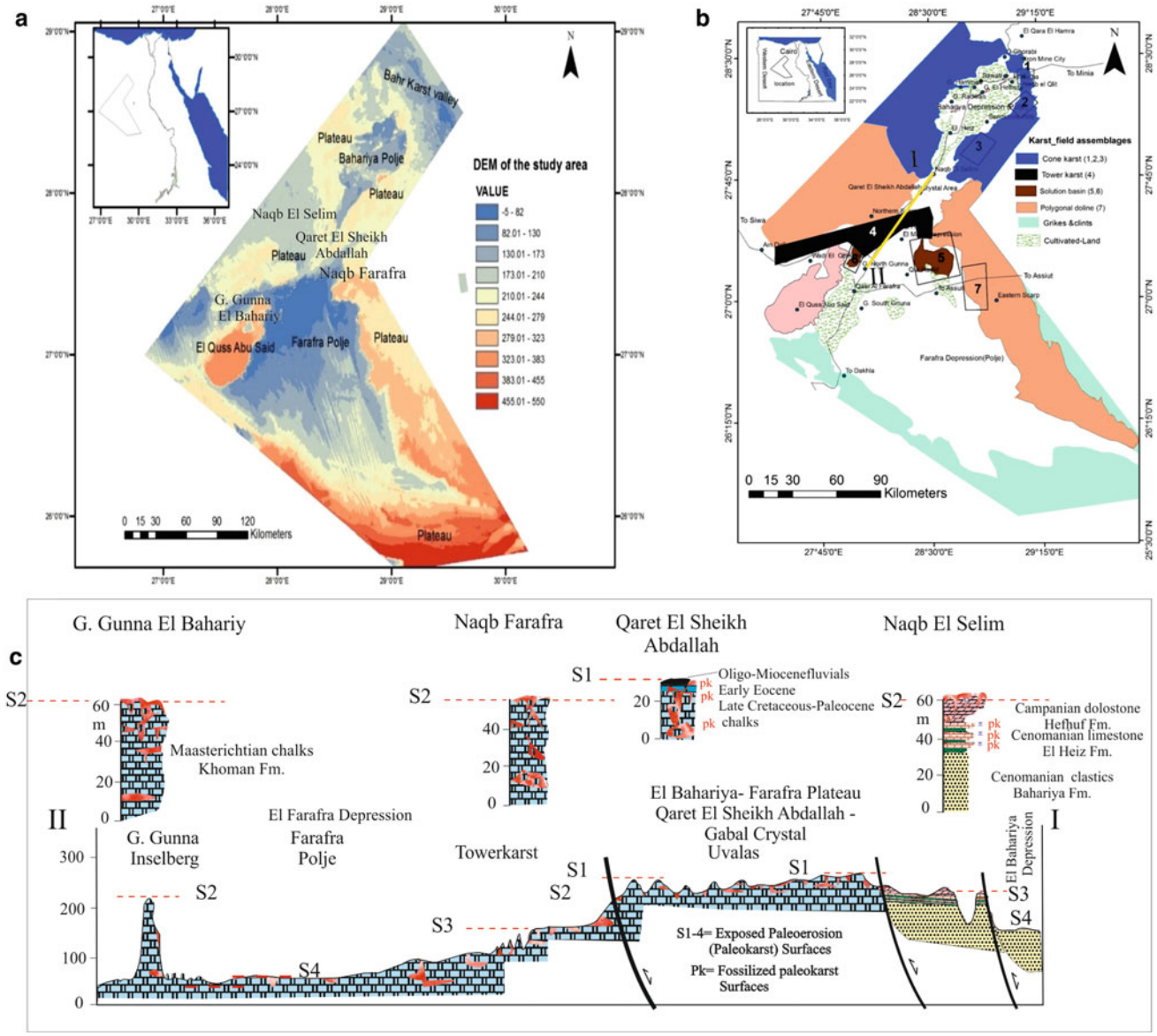

Fig. 29 **a** = GIS layer of the DEM and topographical features of El Bahariya-Farafra karst Territory showing the main karst depressions (El Aref, 2017a), **b** = karst map of El Bahariya-Farafra karst Territory showing the karst landforms zonation's (El Aref, 2017a), **c** = Sketch profile of the exposed paleo-karst surfaces (S1–S4) of El Bahariya-Farafra karst Territory, compiled and modified after Sokker (1991), Abu Khadra et al. (1987), El Aref et al. (2000, 2017a, 2020a, 2020b)

Lutetian-Bartonian paleo-karst, and (b) top Bartonian-Pribonian paleo-karst. The karstified carbonate sequences of this area and the interrupted paleo-karst surfaces were also subjected to post-dated intensive karstification in younger time.

General Comments and Recommendations

(1) The study results emphasize the importance of all types of unconformities especially paleo-karst sequence boundaries as potential sites for ore exploration. It is highly recommended to intensively examine such paleo-karst surfaces and the related soil products (in situ or transported) as a good environment for concentration of varieties of trace or major elements. Furthermore, Karst features are of high economic values for underground storage of water and certain oil and gas products.

(2) The surface landscape and the related features are now considered as a valuable and most significant geo-morphosites showing amazing complex paleo-karst landforms side by side with the present-day arid morphologies, which are very much attractive for geo-tourism and research activities. Therefore, the karst

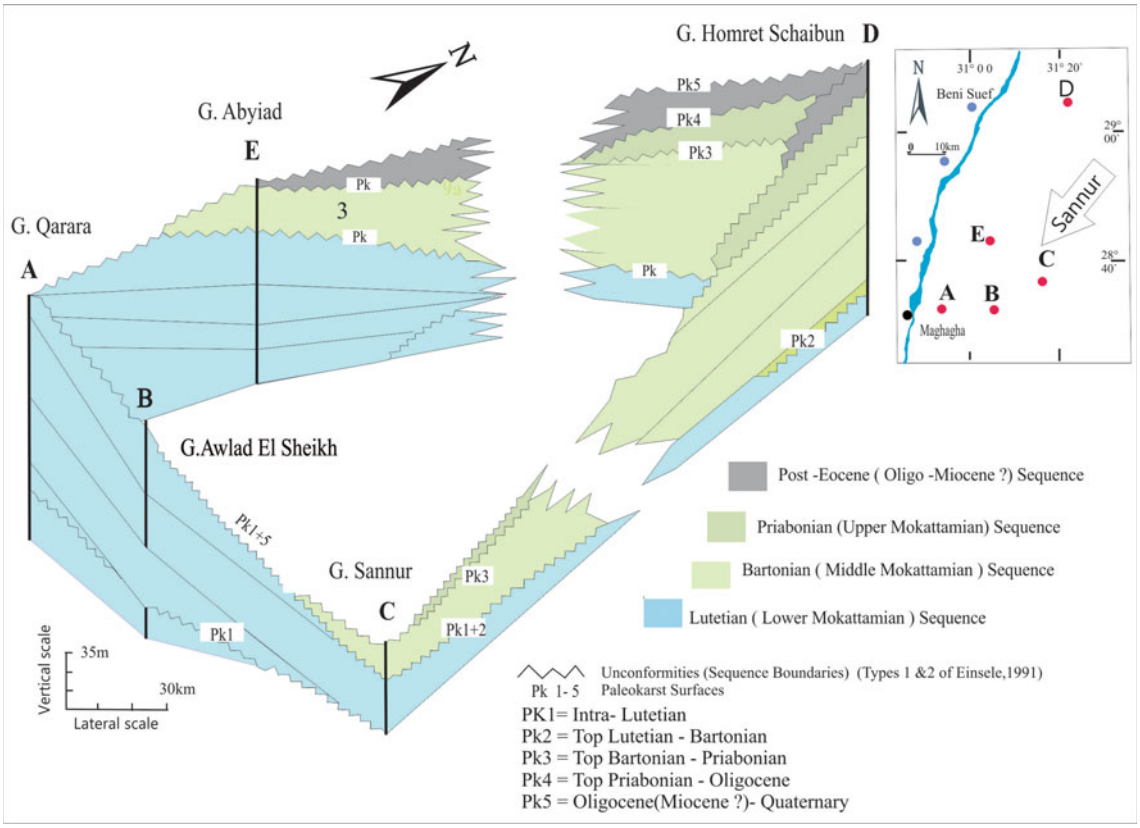

Fig. 30 Isometric panel diagram of Wadi Sannur karst region and the stratigraphic settings of the different time rock units and the associated facies and paleo-karst surfaces. **A**–**E** = measured sections (simplified after Gharieb, 1998, 2003; Philip et al., 1991a)

territories of Siwa Oasis, El Bahariya-Farafra, and Wadi Sannure are declared by Ministerial Decrees as Protected National Geological Parks.

(3) Also, and in order to enhance the economic potentiality of Karst, karst features must be included in every land use planning and urban development.

(4) For accurate determination of the ages of the successive karst events, an extended range of isotope measurements are required, taking into consideration the successive generations of the calcic crystals, as well as intensive paleontological studies on the karst sediments.

(5) Detailed information about the Egyptian karst morphology and karst products are extensively studied and discussed in an ample of publications and M.Sc. and Ph.D. projects, among which are: El Aref (1984, 1993b; 1996, 2000, 2005–2006), El Aref and Amstutz (1983), Ahmed (1986), Abdel Motelib (1987,1996), Lotfy (1989); El Aref and Ahmed (1986), El Aref and Refai (1987), El Aref and Lotfy (1989), El Aref et al. (1985, 1986, 1987, 1991, 1992, 1999a, 2001, 2006a, 2006b, 2017a, 2017b, 2021), Gharieb (1990, 1998, 2003), Sokker (1991), Philip et al. (1991a, 1991b), Halliday (2003), Salama (2006, 2010), Pickford et al. (2006), Mein and Pickford (2010), Hamdan and Lucarini (2013), Salama et al. (2014), Gunnell et al. (2016), Embabi (2004, 2018), Soliman (2018) and Hamdan and Hassan (2020).

5 Cenozoic Stratabound Ore Deposits

5.1 Neogene Rift-Related Ore Deposits

Neogene stratabound/stratiform ore deposits are intimately related to syn-rift facies and syn-rift paleo-karst surfaces (Figs. 1, 31, and 32; Table 1). The Neogene deposition under the Red Sea rifting dynamics led to the formation of a series of faulted clastic, carbonate, and evaporite facies association of variable stratigraphic setup and lateral distributions (El Aref, 1993b; Monetant et al., 1988; Philobbos et al., 1988). The main faulted rock association is classified into four main stratigraphic sequences punctuated by regional unconformities (Fig. 32). The basal Late Oligocene-Early Miocene proto-rift sequence is represented by the of continental clastics, paleosols, and basalt flows of the Ranga Formation in the Red Sea and the Abu Gerfan Formation in the Gulf of Suez. The succeeding Middle Eocene sequence (Um Mahara

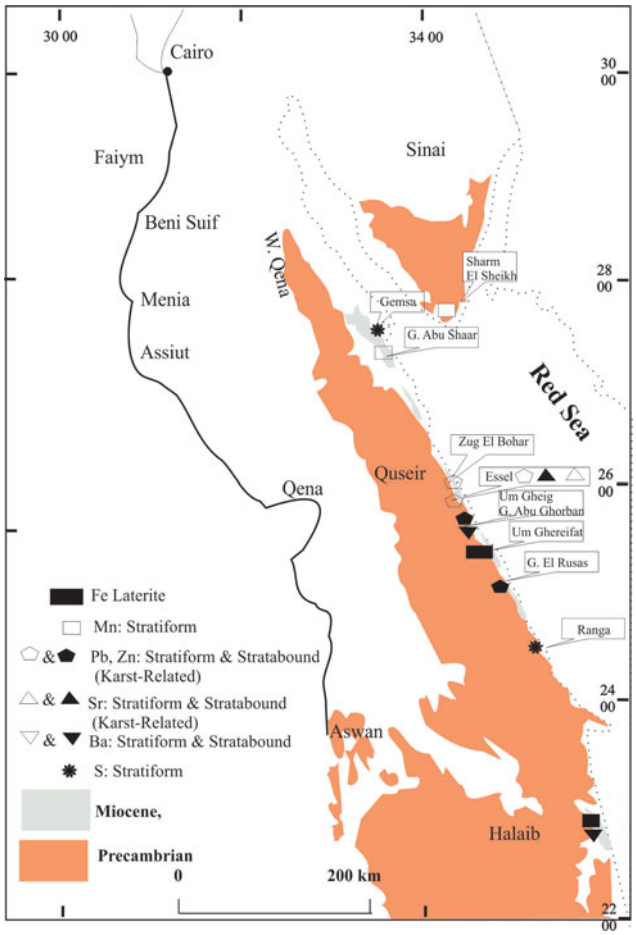

Fig. 31 Location map of the Red Sea Neogene rift-related stratabound and stratiform deposits

Sequence) overlies irregular relief of pre- and syn-rift units and consists of mixed clastics and carbonates of reefal, beach, lagoonal, tidal flat, subtidal-intertidal, and supratidal environments. The upper carbonates of the Um Mahara Formation (sequence) are truncated by a regional paleo-karst surface related to the main phase of rift faulting, postdating the development of this unit. Following this, paleo-karst event is the deposition of subaqueous and sabkha evaporites of the Middle to Late Miocene Abu Dabab sequence. South of Quseir, supratidal-intertiadal dolostones of the Upper Miocene-Paleocene? Um Gheig Sequence terminates the Neogene successions. It either overlies the Abu Dabbab evaporates or in some places (e.g. Um Gheig and Essel mine areas) rests directly on Um Mhahra rock association. Almost all the exposed evaporites and carbonate sequences show remarkable solution karst features and karst sediments, such as allogeneic dray rivers, conekarst and directed cockpits, karst linear ridges, surface depressions, and subsurface solution openings and cavities. The hill summits and hillside slopes are often mantled by relatively thick calcrete crusts or talus sediments derived from the karstified rocks, whereas, the solution openings and cavities are commonly filled by collapse breccia's with or without concentration of some mineral deposits mixed with autochthonous and allochtonous cave sediments. The development of the syn-rift intra-formational and surface karst features is most probably coincided with the evolution of the syn-rift river system of Issawi and McCauley (1992, 1993) and Guiraud et al. (2001) and the post-Late Miocene-Plio-Pliestocene heavy rainy periods (El Aref et al., 1985, 1986, 1987).

5.2 Oligo-Miocene (?) Mn Conglomerates

This stratabound Mn ore is recorded in Sharm El Sheikh, Sinai (Fig. 31) and previously described as post-Oligocene/pre-Pleistocene fault-related mineralized breccia ore type (Omara, 1959). However, El Aref (2020b) has clarified that this ore type represents the basal conglomerates of the syn-rift Miocene clastics of Abu Gerfan Formation of El Azabi and Eweda (1996). It needs more study and evaluation of its economic return.

5.3 Middle Miocene Stratiform Galena of Beach Environment

At Essel and Zug El Bohar mine areas (Figs. 31, 32, and 33), stratiform galena deposit is confined within the basal beach sandstones of the Middle Miocene Um Mahara sequence (Formation), overlaying the Pre-Cambrian rocks. The clastic galena bearing succession consists mainly of mature cross-bedded sandstones including abundant heavy minerals of beach environment. The galena shows typical stratiform and stratabound geometrical patterns forming layers or bedding structures closely symmetrical and concordant with the primary structures of the enclosing sandstones. Galena with or without cerussite constitutes the main cementing materials of the sandstones as they fill the pores or spaces left after diagenetic quartz overgrowths. Galena pore filling is undergrown with a microcrystalline quartz, forming network intergrowth patterns, and with cerussite forming zoning textures. In comparison with the well-led belts of the world, the geologic setting, the nature of the host rocks, the geometric distribution, and sedimentological features of this galena ore, are almost identical with the situation in the Cambrian sandstone around the (partly) buried Pre-Cambrian hills of mine Lamotte of the old Lead Belt, or even at Vibumum in the new Lead Belt of Missouri (USA), Lisvall (Sweden), Maubach-Michernich (Germany), Morocco, etc. (El Aref & Amstutz, 1983). The Egyptian Pb occurrences may represent the most recent stratiform-stratabound lead deposits of this type in the world known today.

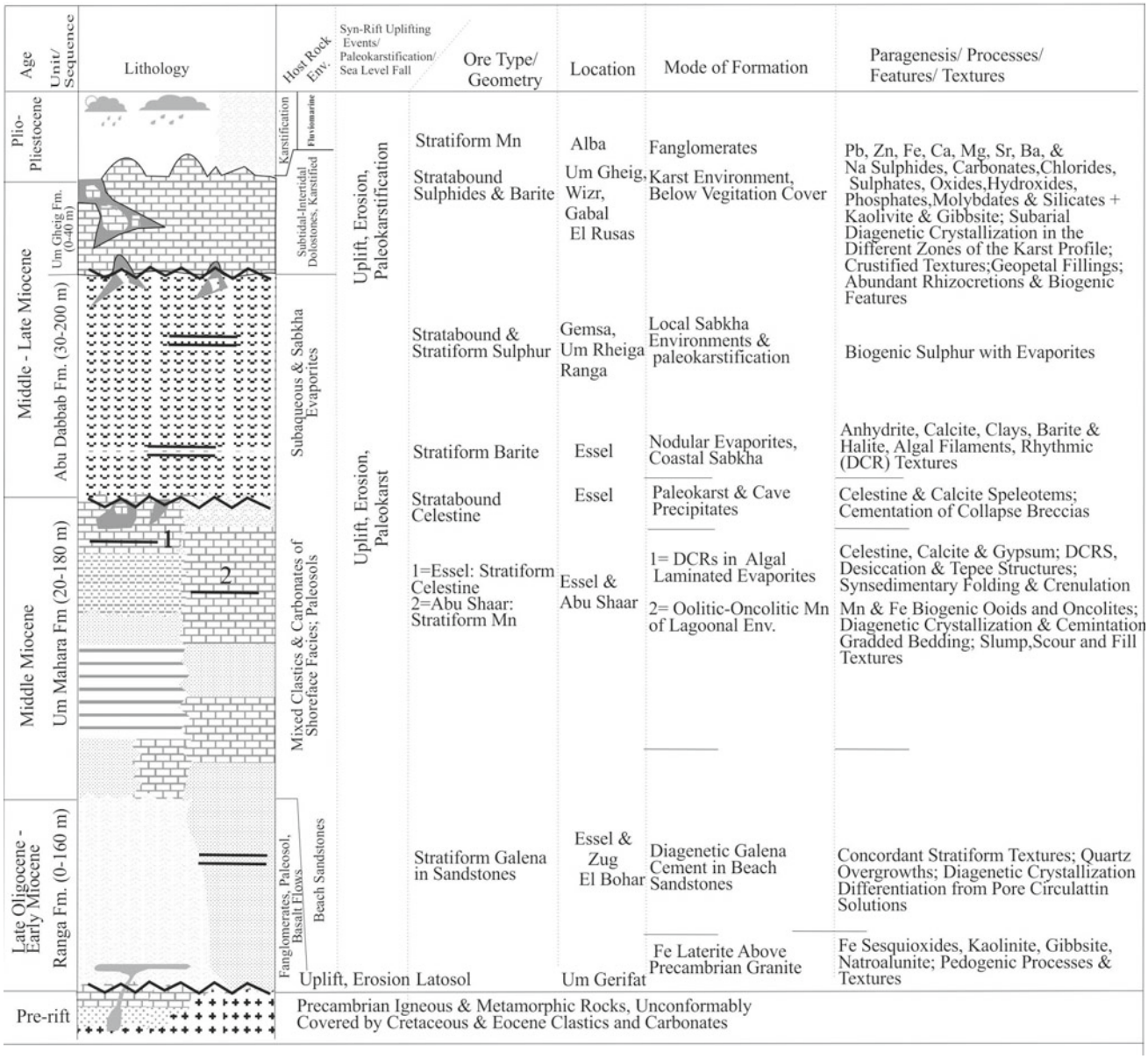

Fig. 32 Syn-rift sedimentation, uplifts, erosion, and related ore deposits in the Red Sea Coastal Zone between latitudes 24° and 28° N (El Aref, 1993b, 1996)

5.4 Middle Miocene Stratiform Oolitic-Oncolitic Mn Ore

This ore type forms a stratified oolitic-oncolitic Mn bed, up to 80 cm thick and of 35.8–45.14 MnO%, encountered within syn-rift Middle Miocene carbonates of reef, shoal, and lagoonal environments (Figs. 1, 34 and 35). The Mn-rich bed is formed by small-scale coarsening-upward cycles of Mn and Fe ooids and oncoids setting in a matrix of earthy manganese and carbonate mud (Fig. 35a and b). The zonation, mineral composition, and geochemical characteristics of this ore type are studied and discussed in detail by Abdel Motelib (1996). The Mn source and the depositional and diagenetic conditions prevailed during the ore formation are also concluded. El Aref (2020b) recommended further exploration survey in order to evaluate the economic potentiality of this ore type.

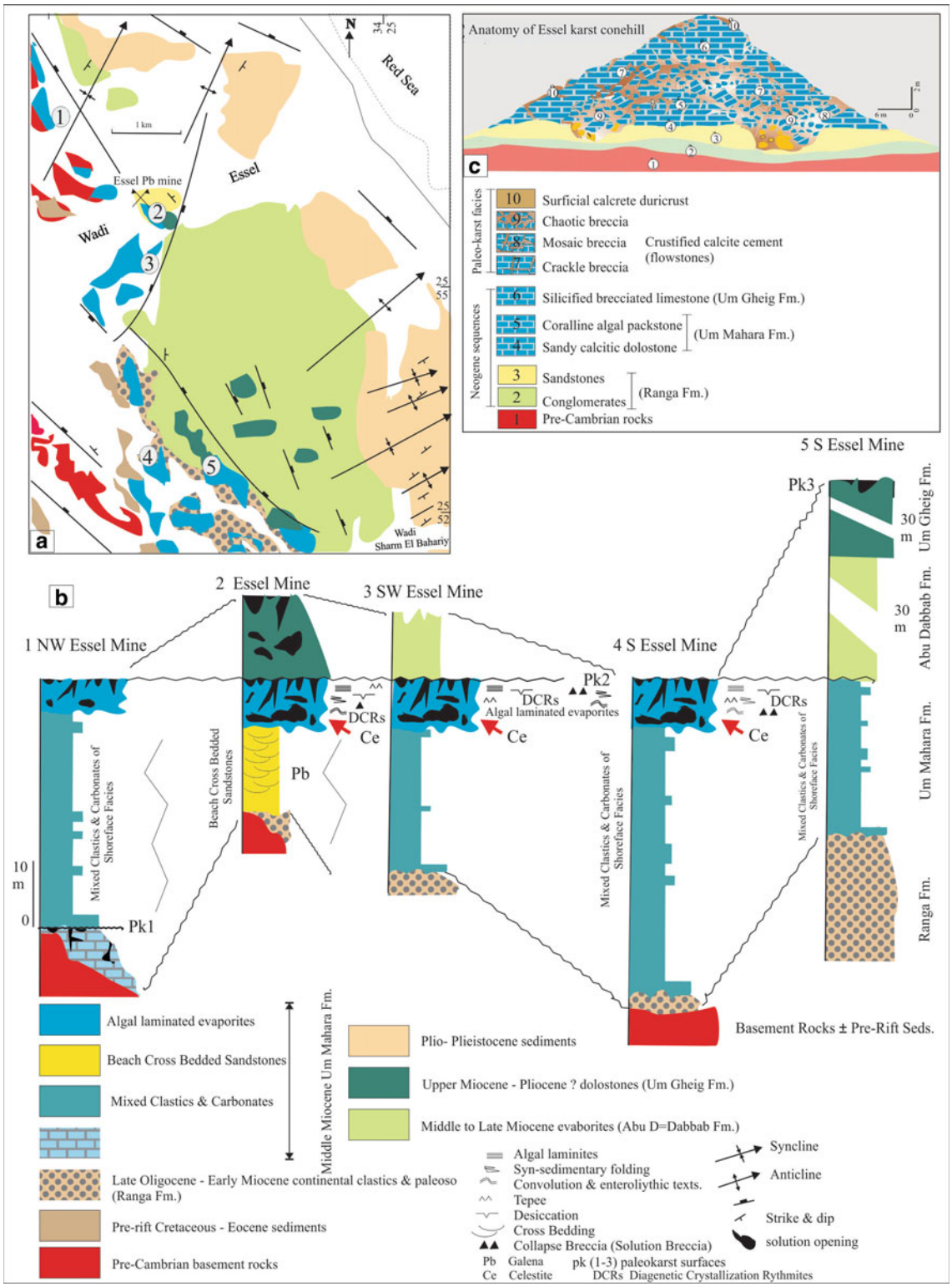

Fig. 33 **a** = Geological map of Essel-Wadi Sharm El Bahary area. **b** = Stratigraphic columns showing the stratigraphic settings of the recognized paleo-karst surfaces and the stratiform and stratabound Pb and Ce deposits, **c** = Schematic representation of isolated cone karst of the Miocene carbonates of Essel mine area, showing the internal cave fills (El Aref, 1993b)

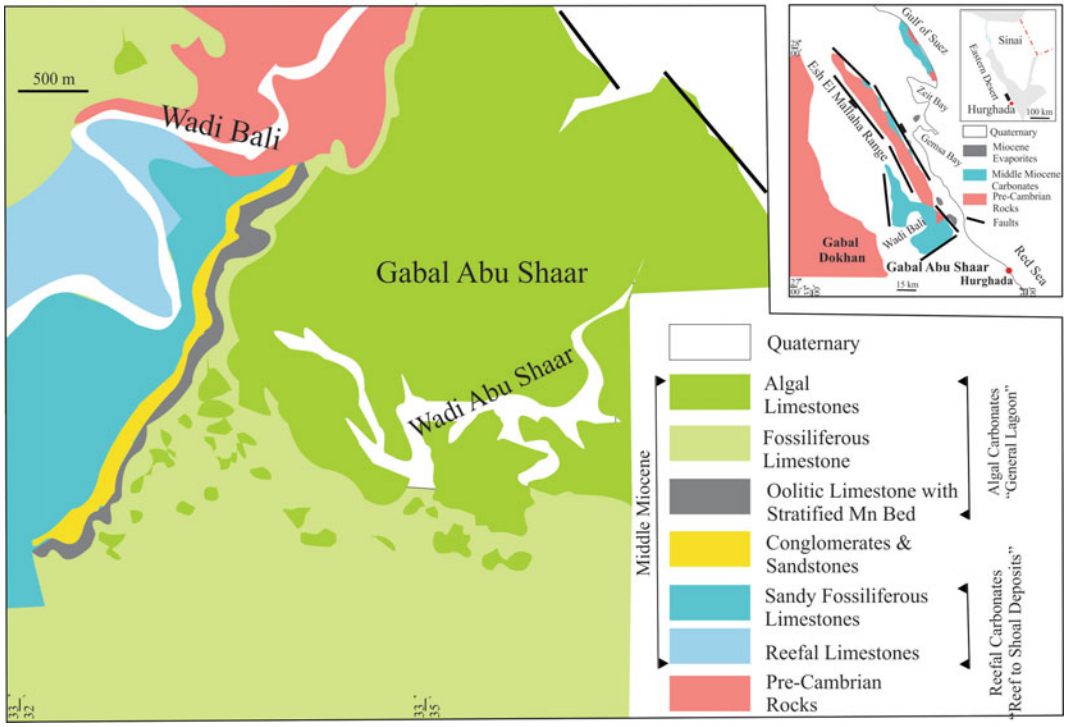

Fig. 34 Simplified geological map of Gabal Abu Shaar El Qebli (after Abdel Motelib, 1996), showing the stratigraphic setting of the oolitic limestone hosting the Mn bed

5.5 Middle Miocene Stratiform and Post-middle Miocene Stratabound Celestite, Essel Mine and South Essel Areas (Stratigraphic Sections 2–5, Fig. 33)

Resting on the tidal flat and galena bearing beach facies of Essel mine area, is a 6–10 m thick celestite bearing supratidal-intertidal facies, representing deposition in a near-shore restricted basin during a period of tectonic stability and constant sea level. This facies comprises alternated beds, 10–50 cm thick, of algal laminated and evaporitic limestones and thin massive calcareous mudstones, dolomitic in part. This succession is topped by paleo-karst surface (pk_2, sections 2 and 3, Fig. 33), where this surface is buried under either mudstones and evaporates of the Abu Dabbab sequence or the karstified bedded dolostones of the Um Gheig sequence. Some tectonic blocks of this facies remained exposed during the deposition of the succeeded Abu Dabbab and Um Gheig sequences and have clearly undergone later intensive weathering during a third karst event postdating the uplifting of Um Gheig sequence (pk3, Fig. 33). Two interesting types of celestite are recognized within this facies, namely (a) stratiform celestite of rhythmic pattern (assigned here as generation I celestite (Fig. 36a and b), and (b) stratabound intra-karstic celestite related to the post-Um Mhara paleo-karst event (generation 2 celestite, Figs. 36c and d). It is recommended to intensify the examination along the unconformity surface between Um Mahara and Abu Dabbab syn-rift sequences for the high probability of discovering new reserves of this ore type.

5.5.1 Middle Miocene Stratiform Celestite (Generation I Celestite, Diagenetic Crystallization Rhythmites, DCRs)

The primary lamination of this bedded facies is formed of 1 mm–3 cm couplets of alternating brownish stromatolitic laminae and celestite-rich laminae, giving rise to characteristic syn-sedimentary rhythmic patterns (Fig. 36a and b), similar to the diagenetic rhythmic texture of Fontboté and Amstutz (1980). This type of rhythmic lamination often forms connected or disconnected domes, up to 40 cm high, encountered within evenly laminated beds. Laminated fenestrae, desiccation cracks, tepee and enterolithic textures, convolute lamination and syn-sedimentary slump folds and faults are frequently observed within evenly laminated beds. Progressive desiccation forms aligned polygonal plates. Slump movement may affect several beds forming small-scale recumbent and tight overturned folds, up to 40 cm in thickness, most of them are flat-based with convex upper surface and usually arranged parallel to the strike of the host strata) Figs. 36 and 37). Some isolated wedge-shaped bodies become highly crumpled, over folded forming disharmonic patterns. The rhythmic characteristic of this celestite type is expressed by parallel algal mats and

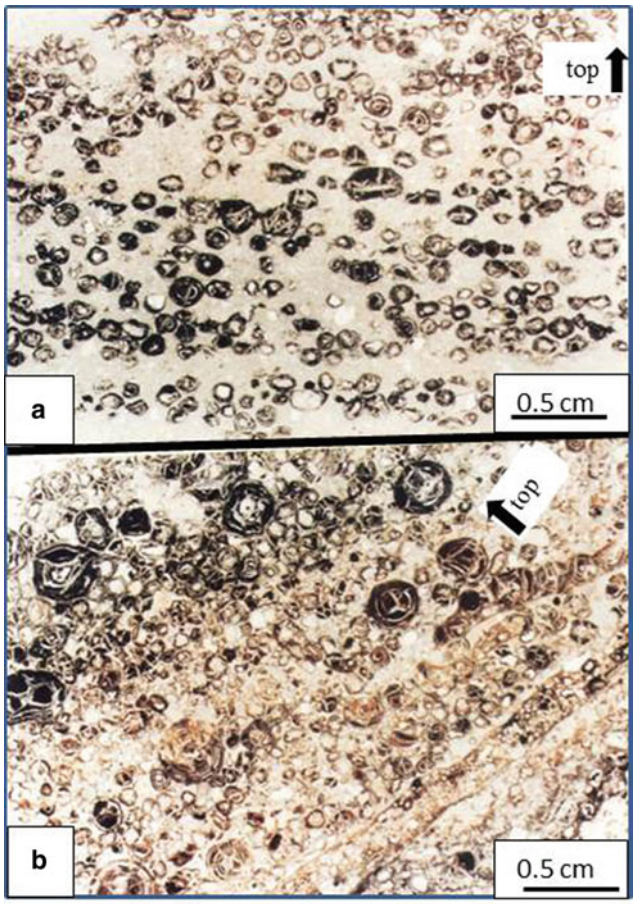

Fig. 35 (**a** and **b**) Thin microphotographs of fairly stratified oolitic-oncolitic Mn (**a**) and Fe (**b**) grainstones, with local grading in the framework components (Abdel Motelib, 1996)

spots rich in ultra-fine-grained celestite mixed with micrite, acting as starting sheets for further crystallization, as well as alternating rosettes or spherules, flat lens-like, fibroradiating coarse-grained celestite and gypsum crystals, growing all around the celestite rich spots or above and below the starting algal mats with idiomorphic termination toward the remaining pore spaces. The remaining pore spaces are usually filled by late coarse-grained celestite, blocky calcite, and gypsum crystals. The paleo-environment and syn-sedimentary fabrics of this Middle Miocene celestite type can be correlated with the syn-genetic celestite deposits elsewhere, e.g. Permian of Greenland (Scholle et al., 1990); Triassic of Bristol area, England (Nickless et al., 1976); Jurassic Hammelete West deposit, Germany (Brodkorb et al., 1982), Late Miocene celestite of Granada basin, Spain (Martin et al., 1984), and the celestite of Wenlock Olso Region, Norway (Olausson, 1981).

5.5.2 Post-middle Miocene Stratabound Celestite (Generation II Celestite, Karst-Related Cavity Filling)

The post-Um Mahara paleo-karst surface, hosting the second celestite ore type, is generally of cuspate form being pitted and rubbly in some places. Near-surface solution joints and channels are often connected with solution cavities of variable diameters (Figs. 36c, d and 37a–c). The solution features show successive stages of widening as a result of dissolution under vadose or transitional vadose-phreatic conditions possibly under progressive lowering of the paleo-water table. Karst effects may extend down to the contact between the hosts karstified celestite-bearing facies and the underlying subtidal-intertidal facies association. Re-precipitation of coarse-grained calcite and celestite (generation II celestite) together with internal geopetal sediments caused partial to complete filling of the intergranular spaces between solution and collapse breccia fragments and the megascopic and microscopic solution openings or may form asymmetrical fringe growing preferentially downwards into open spaces (Figs. 36c, d and 37a–c).

The karst-related calcite and celestite constitute stalactites, stalagmites and flowstones composed of radiaxial fibrous mosaic, bladed and wedge-shaped crystal growing perpendicular to the roofs and floors of the solution features (Fig. 36c–d). These crystals often show increase in size and pyramidal or comb structure against the internal geopetal sediments (mainly a mixture of silt-sized calcite and celestite particles and red-stained calcareous mud), and/or late coarse-grained blocky calcite crystals.

5.6 Middle to Late Miocene Stratiform and Stratabound Barite

The Middle to Late Miocene evaporite sequence includes small-scale occurrences of stratiform barite layers and stratabound barite buckets widely distributed within the intercalated thin dolostone layers. The stratiform barite layers are confined to restricted sabkha facies (Abdel Wahab and Ahmed, 1987), while the stratabound barite fills solution features as well represented in Gabal Abu Ghorban, south Um Gheig mine area (Fig. 38). In this site, barite exhibit well-defined geometrical rhythmic patterns, being composed of rhythmic alternations of dark and light bands and streaks (Fig. 38). The rhythmic characteristics of this barite type are due to repetition of three subsequent generations of crystallization. Generation I (corresponding to the starting sheets of Fontboté and Amstutz, 1980) is represented by dark

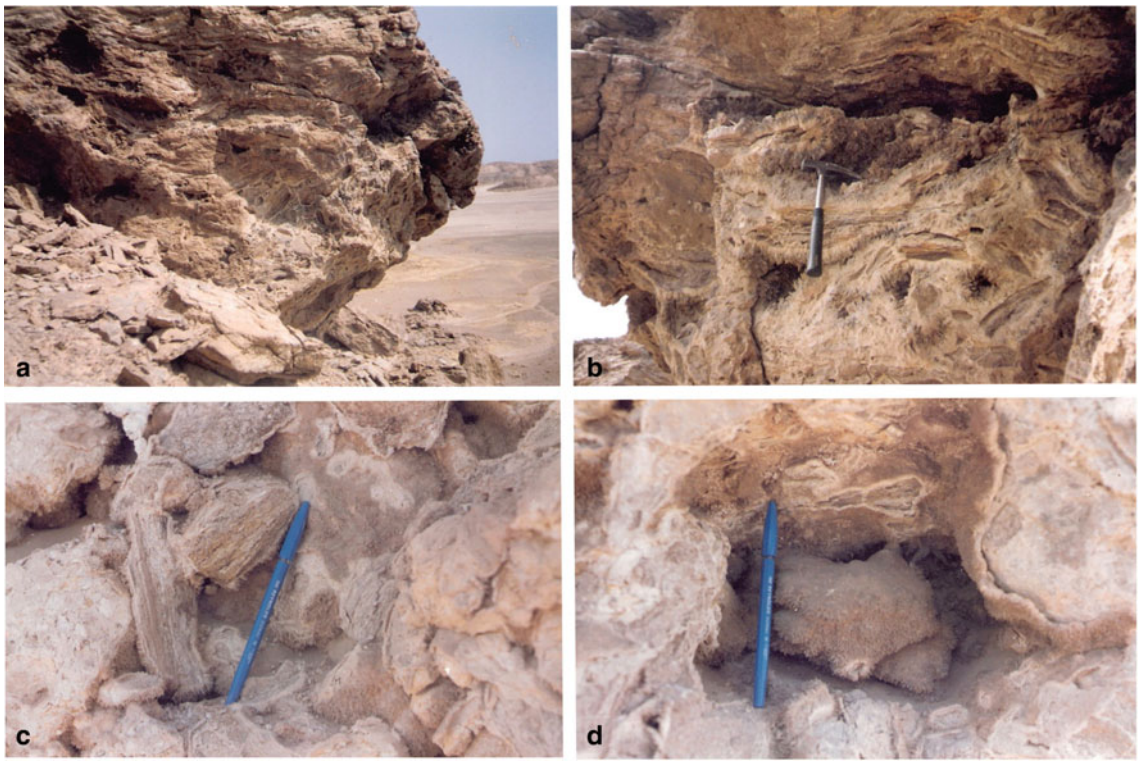

Fig. 36 (**a**–**d**): Field photographs of the stratiform rhythmic celestite (**a**, **b**) showing enlarged solution openings features with precipitated calcite and celestite. **c** = collapse breccia of laminated rhythmic celestite cemented by large celestite and calcite crystals. **d** = solution cavity coated by celestite and calcite

bands, streaks, or spots being composed of cloudy aggregates of fine-grained dolomite together with algal filaments and cellular organic materials. Generation II forms the major parts of the rhythmic light bands consisting of barite crystals symmetrically arranged in bipolar patterns with idiomorphic terminations growing on both sides of generation I. Generation III is displayed by the remaining empty spaces left by generation I which are partially lined or completely filled with celestite, calcite, and/or felty anhydrite. The geologic setting and geometry of this barite type indicate development during "syn-diagenetic" or syn-supergenesis crystallization generations in restricted karst environment. The record of these barite types within the Middle to Late Middle Miocene evaporates of the Abu Dabbab sequence may encourage further and intensive exploration for similar and more promising barite occurrences in this stratigraphic and lithologic evaporitic interval, widely cropping out along the whole Red Sea Coastal Zone.

5.7 Middle to Late Miocene Stratiform and Stratabound Biogenic Sulfur Deposits

Sulfur deposits associated with bituminous materials and/or surface oil seepages are confined to sabkha stromatolitic carbonates and evaporites of the Abu Babbab sequence (e.g. Ranga and Um Reiga occurrences (El Aref, 1984 and Abdel Wahab and Ahmed, 1987) or the coeval Gemsa and Gabal El Zeit occurrences (Shukri & Nakhla, 1955; Wali et al., 1989 and Youssef, 1989). Sulfur has been long extracted from the range occurrence, where it forms as yellow stratiform layers confined to the middle unit of the Middle to Early evaporate section of this location (Fig. 39a and b), overlaying thick biogenic frambouidal pyrite layer and overlain by brecciated limestone. Sulfur, anhydrite, calcite, and bituminous materials are rhythmically arranged, showing well-defined syn-sedimentary and syn-diagenetic textures. The congruent arrangement and the sedimentary textures of these components (Fig. 39c) suggest deposition in a partially closed evaporitic system, under biogenic processes (bacterial metabolisms) and rhythmic crystallization differentiation during the diagenesis (El Aref, 1984).

5.8 Post-late Miocene Stratabound Pb, Zn Sulfides, and Calamine Ore

The stratabound Pb–Zn sulfide deposits of Um Gheig mine (Fig. 40) were extracted since the ancient Pharaoh Time as a main source for lead and zinc. Unfortunately, the mine is now closed and not declared for investment because of the sulfide depletion. The hole mineral assemblage of this mine

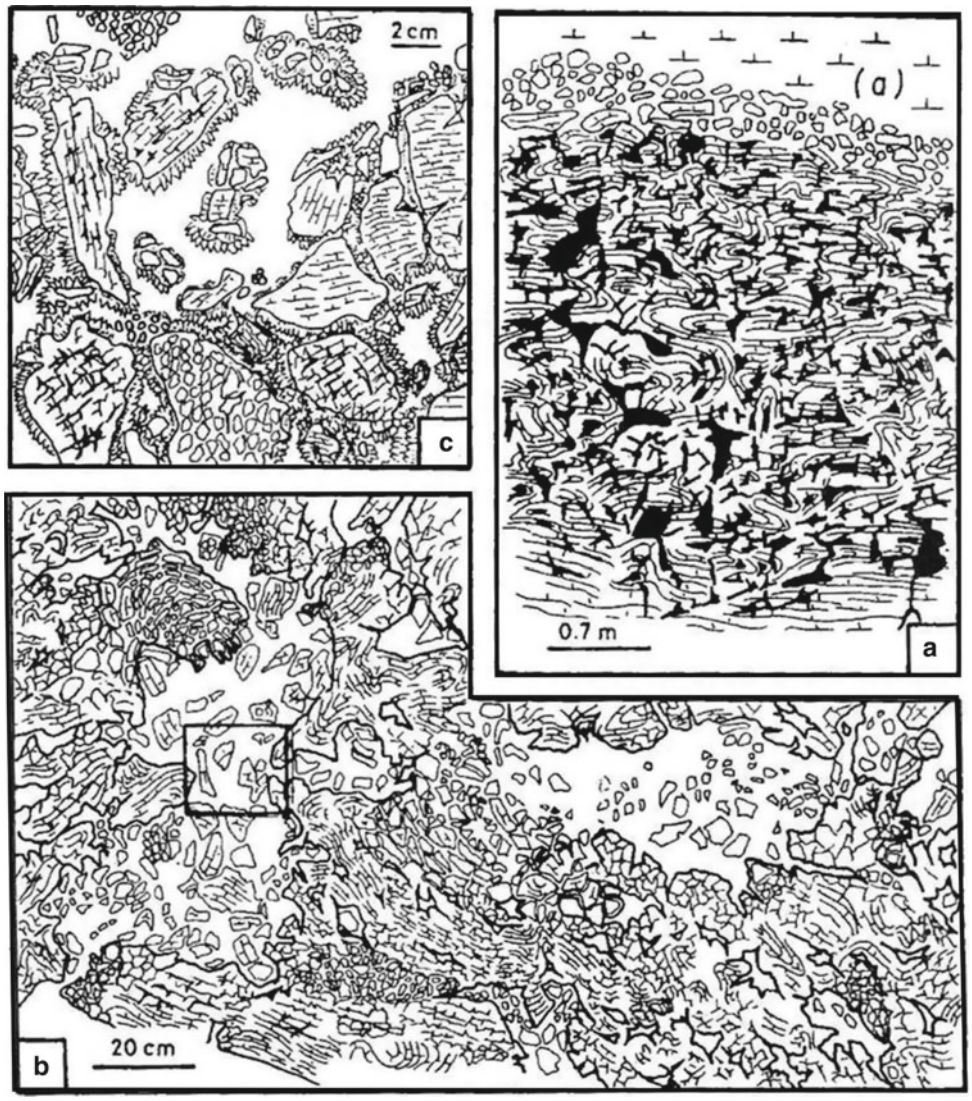

Fig. 37 (**a**–**c**): **a** = Representative cross-sectional drawing of the K2 karst surface beneath Abu Dabbab Fm., notice, the rubbly upper portion and the distribution of solution passages and cavities (in black). **b** = solution cavities and channels with intra-karstic celestite crystals. **c** = enlargement of the channel fill sediments squared in figure **b** showing in situ brecciating of large celestite bearing clasts and encrustation by new generations of calcite and celestite speleothems (from El Aref, 1993b)

is hosted in a fill mass developed along a major NW–SE post-Late Middle Miocene rift fault by water and gravity as a response of Plio-Pleistocene (?) paleo-karst event (El Aref & Amstutz, 1983). This ore type can be correlated to the upper karst-related sulfides of the Mississippi Valley Pb–Zn–Cu deposits (USA) and probably, representing the youngest Mississippi Valley ore type in the world. Among this deposit type are the karst-hosted sulfides of W. Wizr, Gabal El Rusas, Anz and Ranga occurrences. The fill mass of Um Gheig mine consists of chaotic breccia fragments derived from the Middle and Late Middle Miocene carbonates and evaporites (Fig. 40), embedded in soily clayey matrix, that mixed with chemical materials of lead and zinc sulfides, sulfates, carbonates, chlorides, phosphates, molibdates, and silicates as well as Fe oxides and hydroxides, silica, Ca, Mg and Fe carbonates and kaolinite. Three zones are recognized in this ore type (Fig. 40). Based on the Zn content and mineral assemblage, the oxidation (calamine) zone is differentiated into two horizons: (a) an upper varicolored ferruginous Zn-poor horizon (1.01–3.7% PbO and 1.88–3.22% ZnO) being composed mainly of red and yellow earthy ochreous sediments including quartz, hematite, goethite, alunite, jarosite, calcite, gypsum, kaolinite, illite, and montmorillonite, with variable proportion of lead and zinc oxides and (b) a lower white to gray zinc-rich horizon (43–58% Zn% and 2.0–6% PbO%) composed mainly of smithsonite, hydrozincite, and hemimorphite with variable contents of goethite, calcite, quartz, and lead bearing minerals (mainly cerussite). The recent development of worldwide beneficiation techniques for the treatment of the non-sulfide

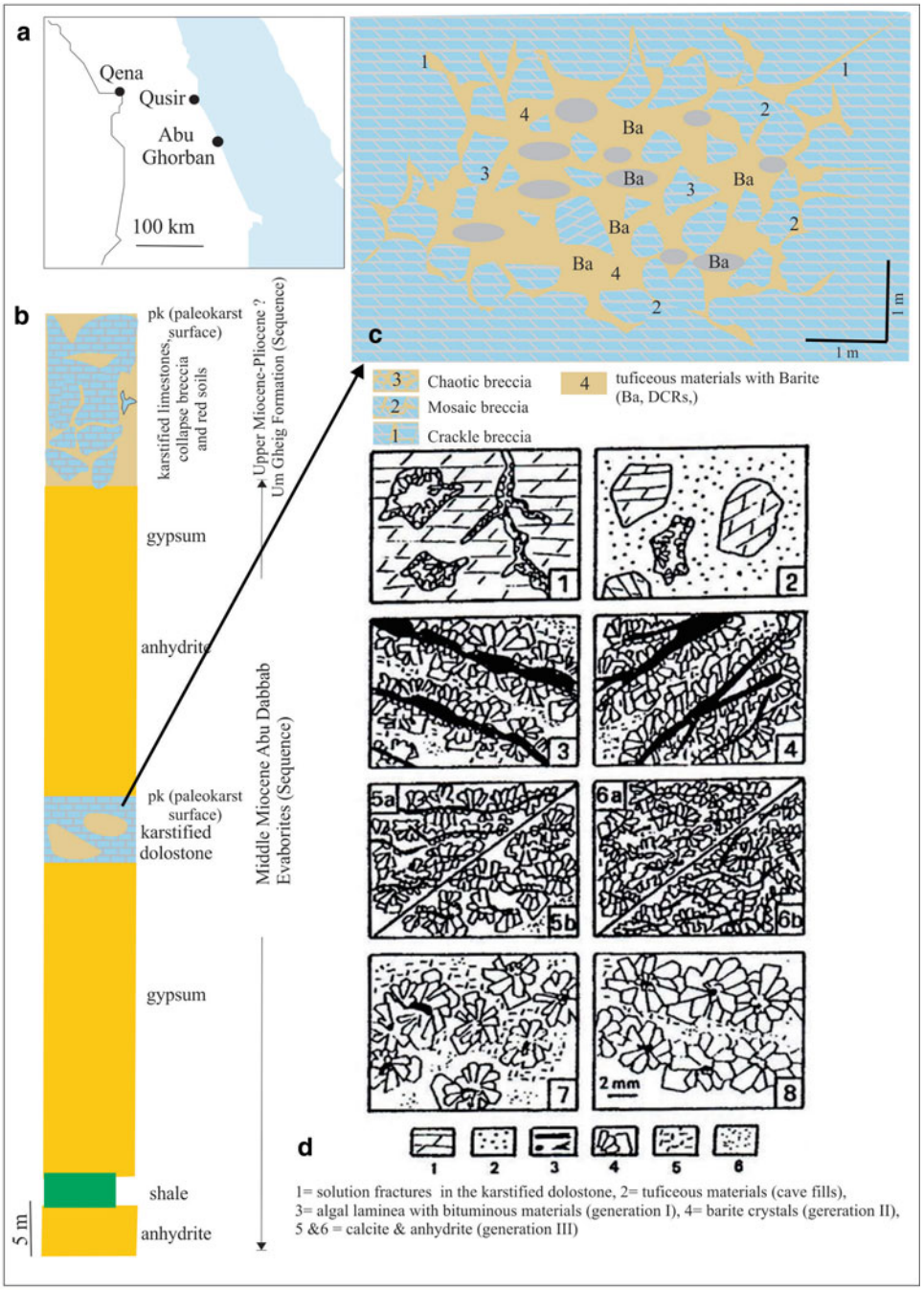

Fig. 38 **a**, **b** = Location and generalized lithostratigraphic section of Abu Dabbab Formation of Gabal Abu Ghorban. **c** = schematic drawing of the karst filling cavity. **d** = geometric distribution patterns of the barite: Type 1 = symmetrical filling of fractures within the host karstified dolostone. Type 2 = drusy filling of geodes, vugs, and grooves within the tufaceous matric of the cave. Types 3–8 = internal fabrics of the barite nodules, 3 and 4 = rhythmic alternations of dark (organic-rich) and light (barite) even (3) or branched (4) bands or streaks. Types 5 a and b = parallel undulated thin rhythmic streaks (5a) or thin interrupted laminae of wavy appearance or flaser-like structure (5b). Types 6 a and b = branched interrupted streaks (6a) and interconnected network pattern (6b). Types 7 and 8 = irregularly distributed (7) or connected spherulitic or orbicular patterns. Notice, the possible transitional evolutions of the rhythmic growing from type to type (after El Aref & Ahmed, 1986)

zinc ores through light into the commercial importance of this calamine ore type, which becomes a major source of zinc metal in this century (Large, 2001). Recent detailed investigations on the oxidation zone (calamine bearing zone) by Farag (2011) and Farag et al. (2011, 2012) confirmed the shearing of the calamine deposits of Um Gheig mine in many characteristics with the typical carbonate-hosted non-sulfide Zn ore (calamine ore type) all over the world.

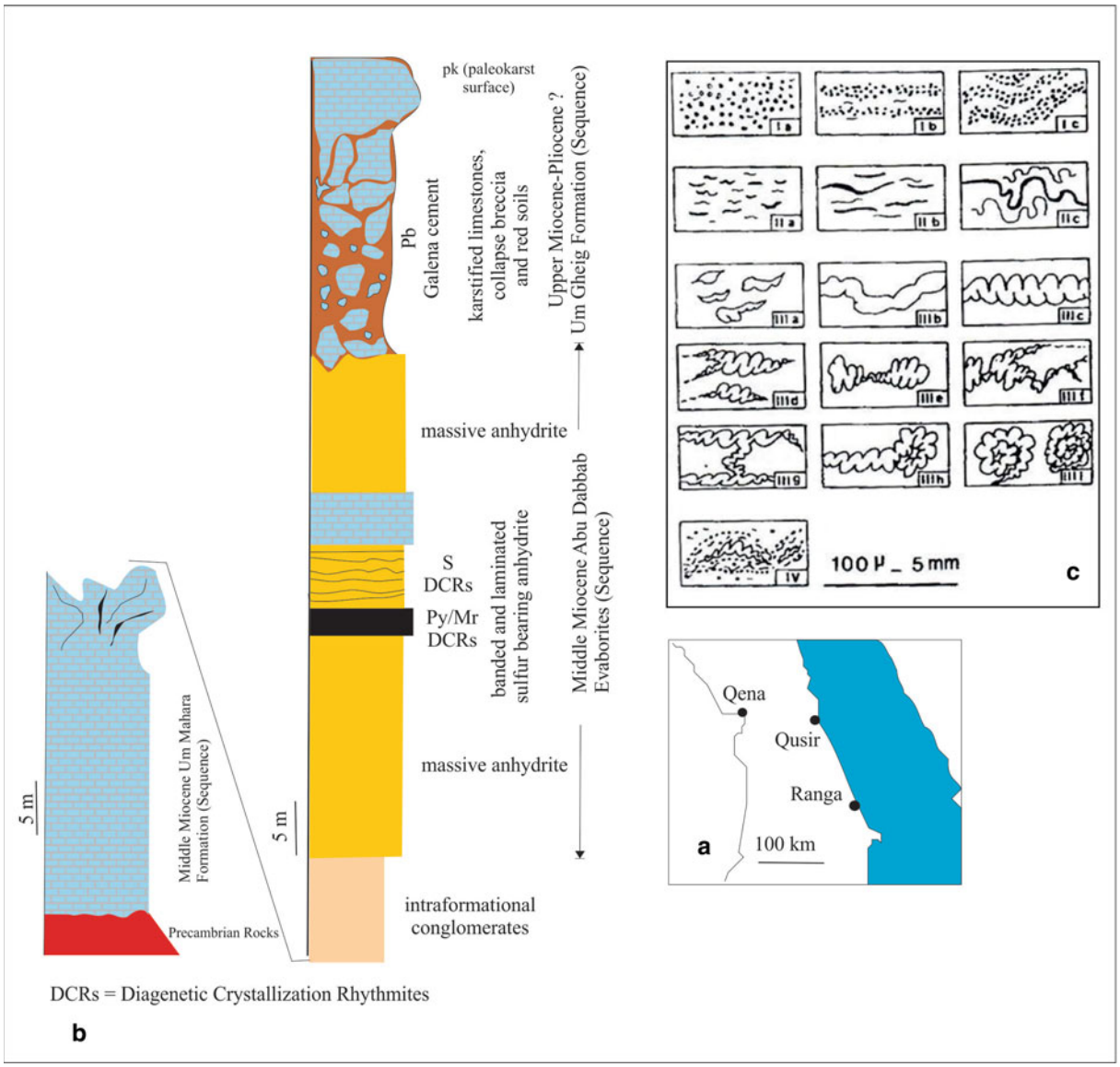

Fig. 39 Location map (**a**) and a composite lithostratigraphic section of the Miocene sequences of the Ranga occurrence (**b**), showing the position of the different ore minerals. **c** = the basic megascopic and microscopic geometric patterns of the sulfur with bitumen. Patterns I a–c = stratified sulfur dust of isotropic appearance (I a), stratified layered pattern (I b) or openly folded pattern (I c). Patterns II a–c = stratiform lenticels gently folded (II a, b) or disharmonically folded (II c). Types III a–i = show examples of derivations of deformed banded segregations as isolated nebulitic-like texture (IIIa) with lateral gradation to stratified complicated and folded bands drawn out in the center and outwards (III b–i). Type IV displays an example of an assemblage of different types in a gently folded arrangement (After El Aref, 1984)

The liberation and mineralogical investigations and mineral evaluation of representative samples of the Zn-rich lower horizon proved that higher degree of liberation (over 90%) between the valuable zinc bearing minerals and their gangues can be achieved below size 0.106 mm at inclination angle (25 1 min (Farag et al., 2012). At these optimum conditions, a concentrate assaying 63.4% ZnO was obtained with a recovery of ~ 93%.

Although the sulfides of Um Gheig mine are highly depleted, the mine should be re-considered as a non-sulfide zinc ore of high potentiality, highly recommended for investment as a calamine ore for the production of Zn metals. The geological setting of Um Gheig mine either as sulfide or non-sulfide ore types can be used as a guide for further exploration for similar deposits.

5.9 Post-Miocene Surficial Mn Deposits

Post-Miocene Mn and Ba deposits (up to 45% Mn) cover the eroded surfaces of Pre-Cambrian and Miocene rocks in Halaib–Elba-Abu Ramad land stretch (Figs. 1 and 31). The

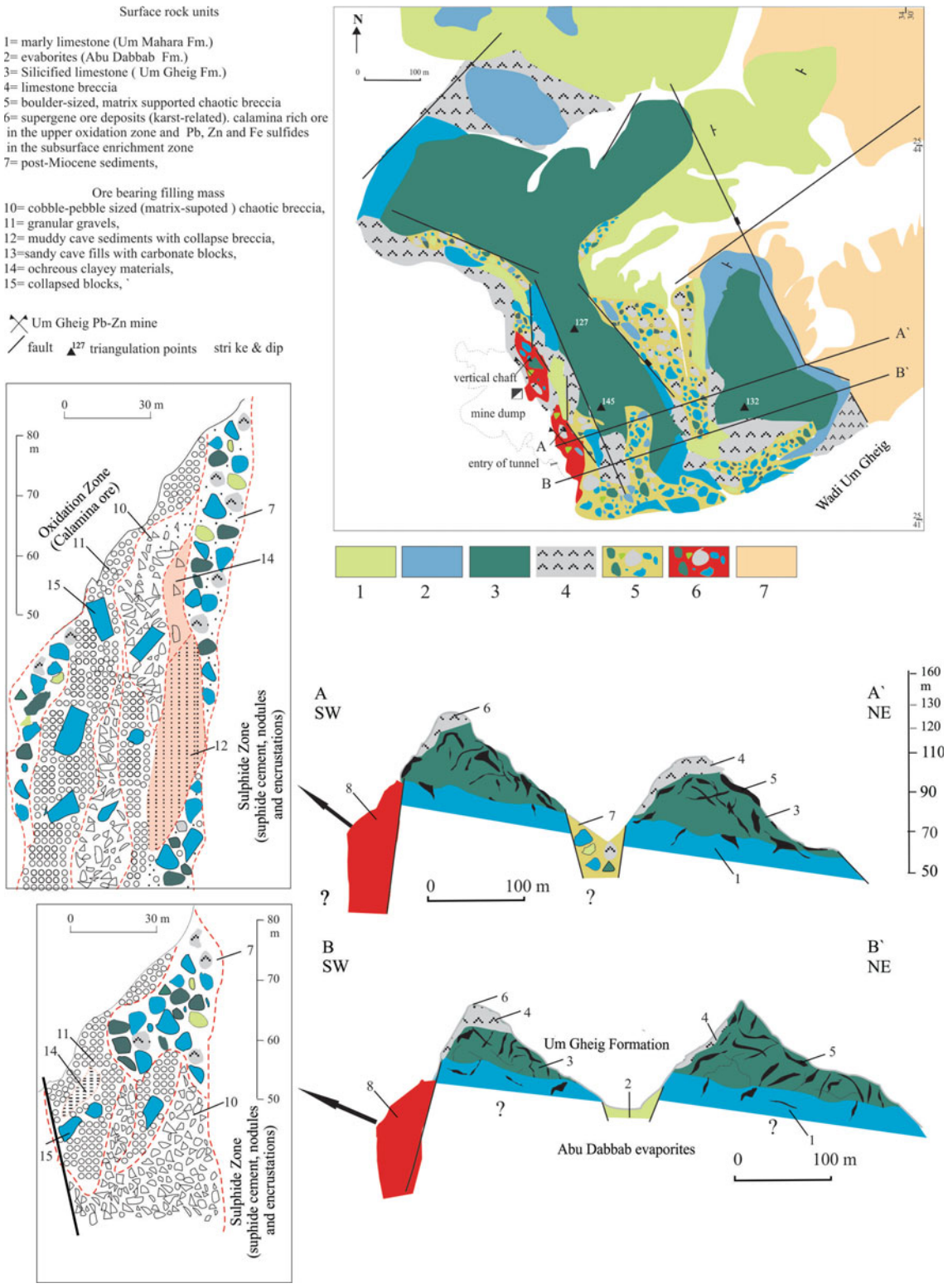

Fig. 40 Simplified geological map of Um Gheig mine area and A–A` and B–B` sketch profiles illustrating the grain size distribution, composition, and vertical zonation of the ore-bearing channel fill materials, (updated and modified after El Aref & Amstutz, 1983)

origin of these deposits is attributed to: (a) weathering of the Pre-Cambrian rocks and supergene deposition (El Shazly, 1957 and El Shazly & Saleeb, 1959), (b) epigenetic low-temperature replacement processes (Basta & Saleeb, 1971), and (c) deposition from deep-seated trans-magmatic ore-bearing solutions (Balkhanov & Razvalyayev, 1981). The surficial setting, mineral paragenesis, and textural characteristics of these deposits described by El Shazly and Saleeb (1959) and Basta and Saleeb (1971) led El Aref (1996, 2020b) to classify this ore type as a Neogene surficial deposits related to Plio-Pleistocene uplifting phase and weathering processes.

5.10 Post-Miocene-Quaternary (?) Surficial Conglomeritic Mn Deposits

This ore type is represented by small occurrences of Mn–Fe bearing rocks recorded in Wadi Araba, Gulf of Suez (Figs. 1 and 31) and suggested to be formed by Mn–Fe solutions of volcanic origin (Abdallah, 1961). The total estimated reserves of these deposits are ~ 4000 tons with 20–65 MnO% (Mineral Map of Egypt, EGSMA, 1979). These deposits form morphogenetic hard cap (surficial crust) of conglomeritic nature forming the summits of isolated small residual hills of Cretaceous clastics and/or Eocene carbonates and represent Post-Miocene to Recent surficial fluvial accumulation during the senile stage of Wadi Araba (El Aref, 1996, 2020b).

Acknowledgements This work is credited to the fruitful scientific cooperation with my colleagues and students at Cairo University, and from local and international universities, institutions, and scientific centers, where we formed together distinguished research teams. I offer them all my sincere thanks and gratitude as much I benefit from them and enjoy their company and cooperation. I must mention the extent to which we enjoy together scientific discussions and exchanges of ideas and knowledge procession to continue to address the difficulties and challenges. I am proud of them as co-researchers and co-authors in my publications or as I am co-author in their published contributions. Difficult here to mention them all and I invite to know them from the attached list of references.

References

Abdallah, A. M. (1961). Note on the manganese-iron deposit in Wadi Araba, Gulf of Suez. *Journal of Geology of the United Arab Republic, 5*(1), 77–79.

Abdallah, A. M. (1992). Paleozoic rocks in Egypt. *Technika Geologicznych Geosynoptyka, Geotermia, 3*, 1–12.

Abdallah, A. M., El Darwish, M. Aref, M. M., & Helba, A. A. (1992). Lithostratigraphy of the pre-cenomanian clastics of North Wadi Qena, Eastern Desert, Egypt. In A. Sadek (Ed.), *Proceedings of the First International Conference on Geology of the Arab World (1992). Geology of the Arab world* (pp. 255–282).

Abdel Motelib, A. (1987). *The cupriferous sediments in West Central Sinai, Egypt* [M.Sc. thesis]. Cairo University, Faculty of Science, Egypt (p. 194).

Abdel Motelib, A. (1996). *Geological and mineralogical studies of some manganese occurrences of Egypt* [Ph.D thesis]. Department of Geology, Faculty of Science, Cairo University (p. 304).

Abdel Wahab, S., & Ahmed, S. M. (1987). Evaporite facies and depositional environment of the Abu Dabbab Formation, Red Sea Coast, Egypt. *Geologie en, Mijnobouw, 66*, 121–138.

Abu Khadra, A., El Aref, M. M., & Sokar, A. (1987). Karst evolution and pedological processes along El Bahariya-El Farafra Road, Western Desert, Egypt. *Presented by El Aref in the 25th Annual Meeting of the Geological Society of Egypt* (Abstract).

Afify, A. M. (2017). *Ironstone occurrences in the northern part of the Bahariya Depression, Western Desert, Egypt: Geology, mineralogy, geochemistry and origin* [Ph.D. thesis]. Universidad Complutense De Madrid, Facultad De Cienias Geolgicas (p. 166).

Afify, A. M., Sanz-Montero, M. E., & Calvo, J. P. (2015a). Ironstone deposits hosted in Eocene carbonates from Bahariya(Egypt)—New perspective on cherty ironstone occurrences. *Sedimentary Geology, 329*, 81–97.

Afify, A. M., Serra-Kielc, J., Sanz-Monteroa, J. M. E., Calvoa, P., & Sallamb, E. S. (2015b). Nummulite biostratigraphy of the Eocene succession in the Bahariya Depression, Egypt: Implications for timing of iron mineralization. *Journal of African Earth Sciences, 120*, 44–55.

Ahmed, S. M. (1986). *Geological, stratigraphical and mineralogical studies on the Miocene sediments of the Red Sea Coast between Quseir and Marsa Alam, Egypt* [Ph.D. thesis]. Department of Geology, Faculty of Science, Cairo University (p 230).

Aita, S. K. (1996). *Geological, mineralogical and geochemical studies on some radioactive anomalies of the Paleozoic sediments of Um Bogma area, West Central Sinai, Egypt* [M.Sc. thesis]. Geology Department, Faculty of Science, Cairo University, Egypt (p. 262).

Baioumya, H. M., Ahmed, A. H., & Khedrd, M. Z. (2014). A mixed hydrogenous and hydrothermal origin of the Bahariya iron ores, Egypt: Evidences from the trace and rare earth element geochemistry. *Journal of Geochemical Exploration, 146*, 149–162.

Balkhanov, V. V., & Razvalyayev, A. V. (1981). The origin of the manganese deposits of the western shore of the Red Sea (in association with rifting). *International Geology Review, 23*(2), 162–166. https://doi.org/10.1080/00206818209467226

Basta, E. Z., & Saleeb, G. R. (1971). Elba manganese ores and their origin, South Eastern Desert, UAR. *Mineralogical Magazine, 38*, 235–244.

Bosworth, W., Darwish, M., Crevello, P., Taviani, M., & Marshak, S. (1996). Stratigraphic and structural evolution of Zabargad Island (Red Sea Egypt) since the Early Cretaceous. In A. Y. Sayed (Ed.), *The third International Conference on Geology of the Arab World* (pp. 161–190). Cairo University, Cairo.

Bosworth, W., Guiraud, R., & Kessler, L. G. (1999). Late Cretaceous (ca. 84 Ma) compressive deformation of the stable platform of NE Africa (Egypt): Far field stress effects of the "Santonian event" and origin of the Syrian arc deformation belt. *Geology, 27*(7), 633–636.

Brodkorb, M. K., Ramos, V., Barbieri, M., & Ametrano, S. (1982). The evaporate celestite-barite deposits of Neuquen, Argentina. *Mineral Deposita, 17*, 423–436.

Ciobotă, V., Salama, W., Tarcea, N., Rösch, P., El Aref, M., Gaupp, R., & Popp, J. (2011). Identification of minerals and organic materials of Middle Eocene ironstones, the Bahariya Depression, Western Desert, Egypt, by means of micro-Raman spectroscopy. *Journal of Raman Spectroscopy, 43*, 405–410.

CMRDI "Central Metallurgical Research and Development Institute, Helwan, Cairo, Egypt". (1998). Evaluation and beneficiation studies of Um-Hebal iron ore deposit, south Aswan, for blast furnace purposes. *Internal Progress Report, 1*, 92.

Darwish, M. (1994). Cenomanian-Turonian sequence stratigraphy, basin evolution and hydrocarbon potentialities of Northern Egypt. In A. Sadek (Ed.), *Proceedings of the 2nd International Conference on Geology of the Arab World, GAW* (Vol. 1, pp. 261–303).

Derocourt, J., Raicu, L. E., & Vrielynck, B. (Eds.). (1993). *Atlas Tethys, Pleo-environmental maps*. Gauthier-Villars (1307, 14 maps, 1 pl).

EGSMA "Egyptian Geological Survey and Mining Authority". (1969–1971). *Reserve calculation plan, El Bahariya Oasis, internal reports*.

El Aref, M. M. (1984). Strata-bound and stratiform iron sulfides, sulfur and galena in the Miocene evaporites, Ranga, Red Sea, Egypt (with special emphasis on their diagenetic crystallization rhythmites). In A. Wauschkuhn (Ed.), *Syngenesis and epigenesis in the formation of mineral deposits* (pp. 457–467). Springer.

El Aref, M. M. (1993a). Pedogenesis and related gibbsite and natroalunite formation in Um Gereifat area, Red Sea Coastal Zone, Egypt. *Egyptian Journal of Geology, 37*(1), 307–333.

El Aref, M. M. (1993b). Paleo-karst surfaces in the Neogene succession of Wadi Essel-Wadi Sharm El Bahari area, Egyptian Red Sea Coast, as indication of uplifting and exposure. In B. H. Purser & E. R. Philobbos (Eds.), *Proceedings of the International Conference on Geodynamics and Sedimentations of the Red Sea-Gulf of Aden Rift System, Cairo, 1993. Egyptian Journal of Geology* (Vol. 1, pp. 205–231).

El Aref, M. M. (1996). Phanerozoic stratifrm and stratabound deposits of Egypt; their stratigraphic, paleo-geographic, -topographic and -environmental controls. In A. Sadek (Ed.), *Proceedings of the 2nd International Conference on Geology of the Arab World, GAW (1994)* (pp. 97–124). Cairo University, Egypt.

El Aref, M. M. (1999). Achievements of the Egyptian iron exploration project (IEP, 1993–1997). In Hafez et al. (Eds.), *Proceedings of the 4th International Conference on Geology of the Arab World, GAW (1998)* (pp. 10–22). Cairo University, Egypt.

El Aref, M. M. (2000). Paleo-karst surfaces and Karst morphology of the Western Desert of Egypt, history and economic potentialities. *Presented in the International Conference on the Western Desert of Egypt: Geological Environment and Development Potentials, NARSS, EGSMA, BOSTON UNIVERSITY, UNDP, UNESCO* (pp. 17–20).

El Aref, M. M. (2001). Phanerozoic stratabound ore deposits. In *The metallogenic map of Egypt, scale 1:1000.000 (Dardir et al., 2001), Part Three* (pp. 26–43).

El Aref, M. M. (2005, 2006). Egyptian Karst morphology and processes, its economic potentiality and environmental impacts. In *Invited lectures, presented in the Annual Meeting of the Sedimentary Society of Egypt (2005) and the Annual Meeting of the Geological Society of Egypt (2006)*.

El Aref, M. M. (2020a). Iron ores in Egypt. In Z. Hamimi et al. (Eds.), *The geology of Egypt* (pp. 522–529). Springer Nature Switzerland, AG 2020 (Chapter 14.1). ISSN 2364-6438, ISSN 2364-6446 (electronic), Regional Geology Reviews, ISBN 978-3-030-15264-2, ISBN 978-3-030-15265-9 (eBook).

El Aref, M. M. (2020b). Egyptian manganese deposits. In Z. Hamimi et al. (Ed.), *The geology of Egypt* (pp. 570–578). Springer Nature Switzerland, AG 2020 (Chapter 14.9). ISSN 2364-6438, ISSN 2364-6446 (electronic), Regional Geology Reviews, ISBN 978-3-030-15264-2, ISBN 978-3-030-15265-9 (eBook).

El Aref, M. M., Abdel, W. S., & Ahmed, S. (1985). Surficial calcareous crust of caliche type along the Red Sea Coast, Egypt. *Geologische Rundschau, Sonderdruck, Geologische Vereinigung, Mending, 74* (1), 155–163.

El Aref, M. M., & Abdel Motelib, A. (2001). Geology, facies distribution and environments of the Carboniferous stratabound Mn deposits of Um Bogma region, Sinai, Egypt. In *Proceedings of the 2nd Conference on the Geology of Africa* (pp. 61–77). Assiut University, IA.

El Aref, M. M., Abu Khadra, A. M., & Lotfy, Z. H. (1987). Karst topography and karstification processes in the Eocene limestone plateau of El Bahariya Oasis, Western Desert, Egypt. *Zeitschrift für Geomorphologie. N.F. Gebrüder Borntrager, Berlin-Stuttgart, 31* (1), 45–64.

El Aref, M. M., & Ahmed, S. (1986). Diagenetic crystallization rhythmites (DCRs) of dolomite—barite—calcite in karst environment, Gabal Abu Ghorban, Red Sea Coastal Zone, Egypt. In R. Rodriguez-Clemente, Y. Tardy (Eds.), *Proceedings of the International Meeting "Geochemistry of the Earth Surface and Processes of Mineral Formation" held in Granada (Spain)*, March 16–22, 1986 (pp. 611–622).

El Aref, M. M., & Amstutz, G. C. (1983). Lead-zinc deposits along the Red Sea Coast of Egypt. In *New observations and genetic models on the occurrences of Um Gheig, Wizr, Essel and Zug El Bohar. Monograph series on mineral deposits* (Vol. 21, p. 103). Gebrüder Borntraeger.

El Aref, M. M., Awadalah, F., & Ahmed, S. (1986). Karst landform development and related sediments in the Miocene rocks of the Red Sea Coastal Zone, Egypt. *Geologische Rundschau, Sonderdruck, Geologische Vereinigung, Mending, 75*(3), 781–790.

El Aref, M. M., El Dougdog, A. A., & Mesaed, A. A. (1991). Landform evolution and formation of ferricrete duricrusts, El Heiz area, El Bahariya Depression, Western Desert, Egypt. *Egyptian Journal of Geology, 34*(1 and 2), 1–39.

El Aref, M. M., El Dougdog, A. A., & Mesaed, A. (1992). Petrography and diagenesis of the high-laying ferricrete of El Bahariya depression, Western Desert, Egypt. *Egyptian Mineralogist, 4*, 23–53.

El Aref, M. M., El Sharkawi, M. A., & Khalil, M. (1999a). Geology and genesis of the stratabound and stratiform Cretaceous-Eocene iron ore deposits of El Bahariya region, Western Desert, Egypt. In Hafez et al. (Eds.), *Proceedings of the 4th International Conference on Geology of the Arab World, Cairo University, Egypt. 1998. Geology of the Arab World* (pp. 450–475).

El Aref, M. M., El Sharkawi, M. A., & Mesaed, A. (1999b). Depositional and diagenetic microfabric evolution of the Cretaceous oolitic ironstone of Aswan, Egypt. Research Studies on Some Cretaceous Sequences of Egypt. *Geological Society of Egypt Special Publications, 2*, 280–312.

El Aref, M. M., Helba, A. A., & Saad, F. (2001). Lutetian ramp carbonate facies, hierarchy and environments, northeast El Bahariya depression. In *Proceedings of the 2nd International Conference on the Geology of Africa* (pp. 385–403). Assiut University, IB.

El Aref, M. M., Hussein, H. A., El Aassy, I. E. and Aita S. K. (1998). Mineralogy and Geochemistry of the Carboniferous stratabound U karst Latosol of Um Bogma Region, West Central Sinai, Egypt. In Hafez et al. (Eds.), *Presented by El Aref in the 4th International Conference on Geology of the Arab World, GAW4*. Cairo University (Abstract).

El Aref, M. M., & Lotfy, Z. H. (1989). Genetic karst significance of the iron ore deposits of El Bahariya Oasis, Western Desert, Egypt. *Annals of the Geological Survey of Egypt, XV*, 1–3.

El Aref, M. M., Mesaed, A. A., Khalil, M. A., & Salama, W. S. (2006a). Stratigraphic setting, facies analyses and depositional environments of the Lutetian Ironstones of Gabal Ghorabi mine area, El Bahariya Depression, Western Desert, Egypt. *Egyptian Journal of Geology, 50*, 29–57.

El Aref, M. M., Mesaed, A. A., & Salama, W. S. (2006b). Microbialite morpho-structures and biogenic accretion mechanism of the Lutetian Ironstones of Gabal Ghorabi mine area, El Bahariya Depression, Western Desert, Egypt. *Egyptian Journal of Geology, 50*, 59–81.

El Aref, M. M., & Refai, E. (1987). Paleo-karst processes in the Eocene limestones of the Pyramids Plateau, Giza, Egypt. *Journal of African Earth Sciences, Great Britain, 6*(3), 367–377.

El Aref, M., Salama, A., & Hammed, M. (2021). Morphotectonic evolution of Qaret El Sheikh Abdallah depressions and Denuded

paleo-karst in the White Desert, El Bahariya-Farafra Karst Territory, Egypt. *Egyptian Journal of Geology, 65*, 27–53.

El Aref, M. M., Saleh, M. H., & Salama, A. (2017a). Geomorphological classification and zonation of the exposed karst landforms in Bahariya-Farafra region, Western Desert Egypt. *International Journal of Science and Research (IJSR), 6*(5), 956–965.

El Aref, M. M., Saleh, M. H., & Salama, A. (2017b). Inventory and assessment of the geomorphosites of Bahariya-Farafra Territory, Western Desert, Egypt. *International Journal of Sciences: Basic and Applied Research (IJSBAR), 33*(2), 128–143.

El Azabi, M., & Eweda, S. (1996). Clastic-carbonate sequence of Gabal El Sara, Sharm El Sheikh Area, southern Sinai, Egypt. *Egyptian Journal of Geology, 40–2*(1996), 805–844.

El Kammar, A. (2020). Phosphae deposits of Egypt: Composition, origin and utilization. In Z. Hamimi et al. (Eds.), *The geology of Egypt* (pp. 590–563). Springer Nature Switzerland, AG 2020 (Chapter 15.1). ISSN 2364-6438 ISSN 2364-6446 (electronic), Regional Geology Reviews, ISBN 978-3-030-15264-2, ISBN 978-3-030-15265-9 (eBook).

El Manawi, A. W. (2006). Geologic setting and mineralogical investigations of Cenomanian ironstones, Wadi Dara, north Eastern Desert, Egypt. *Egyptian Journal of Geology* (Abstract and Prof. El Manawi personal communication).

El Miligy, A., & El Aref, M. M. (2004–2006). *The Guide (investment) map for limestone ore in Egypt* (Progress and final reports 1–6). The Egyptian Academy of Scientific Research and Technology, Cairo, Egypt.

El Sharkawi, M. A., El Aref, M. M., & Abdel Motelib, A. (1990a). Syngeneic and paleo-karstic copper mineralization in the Paleozoic platform sediments of West Central Sinai, Egypt. In J. Parnell et al (Eds.), *Sediment-hosted mineral deposits. Special publication, The international association of sedimentologists* (Vol. 11). Black Well Scientific Publications (pp. 159–172).

El Sharkawi, M. A., El Aref, M. M., & Abdel Motelib, A. (1990b). Manganese deposits in Carboniferous paleo-karst profile, Um Bogma region, West Central Sinai, Egypt. *Mineralium Deposita, 25*, 34–43.

El Sharkawi, M., El Aref, M. M., & El Manawi, A. W. (1989). Paleo-environments, classification and diagenetic aspects of ironstones in the Mesozoic sediments of El Maghara Area, Egypt. *Mineralogist, 1*, 1–25.

El Sharkawi, M. A., El Aref, M. M., & Mesaed, A. (1999). Stratigraphic setting and paleo-environment of the Coniacian-Santonian Ironstones of Aswan, South Egypt. *Geological Society of Egypt Special Publications, 2*, 243–278.

El Sharkawi, M. A., & Khalil, M. A. (1977). Glauconite, a possible source of iron for El Gedida iron ore deposits, Bahariya Oases, Egypt. *Egyptian Journal of Geology, 21*, 109–116.

El Shazly, E. M. (1957). Classification of Egyptian mineral deposits. *The Egyptian Journal of Egypt, I*(1), 1–21.

El Shazly, E. M., & Saleeb, G. R. (1959). Contribution to the mineralogy of Egyptian manganese deposits. *Economic Geology, 54*, 59–71.

Embabi N. S. (2004) *The geomorphology of Egypt, landforms and evolution. Volume I: The Nile Valley and the Western Desert. The Egyptian Geographical Society, Special Publication* (p. 447).

Embabi, N. S. (2018). Landscapes and landforms of Egypt: Landforms and evolution. In *World geomorphological landscapes* (p. 336).

Farag, M. Z. (2011). *Mineral evaluation and beneficiation of the oxidation zone Um Gheig Pb–Zn deposits, Red Sea Coast, Egypt* [MSc. Thesis]. Faculty of Science, Cairo University (p. 163).

Farag, M. Z., Abdel Khalek, N. A., El Aref, M. M., Hassan, M. S., & El Manawi, M. A. (2011). Characterization and gravity separation of non-sulfide Zn deposit from Um Gheig Mine, Red Sea Coast, Egypt. *Journal of Engineering Sciences (JES), Faculty of Engineering, Assiut University, 39*(1).

Farag, M. Z., Abdel Khalek, N. A., Hassan, M. S., El Aref, M. M., & El Manawi, A. W. (2012). Upgrading of Egyptian non-sulfide zinc ore by gravity separation techniques. *Journal of Metallurgical Engineering (ME), 1*(1), 6–13.

Fontboté, L., & Amstutz, G. C. (1980). New observations on diagenetic crystallization rhythmites in the carbonate facies of the Triassic of the Alpujarrides (Betic Cordillera, Southern Spain). Comparison with other diagenetic rhythmites. I. sym. diagenesis, Barcelona, 1980. *Revista del Instituto de Investigaciones Geológicas de la Diputación de Barcelona, 34*, 293–310

GAW. (1994). In A. Sadik (Ed.), *2nd International Conference on the Geology of the Arab World (GAW) Conference Proceedings, Cairo* (p 553).

Germann, K., Mocke, A., Doering, T., & Fisher, K. (1987). Late Cretaceous laterite-derived sedimentary deposits (oolitic ironstones, kaolins, bauxites) in Upper Egypt. *Berliner Geowissenschaftliche Abhandlungen, 73*(3), 727–758.

Gharieb, S. E. M. (1990). *Geological and geomorphological studies on limestones, East of the Nile* [M.Sc. thesis]. Department of Geology, Faculty of Science, Cairo University (p. 168).

Gharieb, S. E. M. (1998). *Geological studies on the Eocene rocks and the associated karst features and facies in the east Bei Suief area, North Eastern Desert, Egypt* [Ph.D. thesis]. Department of Geology, Faculty of Science, Cairo University (p. 226).

Gharieb, S. E. M. (2003). Eocene rocks and associated karst features in the East Beni Suef area, North Eastern Desert, Egypt. *Göttinger Arbeiten zur Geologie und Paläontologie Sb, 5*, 7–22, Gottingen, 7–21.

Glenn, C. R., & Arthur, M. A. (1990). Anatomy and origin of a Cretaceous phosphorite-greenand giant, Egypt. *Sedimentology, 37*, 123–154.

Guiraud, R., & Bosworth, W. (1999). Phanerozoic geodynamic evolution of the northeastern Africa and the northeastern Arabian platform. *Tectonophysics, 315*(1999), 73–108.

Guiraud, R., Bosworth, W., Thierry, J., & Delplanque, A. (2005). Phanerozoic geological evolution of Northern and Central Africa. *Journal of African Earth Sciences, 43*(2005), 83–143.

Guiraud, R., Issawi, B., & Bosworth, W. (2001). Phanerozoic history of Egypt and surrounding areas. In P. A. Ziegler, W. Cavazza, A. H. F. Robertson, & S. Crasquin-Solean (Eds.), *Peri-Tethys Memoir 6: Peri-Tethyan/Rift/Wrench Basins and Passive Margins. Mémoires du Museum national d'histoire naturelle* (Vol. 186, pp. 469–509). Paris. ISBN: 2-85653-528-3.

Gunnell, G. F., Winkler, A. J., Miller, E. R., Head, J. J., El-Barkooky, A. N., Abdel, G. M., Sanders, W. J., & Gingerich, P. D. (2016). Small vertebrates from Khasm El-Raqaba, late middle Miocene, Eastern Desert, Egypt. *Historical Biology, 28*(1–2), 159–171.

Halliday, W. R. (2003). Caves and karsts of Northeast Africa. *International Journal of Speleology, 32*(1/4), 19–32.

Hamdan, M. A., & Hassan, F. A. (2020). *Quaternary of Egypt. In the Geology of Egypt (Hamami et al., 2020), Regional Geology Reviews*. ISSN 2364-6438 ISSN 2364-6446 (electronic), ISBN 978-3-030-15264-2 ISBN 978-3-030-15265-9 (eBook), © Springer Nature Switzerland AG 2020. https://doi.org/10.1007/978-3-030-15265-9

Hamdan, M. A., & Lucarini, G. (2013). Holocene paleo-environmental, paleo-climatic and geoarchaeological significance of the Sheikh El-Obeiyid area (Farafra Oasis, Egypt). *Quaternary International, 320*, 154–168.

Hassan, M. M. (1990). Studies on lead-zinc sulphide mineralization in the Red Sea Coastal zone, Egypt. In *Proceedings of Eighth Quadrennial IAGOD Symp. Schweitzer Bartsche-Verlags bunch handlung*.

Hassan, M. M. (2002). Genesis of miocene polymetals mineralization, Western coastal zone, Egypt. *Journal of Sedimentology, Egypt, 10*.

Hassan, M. M. (2016). Phanerozoic rifting phases and mineral deposits. *EGU, 18*, 2016–3304.

Hassan, M. M. (2018). The Red Sea polymetallogenic province: the newest of the world. In *The Annual 56th Meeting of the Geological Society of Egypt, November, 2018, Invited Talk, Abstract* (pp. 1–4).

Hassan, M. M., Awed, M. H., El Sweifi, B., & El Nadeem, G. A. (2004). The South East Aswan iron ore deposits: An approach for qualitative evaluation. In *14th Symposium Planer and Development, Egypt* (pp. 99–120). May 2004.

Hassan, M., El-Afandy, H., El-Desoky, A., Hatem, A. M., Hassan, A., & Soliman, O. A. (2006). Studies on ferrugination in Gabal Agib Ring Complex, South Eastern Desert, Egypt. *Nuclear Sciences Scientific Journal, 4*, 1–18.

Hassan, M. M., El Dosoky, H., Salem, S., El Afendy, A., & Soliman, O. A. (2018). Genesis of iron deposits in Bir Um Hebal area, Southeast Aswan, Egypt: Remote sensing-structural-lithological-ore mineralogical contributions. *Middle East Journal of Applied Sciences, 8*(1), 19–36.

Helba, A. A., El Aref, M. M., & Saad, F. (2001). Lutetian oncoidal and ooidal ironstone sequences; Depositional setting and origin, northeast El Bahariya depression, Western Desert, Egypt. *Journal of Geological Society of Egypt, 45*(1A), 325–351.

Helba, A., El Manawy, A. W., & El Aref, M. M. (2003). Syn-depositional lateritic alteration and clastics starvation as pathways in the formation of the oolitic ironstones of North Wadi Qena, Eastern Desert, Egypt. *Egyptian Journal of Geology, 47*(1), 255–274.

Hermina, M., Klitzch, E., & List, F. K. (1989). *Stratigraphic Lexicon and explanatory notes to the geological map of Egypt 1; 500000* (p. 251). Conoco Co. Inc.

Hilmy, M. E., Ghozlan, A. E., & Sleem, Y. S. (1958). Uranium in some manganese ores, Um Bogma, Sinai. In *3rd Scientific Arab Conference, Beirut* (pp. 350–355).

Hilmy, M. A., & Hussein, A. (1978). A proposed classification for mineral deposits and occurrences in Egypt. *Precambrian Research, 6* (Abstract).

Hilmy, M. E., & Mohsen, L. (1965). Secondary copper minerals from West Central Sinai. *Journal of Geology UAR, 9*, 1–2. https://doi.org/10.1007/978-3-030-15265-9

Hussein, H. A., El Assy, I. E., El Aref, M. M., & Aita, S. K. (1998). Paleozoic stratabound Th and U latosol type of Um Bogma Region, Egypt, their geological setting and mode of formation. In A. Hafez et al. (Eds.), *4th International Conference, Geology of the Arab World* (*GAW*) (p. 117). Geology Department, Faculty of Science, Cairo University (Abstract).

Hussein, H. A., & El Sharkawi, M. (1990). Mineral deposits. In R. Said (Ed.), *The geology of Egypt* (pp. 511–566). A. A. Balkema, Brookfield (Chapter 26).

IEP "Iron Exploration Project". (1993–1997). *Iron exploration project, reports of phases 1–3, El Bahariya and Aswan Regions (Geol. Naim N (leader of the consortium), El Sharkawi M. and El Aref M. M. (Principle Investigators).* Geology Department, Cairo University and Geological Survey of Egypt (EGSMA). Phase I Report (1994, 147p), Phase II Report (1995, 162p), Phase III Report (1997, 287p).

ISCo, Iron Steel Company. (1987–1977, 2010). Exploration and re-evaluation of the iron ores of El Bahariya Oasis Ghorabi, Naser, El Harra, El Gedida. In *Annual internal technical reports*.

Issawi, B. (2002). Egypt during the phanerozoic. In Sadik et al. (Ed.), *5th International Conference on the Geology of the Arab World (GAW V1), Cairo* (pp. 401–440).

Issawi, B., El Hinawi, M., Francis, M., & Mazhar, A. (1999). *The phanerozoic geology of Egypt; geodynamic approach. Special publication* (Vol. 76, p. 462). Egyptian Geological Survey.

Issawi, B., Francis, M., Youssef, E. A., & Osman, R. I. (2009). The phanerozoic geology of Egypt, a geodynamic approach. In *Ministry of petroleum, the Egyptian mineral resources authority, Special publication* (Vol. 81, 2nd ed., p. 589).

Issawi, B., & McCauley, J. (1992). The Cenozoic rivers of Egypt: the Nile problem. In R. Hriedman & B. Adams (Eds.), *The flowers of horus, Egyptian studies association publication 2, Oxbow monograph* (Vol. 20, pp. 121–145).

Issawi, B., & McCauley, J. (1993). The Cenozoic landscape of Egypt and its river systems. *Annals of the Geological Survey of Egypt, 19*, 357–384.

Issawi, B., & Osman, R. (1993). Tectono-sedimentary synthesis of the Paleozoic-Cretaceous clastics, southwest Aswan, Egypt. *Journal of Sedimentary, 1*, 11–21.

Klitzsch, E. (1984). Northwestern Sudan and bordering areas: Geological development since Cambrian time. *Berliner Geowissenshaftliche Abhandlungen, 50*, 23–45.

Klitzsch, E. (1986). Plate tectonics and cratonal geology in Northeast Africa (Egypt and Sudan). *Geologische Rundschau, 75*(3), 753–768.

Klizsch, E. (1990). Paleozoic. In R. Said (Ed.), *The geology of Egypt* (pp. 393–406). A. A. Balkema, Brookfield (Chapter 21).

Klitzsch, E., & Wycisk, P. (1987). Geology of the sedimentary basins of northern Sudan and bordering areas. *Berliner Geowissenshaftliche Abhandlungen, 75*(1), 97–136.

Large, D. (2001). The geology of non-sulphide zn deposits—An overview. *Eazmetall, 54*, 264–276.

Lotfy, Z. H. (1989). *Geological, sedimentological and mineralogical study of the Northeastern Plateau, Bahariya Oasis* [Ph.D. thesis]. Department of Geology, Faculty of Science, Cairo University (p. 290).

Martin, J. M., Ortega, H. M., & Torres-Ruiz, J. (1984). Genessis and evolution of strontium deposits of the Granada Basin (Southeastern Spain): Evidence of diagenetic replacement of stromatolite belt. *Sedimentary Geology, 39*, 281–298.

McCauley, J. E., Schaber, G. G., Breed, C. S., Grolier, M. J., Haynes, C. V., Issawi, B., Elchi, C., & Blom, R. (1982). Subsurface Valleys and geochronology of the Eastern Sahara revealed by shuttle Radar. *Science, 218*(4516), 1004–1020.

Mein, P., & Pickford, M. (2010). Vallesian rodents from Sheikh Abdallah, Western Desert, Egypt. *Historical Biology, 22*(1–3), 224–259.

Meneisy, M. S. (1990). Vulcanicity. In R. Said (Ed.), *The geology of Egypt* (pp. 157–172). A. A. Balkema, Brookfield (Chapter 9).

Mesaed, A. A., Khalil, M. A., Salama, W. S., & El Aref, M. M. (2005). Diagenetic history and mineral evolution of the Lutetian ironstones of Gabal Ghorabi mine area, El Bahariya Depression, Western Desert, Egypt. In *Annual Meeting of the Egyptian Geological Society* (Abstract).

Meshref, W. M. (1990). Tectonic framework. In R. Said (Ed.), *The geology of Egypt* (pp. 113–156). A. A. Balkema, Brookfield (Chapter 8).

Mineral Map of Egypt, EGSMA. (1979). In M. S. Afia & I. Imam (Ed.), *Mining authority* (p. 44).

Monetant, C., Ott D'Estevou, P. O., Purser, B. H., Buroller, P. T., Jarrige, J. J., Orszag-Sperber, F., Philobbos, E. R., Plaziat, J.-C., Part, P., Richert, J. P., Roussel, N., & Thiriet, J. P. (1988). Tectonic and sedimentary evolution of the Gulf of Suez and the northwestern Red Sea. *Tectonophysics (Amsterdam), 153*, 161–177.

Morgan, P. (1990). Egypt in the framework of global tectonics. In R. Said (Ed.), *The geology of Egypt* (pp. 91–111). A. A. Balkema, Brookfield (Chapter 7).

Moustafa, A. R., Saoudi, A., Moubasher, A., Ibrahim, I. M., Molokhia, H., & Schwartz, B. (2003). Structural setting and tectonic evolution of the Bahariya Depression, Western Desert, Egypt. *GeoArabia. Gulf Petrolink, Bahrain, 8*(1).

Nickless, E. F. P., Booth, S. J., & Mosley, P. N. (1976). The celestite resources of the area northeast of Bristol. *Institute of Geological Science, Mineral Assessment Report, 25*, 83p.

Olausson, S. (1981). Formation of celestite in the Wenlock, Oslo Region, Norway, evidence of evaporitic deposition environments. *Journal of Sedimentary Research, 51*, 37–46.

Omara, S. (1959). The geology of Sharm El Sheikh Sandstone, Sinai. *Egyptian Journal of Geology, III*(1), 107–120.

Omran, M. (2015). *Micriwave dephosphorisation of high phosphorus iron ores of the Aswan region* (p. 427). University of Oulu Graduate School, University of Oulu, Faculty of Technology.

Omran, M., Fabritius, T., Abdel-Khalek, A., El-Aref, M., Elmanawi, A., Nasr, M., & Elmahdy, A. (2014). Microwave assisted liberation of high phosphorus oolitic iron ore. *Journal of Minerals and Materials Characterization and Engineering, 2*, 414–427.

Omran, M., Fabritius, T., Elmahdy, A., Abdel-Khalek, A., El-Aref, M., & Elmanawi, A. (2015). XPS and FTIR spectroscopic study on microwave treated high phosphorus iron ore. *Applied Surface Science, 345*(2015), 127–140.

Philip, G., El Aref, M. M., Darwish, M., & Ewais, S. (1991a). Paleo-erosion surfaces and karst manifestations including "Egyptian Alabaster". In *Gabal Homret Schaibun—Gabal Sannur Area, East of the Nile Valley, Egypt. Egyptian Journal of Geology, 34*(1 and 2), 41–79.

Philip, G., El Aref, M. M., Darwish, M., & Ewais, S. (1991b). Organic and inorganic fabrics of paleo-karst sediments, east of Bani Suef, Nile Valley, Egypt. In *Twenty Ninth Annual Meeting, Abstract. Egyptian Journal of Geology*.

Philobbos, E. R., Plaziat, J.-C., Part, P., Richert, J. P., Roussel, N., & Thiriet, J. P. (1988). Tectonic and sedimentary evolution of the Gulf of Suez and northwestern Red Sea. *Tectonophysics (Amsterdam), 153*, 161–177.

Pickford, M., Wanas, H., & Soliman, H. (2006). Indications for a humid climate in the Western Desert of Egypt, 1–10 Myr ago: Evidence from Galagidae (Primates, Mammalia). *Paleo-ecology, 5*, 935–943.

Said, R. (1990a). Cretaceous paleo-geographic maps. In R. Said (Ed.), *The geology of Egypt* (pp. 439–450). A. A. Balkema, Brookfield (Chapter 23).

Said, R. (1990b). Cenozoic. In R. Said (Ed.), *The geology of Egypt* (pp. 451–486). A. A. Balkemam, Brookfield (Chapter 24).

Said, R. (1990c). In R. Said (Ed.), *The geology of Egypt* (p. 734). A. A. Balkema.

Said, R., & Mansour, A. (1971). The discovery of new kaolin deposits in Wadi Kalabsha, Western Desert, Egypt. *Geological Survey of Egypt, 54*, 138.

Said, R., Sabet, A., Zalata, A., Teniakov, V., & Porkyshkin, V. (1967). A review of theories on the geological distribution of bauxite and their application for bauxitic prospecting in Egypt. *Annals of the Geological Survey of Egypt, 6*, 6–32.

Salama, W. S. (2006). *Geology and genesis of Ghorabi iron ore and associated barite and manganese rich deposits, El Bahariya Depression, Western Desert, Egypt* [M.Sc. thesis]. Faculty of Science, Cairo University (p. 201).

Salama, W. S. (2010). *Geological and mineralogical studies on the microbially mediated Ironstone Facies, El Bahriya Depression, Western Desert, Egypt* [Ph.D. thesis]. Faculty of Science, Cairo University (p. 245).

Salama, W. S. (2014). Paleo-environmental significance of aluminum phosphate-sulfate minerals in the upper Cretaceous ooidal ironstones, E-NE Aswan area, southern Egypt. *International Journal of Earth Sciences (geologische Rundschau), 103*, 1621–1639.

Salama, W. S., El Aaref, M. M., & Gaupp, R. (2012). Mineralogical and geochemical investigations of the Middle Eocene ironstones, El Bahariya Depression, Western Desert, Egypt. *Gondwana Research, 22*, 717–736.

Salama, W. S., El Aaref, M. M., & Gaupp, R. (2013). Mineral evolution and processes of ferruginous microbialite accretion—An example from the Middle Eocene stromatolitic and ooidal ironstones of the Bahariya Depression, Western Desert, Egypt. *Geopiology, 11*, 15–28.

Salama, W. S., El Aaref, M. M., & Gaupp R. (2014). Facies analysis and palae-oclimatic significance of ironstones formed during the Eocene greenhouse. In *Sedimentology 2014, International Association of Sedimentologists* (pp. 1–31).

Salama, W. S., El Aaref, M. M., & Gaupp, R. (2015). Spectroscopic characterization of iron ores formed in different geological environments using FTIR, XPS, Mssbauer spectroscopy and thermoanalyses. *Spectrochimica Acta Part A: Molecular and Biomolecular Spectroscopy, 136*, 1816–1826.

Schandelmeir, A., Klitzsch, E., Hendrix, F., & Wycisk, P. (1987). Structural development of northeast Africa since Pre-Cambrian times. *Berliner Geowissenshaftliche Abhandlungen, 75*(1), 5–25.

Scholle, P. A., Stemmerik, I., & Harpoth, O. (1990). Origin of karst-associated celestite mineralization in Karstryggen, Central East Greenland. *Journal of Sedimentary Research, 60*, 397–410.

Sehim, A. A. (1993). Cretaceous tectonics in Egypt. *Egyptian Journal of Geology, 37*(1), 335–372.

Shukri, N. M., & Nakhla, F. M. (1955). The sulfur deposits of Ras Gemsa coast. In *Symposium on Applied Geology in the Near East* (pp. 114–123). UNESCO, Ankara.

Smith, A. G. (1981). Phanerozoic equal area maps. *Geologische Rundschau, 1*, 91–127.

Sokker, A. M. (1991). *Geomorphological, petrological and mineralogical studies on the carbonate sediments between Bahariya-Farafra, Western Desert, Egypt* [M.Sc. thesis]. Faculty of Science, Cairo University (p. 256).

Soliman, A. S. M. (2018). *Geology, genetic classifications and inventory of paleo-karst related landforms of the Cretaceous-Tertiary carbonate sequences, Bahariya-Farafra Territory, Western Desert, Egypt* [Ph.D. thesis]. Department of Geology, Faculty of Science, Cairo University (p. 249).

Stern, R. F. (1994). Arc assembly and continental collision in the Neoproterozoic East African orogeny; implication for the consolidation of Gondwanaland. *Annual Reviews of Earth Band Planetary Sciences, 22*, 319–351.

UEC 'United Engineering Consultant". (1976). *Development of iron ore deposits, Bahariya Oasis* (Project 4741, report). USS "United State Steel Engineering and Consultants INC.

Wali, A. M., El Dougdoug, A. A., & Aref M. A. (1989). Geology, isotope geochemistry and the role of salt spines sulfur genesis, Gemsa area, Red Sea, Egypt. *Annals of the Geological Survey of Egypt, XVI* (1986–1989).

Weissbrod, T. (1969). The Paleozoic of Israel and adjacent countries. Part I, the subsurface Paleozoic stratigraphy of S Israel. In *Bulletin —geological survey of Israel, 1–25; Part II, the Paleozoic outcrops in SW00 Israel and their correlation with those of S Israel* (Vol. 48, pp. 1–32).

Wilson, M., & Guiraud, R. (1998). Late permian to recent magmatic activity of the Africa-Arabian Margin of the Tethys. In D. S. MacGregor, T. J. Moody, & D. D. Clark-Lowes (Eds.), *Hydrocarbon geology of North Africa. Special publication, Geological society of London* (Vol. 132, pp. 231–263).

Yahiya A. (2007): Beneficiation of Aswan iron ores. In *Iron Symposium*. Central Metallurgical Research and Development Institute, Cairo, Egypt.

Youssef, E. A. (1989). Geology and genesis of sulfur deposits at Ras Gemsa area, Red Sea coast, Egypt. *Geology, 17*, 797–801.

Mortada Mourad Taha El Aref is a professor of ore geology in the Geology Department, Faculty of Science, Cairo University, Egypt. Prof. El Aref has worked on and deeply investigated different types of metallic and non-metallic stratabound ore deposits of the Eastern and Western Deserts of Egypt and Sinai. He has led several regional projects in the field of ore exploration and beneficiation. He was the Director of the Regional Centre for Training and Technology Transfer for Arab States (Cairo-BCRC), Basel Convention on the Control of Transboundary Movements of Hazardous Wastes and their Disposal, UNEP, (2003–2008). He became interested in environmental sciences and management since his election as a director of the Cairo University Centre for Environmental Hazard Mitigation (CEHM) from 2003 to 2008. He has supervised numerous environmental protection mega projects, including air pollution, noise, environmental impact assessment (EIA) studies, hazard mitigation studies, and urban land use planning. Currently, Prof. El Aref holds the position of Chairman of the Board of Directors of the Iron and Steel Company for Mines and Quarries (ISMQ).